Oscillons: localized patterns in a periodically forced system

Abeer Saleh Alnahdi

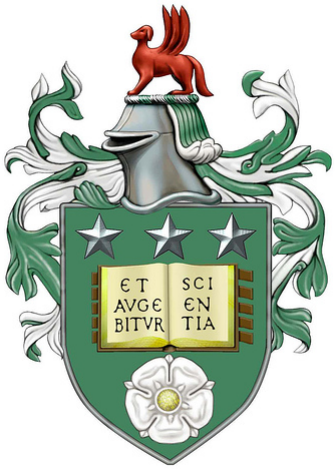

Department of Applied Mathematics

University of Leeds

Submitted in accordance with the requirements for the degree of

Doctor of Philosophy

March 2015

The candidate confirms that the work submitted is her own, except where work which has formed part of jointly-authored publications has been included. The contribution of the candidate and the other authors to this work has been explicitly indicated below. The candidate confirms that appropriate credit has been where reference has been made to the work of others.

- Chapter 2 is based on A. S. Alnahdi, J. Niesen, A. M. Rucklidge, "Localized patterns in periodically forced systems", SIAM J. Appl. Dyn. Syst., **13** (2014), pp. 1311-1327.

The construction of the paper "Localized patterns in periodically forced systems" was my original idea which I accomplished with the co-authors, J. Niesen and A. M. Rucklidge, for all derivations of the equations (the analysis of the model) and numerical results. The contribution was equal. Moreover, I wrote the draft of the paper which, after all the co-author's amendments, was brought to a publishable form.

To my parents, Saleh and Fatimah

Abstract

Spatially localized, time-periodic structures, known as oscillons, are common in pattern-forming systems, appearing in fluid mechanics, chemical reactions, optics and granular media. This thesis examines the existence of oscillatory localized states in a PDE model with single frequency time dependent forcing, introduced in [70] as phenomenological model of the Faraday wave experiment. Firstly in the case where the prefered wavenumber at onset is zero, we reduce the PDE model to the forced complex Ginzburg–Landau equation in the limit of weak forcing and weak damping. This allows us to use the known localized solutions found in [15]. We reduce the forced complex Ginzburg–Landau equation to the Allen–Cahn equation near onset, obtaining an asymptotically exact expression for localized solutions. In the strong forcing case, we get the Allen–Cahn equation directly. Throughout, we use continuation techniques to compute numerical solutions of the PDE model and the reduced amplitude equation. We do quantitative comparison of localized solutions and bifurcation diagrams between the PDE model, the forced complex Ginzburg–Landau equation, and the Allen–Cahn equation. The second aspect in this work concerns the investigation of the existence of localized oscillons that arise with non-zero preferred wavenumber. In the limit of weak damping, weak detuning, weak forcing, small group velocity, and small amplitude, asymptotic reduction of the model PDE to the coupled forced complex Ginzburg–Landau equations is done. In the further limit of being very close to onset, we reduce the coupled forced complex Ginzburg–Landau equations to the real Ginzburg–Landau equation. We have qualitative prediction of finding exact localized solutions from the real Ginzburg–Landau equation limited by computational constraints of domain size. Finally, we examine the existence of localized oscillons in the PDE model with cubic–quintic nonlinearity in the strong damping, strong forcing and large amplitude case. We find two snaking branches in the bistability region between stable periodic patterns and the stable trivial state in one spatial dimension in a manner similar to systems without time dependent forcing. We present numerical examples of localized oscillatory spots and rings in two spatial dimensions.

Acknowledgements

Doing a PhD is very hard work, and can not be easy to do without all the support and help that I got from many people around me. I would like to thank all the people who have made my time during my PhD enjoyable and to who contributed in any way to making it happen.

I would first like to thank my supervisors, Prof. Alastair Rucklidge and Dr Jitse Niesen for all the support, guidance, and for being patient throughout my PhD studies. I have learnt so much from them throughout this thesis. The research environment they provided always enhanced me to do my best. They encouraged me to participate in many conferences, which was very useful. I really appreciate their valuable advice and willingness to proof-read throughout my studies. At this point, I would also like to thank Andrew Dean for his interest and discussion in some of our regular meetings.

I was very lucky to get this project after I finished my MSc under the supervision of Prof. Alastair Rucklidge and Dr Thomas Wagenknecht. It was a pleasure to work with Thomas in the dissertation for my master degree and the first year and a half of my PhD study. Thomas was very helpful person. I learnt a lot from him especially with continuation, AUTO. In fact, I knew nothing about AUTO before Thomas taught me. We sat for hours in his office trying to help me to understand how it works. His sense of humor was always inspiration for me. I will always be glad that I had the chance to know him.

I am greatly thankful to the school of Mathematics for the friendly and highly organized environment for postgraduate student. Many thanks to all the administrative Staff for being very helpful and kind. I am very pleased to do my PhD at the University of Leeds, and I would highly recommend it to any graduate students. I would also like to thank my entire friends who I met in the school of Mathematics during my study.

Finally, I am more than grateful to my parents Saleh and Fatimah for their support and help in everything in my life. My special thanks are reserved for my wonderful husband

Bandar for his love, support, encouragement, compassion and unwavering belief in my ability at every step of the way. Moreover, I would like to thank all my family and friends for their source of joy and support; especially my brother Sultan.

Throughout my PhD I was supported by King Abdullah Foreign Scholarship Program. I also acknowledge the support from Imam Muhammad bin Saud Islamic University in my last year.

This thesis is dedicated to the memory of Dr Thomas Wagenknecht.

Contents

List of figures

List of tables

Chapter 1

Introduction

1.1 Patterns

Patterns appear throughout nature, including convection, animal coat markings, fingerprints, ripples on flat sandy beaches and desert dunes. The observation of pattern formation has attracted the attention of scientists for a long time, and has motivated both theoretical and experimental research. When a control parameter of a homogeneous system is increased above a critical value, spatially periodic structures can emerge. The study of convection between two horizontal plates (Rayleigh–Bénard convection) is one famous physical example of pattern formation [41], in which a container of fluid is heated from below. As the heat is applied from underneath the container, the fluid expands at the bottom and becomes less dense. Thus, the fluid rises through the colder fluid at the upper boundary to be away from the heat source, it cools and becomes denser than the fluid at the lower boundary, so that it sinks. As a consequence of this, the fluid falls from the upper surface back down to the bottom. Repeated rising and sinking in different locations causes the fluid to form spatial patterns. An important review of theoretical and physical examples of pattern formation is the paper by Cross and Hohenberg [25], and an introduction to common analytical methods that are used to study pattern formation mathematically can be found in the book by Hoyle [41].

Figure 1.1: Soliton-like structure on the surface of a ferrofluid generated by applying magnetic field vertically. Figure is reprinted from [68], and the copyright (2005) is by the American Physical Society.

Turing patterns are steady patterns that arise in reaction–diffusion systems, predicted in Turing's original paper [81]. Non-oscillatory Turing patterns appear through a linear instability when there are two reacting and diffusing chemicals, with one diffusing much faster than the other. Steady localized states near the Turing instability can exist if the system has bistability [22, 85, 91]. This occurs when the Turing instability is subcritical, and so a stable zero state, a small amplitude unstable pattern, and larger amplitude stable pattern can all coexist. The localized solution consists of a patch of stable pattern surrounded by the stable zero state [27, 52, 53], rather than having the periodic pattern filling the whole domain.

An example of spatially localized states was observed on the surface of a ferrofluid [68] (see Figure 1.1). This fluid is placed in a spatially homogeneous time-independent vertical

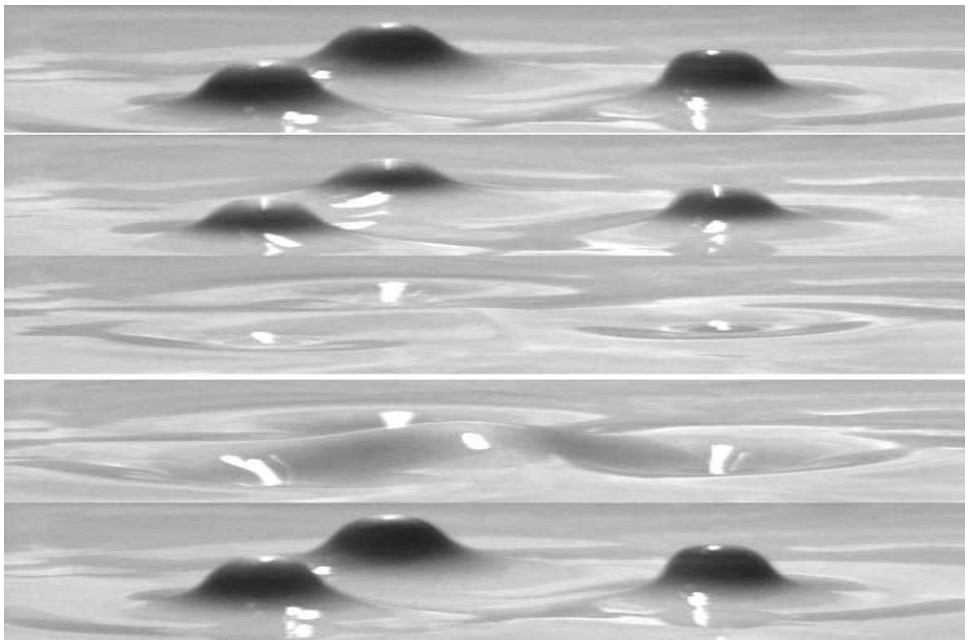

Figure 1.2: A triad of oscillons in a in a vertically vibrated colloidal suspension by O. Lioubashevski, Y. Hamiel, A. Agnon, Z. Reches, and J. Fineberg, taken from [51], Physical Review Letters, 1999.

magnetic field. The deformation in the surface of the fluid creates one or more stationary, isolated peaks [68].

Spatially localized structures appear in many other pattern-forming systems driven by external forcing. The formation of localized states has been of interest to the scientific community for many years. Localized states have been found in many experiments, such as in ferromagnetic fluids [68], in fluid surface wave experiments [4, 50, 76, 89], chemical reactions [47,49,65,84,87], colloidal suspensions [51], and granular media [10,54,83,92]. Examples of spatially localized structures have also been observed in theoretical studies, for example in optics [19, 33, 79], and in mathematical neuroscience, where localized bursts of activity might be related to short-term memory formation [48, 74], as well as in models of granular media [16, 30], surface wave in fluids [59, 60] and chemical reactions [84, 86].

Our interest in this thesis is to investigate specific types of localized structures, called

oscillons. Much progress has been made on steady problems, where bistability between a steady pattern and the zero state leads to steady localized patterns bounded by stationary fronts between these two states [13, 26]. In contrast, oscillons, which are oscillating localized structures in a stationary background, are relatively less well understood. Oscillons have been found experimentally in fluid surface wave experiments [4, 50, 51, 76, 89], chemical reactions [65], and vibrated granular media problems [9, 54, 82, 83]. In the surface wave experiments, the fluid container is driven by vertical vibrations. When these are strong enough, the surface of the system becomes unstable (the Faraday instability) [32], and standing waves are found on the surface of the fluid. Oscillons have been found when this primary bifurcation is subcritical [24], and these take the form of alternating conical peaks and craters against a stationary background. Figure 1.2 shows an example with three oscillons in a colloidal suspension.

A second striking example of oscillons was found in a vertically vibrated thin layer of granular particles [83]. As with the surface wave experiments, oscillons take the shape of alternating peaks and craters: Figure 1.3 shows spatially localized oscillons in a thin layer of bronze beads.

The observation of oscillons in these experiments has motivated our theoretical investigation into the existence of these states and their stability. In both of these experiments, the forcing (vertical vibration) is time-periodic, and the oscillons themselves vibrate with either the same frequency as the forcing (harmonic) or with half the frequency of the forcing (subharmonic).

Previous studies to these parametrically forced problems have averaged over the fast timescale of the forcing and have focused on PDE models where the localized solution is effectively steady [3, 15, 24]. In a variety of pattern-forming systems, stable oscillons arise in numerical simulations of these PDEs. Models like the Swift–Hohenberg equation [24, 36], the forced complex Ginzburg–Landau equation [15, 21, 58, 61, 90], the forced complex Ginzburg–Landau equation with a conservation law [28], and the nonlinear

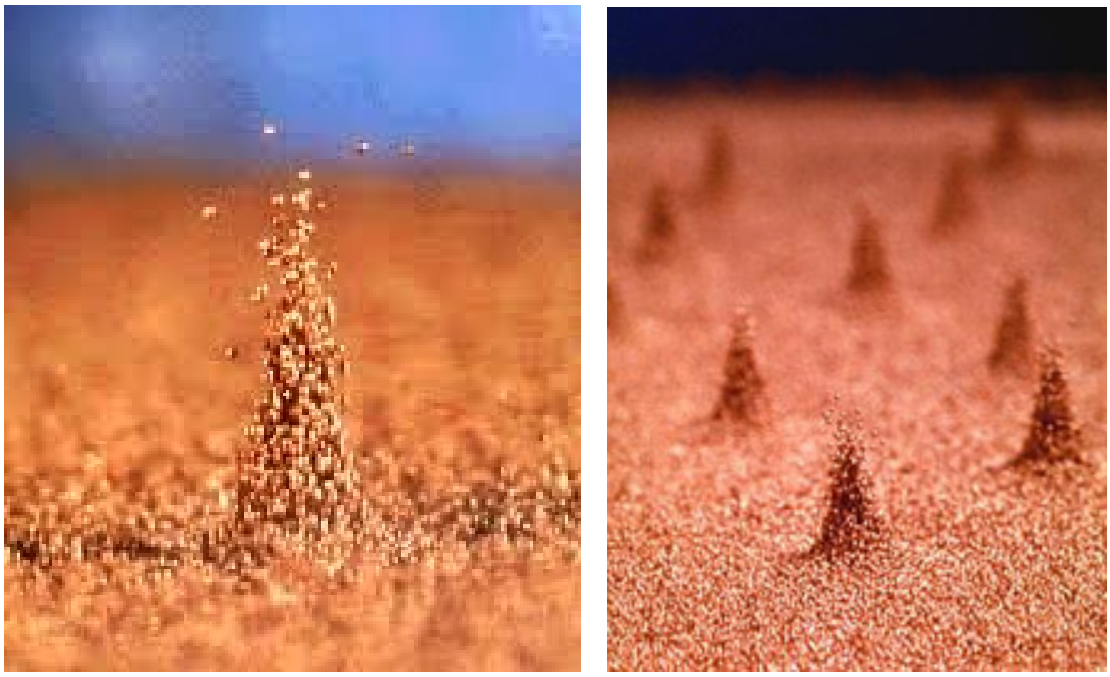

Figure 1.3: Localized oscillon in a vertically-vibrated layer of bronze beads (photo courtesy of Paul Umbanhowar, Northwestern University).

Schrödinger equation [5, 59] are designed to capture the features of pattern-forming systems in one-, two- and three- dimensions. In all these models, numerical study revealed that the equations give a qualitative explanation of the observations of patterns in experiments.

We will discuss first the existence of localized solutions with zero wavenumber at onset (Chapter 2), because we know that in this case the amplitude equation is in the form of the forced complex Ginzburg–Landau equation [21], which is given by

$$A_T = (\tilde{\mu} + i\nu)A + (1 + i\kappa)A_{XX} - (1 + i\rho)|A|^2 A + \Gamma\bar{A}, \tag{1.1}$$

where A is a complex amplitude representing the oscillation in a continuous system near a Hopf bifurcation point in one spatial dimension; and the real coefficients $\tilde{\mu}$ is the distance from the onset of the oscillatory instability, ν is the detuning between the Hopf frequency and the driving frequency, κ represents the dispersion, ρ is the nonlinear

frequency correction, and Γ is the forcing amplitude. We also know from [15] that the forced complex Ginzburg–Landau equation has localized states. By carrying out all stages of the calculation explicity, we are able to make a quantitative connection from start to finish.

However, in the Faraday wave experiment, the preferred wavenumber at the onset of pattern formation is non-zero [64, 77]. We consider this more complicated case in Chapters 3 and 4, and derive the *coupled forced complex Ginzburg–Landau equations*:

$$\begin{aligned}\frac{\partial A}{\partial T} &= (\rho + i\nu)A - 2(\alpha + i\beta)\frac{\partial^2 A}{\partial X^2} + v_g\frac{\partial A}{\partial X} + C\left(|A|^2 + 2|B|^2\right)A + i\Gamma\bar{B}.\\ \frac{\partial B}{\partial T} &= (\rho + i\nu)B - 2(\alpha + i\beta)\frac{\partial^2 B}{\partial X^2} - v_g\frac{\partial B}{\partial X} + C\left(2|A|^2 + |B|^2\right)B + i\Gamma\bar{A},\end{aligned} \tag{1.2}$$

where A and B represent the amplitudes of slowly varying left- and right-travelling waves; and ρ, ν, α, β, v_g and Γ are real parameters and measure the dissipation, detuning, diffusion, dispersion, group velocity and forcing of the wave; C is a complex parameter.

Throughout this thesis we will seek localized oscillatory states in a PDE with explicit time dependent parametric forcing that is based on the PDE in [70]. We will present this PDE model in section 1.4. We find excellent agreement between oscillons in this PDE and steady structures found in appropriate amplitude equations; this is the first complete study of oscillatory localized solutions in a PDE with explicit time dependent forcing.

In the next sections we will discuss some basic theoretical approaches in order to study localized states.

1.2 Theoretical approaches

A fundamental theoretical approach to studying pattern-forming problems is based on describing the slow dynamics of a driven system as a phase transition or symmetry-breaking bifurcation. The basic idea is to study the transition in stability of a trivial state

as a control parameter (in our study, F) passes through its critical value, with the critical value determined from a linear stability analysis. The analysis then lies in the study of weakly nonlinear dynamics of the problem slightly beyond the instability point.

If we consider the linearized problem about the trivial state and examine the stability of Fourier modes $e^{\sigma t+ikx}$ where k is a wavenumber, the trivial state is linearly stable if the real part of the growth rate σ is negative for all k. An instability corresponds to the real part of σ (for some wavenumber) first passing through zero; we define the corresponding F value as $F = F_c$. The critical wavenumber $|k| = k_c$ for which this determines whether the bifurcation is finite-wavelength ($k_c > 0$) or uniform ($k_c = 0$). The amplitude of the unstable modes will grow exponentially until nonlinear effects become important.

The theoretical analysis of pattern-forming systems can be often described by reducing the governing equations to their amplitude equations (equations for the nonlinear evolution of the amplitude of the unstable modes) by studying dynamics between different modes: active modes, which are growing, and passive modes, which are decaying, or neutrally stable modes, which are neither growing nor decaying. Amplitude equations have become an important tool in the study of pattern formation problems. They have been successfully applied to a wide range of physical systems. Amplitude equations are often studied as general models for pattern formation phenomena as they are the simplest nontrivial models that enjoy the correct properties. In large or infinite boxes, the amplitude equations are known as envelope equations. In this case the behavior of the active modes is modulated by the envelope over a slow timescale and a large spatial scale [62]. Often the term *amplitude* equation is used to refer to both amplitude and envelope equations.

Fourier modes of the form $e^{i(\Omega t+kx)}$, with real frequency Ω and wavenumber k, are travelling waves, and move from place to place with constant speed, and transport energy. Standing waves refer to waves that remain in a constant position. They can arise as a result of interference between two waves travelling in opposite directions. When the amplitude of the wave is modulated, the variation in the amplitude is called the envelope of the wave.

Modulated waves can vary in space and time.

The behavior of a system near the bifurcation point with a slowly varying envelope was studied by Newell and Whitehead [63] and Segel [75]. They investigated the formation of stationary patterns in convection systems. Amplitude equations also appear in the work of Ginzburg and Landau, though their study was in superconductivity [35].

In this thesis, we use weakly nonlinear analysis in order to derive the amplitude equations of a particular PDE model. We will briefly talk about the procedure of this method in the next section.

1.2.1 Weakly nonlinear analysis

The governing equations of motion in most pattern-formation systems are nonlinear and can not be solved analytically. Weakly nonlinear analysis is a common approach to analyzing such equations, dating back to the middle of the last century [56]. The presentation of the method in this section follows [41,88]. We consider a nonlinear system of the form

$$LU = f_{non}(U, x, t, F), \tag{1.3}$$

where $U(x,t)$ is a (vector-valued) complex function, L is a (matrix) linear operator (which can include the forcing F and differentiation in time and space), and f_{non} is a function that contains the nonlinear and forcing terms. We assume that F is the control parameter of the system (1.3). Usually, the zero flat state loses stability at a critical value $F = F_c$, and the critical eigenfunction can have zero or non-zero wavenumber and frequency.

Weakly nonlinear theory is a method that is used for studying the dynamics of a system when F is close to the critical value F_c. Thus, the amplitude of the perturbations is just large enough for the nonlinear terms to become relevant. In this case there are only a few unstable modes. The purpose of using weakly nonlinear analysis is to get a set of reduced amplitude equations that describes the motion of the governing equation, and

which captures the nonlinear interaction between the few unstable modes.

However, using weakly nonlinear theory can be very tricky to approach. The difficulty comes from the fact that there are a number of ways of constructing weakly nonlinear equations, and also because the methodology and the result are not unique. However, the key is to determine, ahead of time, the type of dynamics we aim for. Over time, it gets easier to do the reduction by experience and practice. Additionally, the method will determine whether a subcritical or supercritical bifurcation occurs. A small parameter is introduced, using the distance above the bifurcation point $|F - F_c|$ in a multiple scales analysis. Therefore, we begin the analysis with the near-threshold condition $F = F_c(1 + \epsilon^2 F_2)$, where $0 < \epsilon \ll 1$.

In order to modulate the envelope of the wave $e^{ik_c x}$, so that the amplitude of the governing equation varies in slow time and slow space, we apply an appropriate multiple scales analysis. Thus we introduce the temporal and spatial variables, $T = \epsilon^i t$ and $X = \epsilon^j x$, for some integers i and j. We then expand the variable $U(x, t)$ as series in powers of ϵ:

$$U = \sum_{m=1}^{\infty} \epsilon^m U_m, \tag{1.4}$$

where U_m is $O(1)$ complex functions for all $m \in Z^+$.

We substitute (1.4) into (1.3), and then we solve the problems that occur at successive orders of ϵ. The linear analysis appears at the lowest order of ϵ. As we mentioned before, it takes some thought to get the scaling right (selecting correct values of i and j) until eventually we end up with the required nonlinear amplitude equation.

At $O(\epsilon)$, the linear problem arises

$$LU_1 = 0, \tag{1.5}$$

which normally has a non-zero explicit solution that contains a combination of components evolving over the fast scales of space x and time t, multiplied by the

modulation of the amplitudes in slow space and time. At higher order of ϵ, we can determine the evolution of these amplitudes. At a specific order (m) of ϵ, we get problems of the following form

$$LU_m = f_{non}^m, \tag{1.6}$$

where f_{non}^m refers to the slow derivatives, forcing, and nonlinear terms at $O(\epsilon^m)$. We must ensure that there are no resonant terms at the equation of U_m, so that U_m is bounded.

Another way to investigate this problem is to look at the adjoint linear operator of (1.5). The adjoint linear operator $L^\dagger$ is defined by

$$\langle f(x,t), Lg(x,t)\rangle = \langle L^\dagger f(x,t), g(x,t)\rangle, \tag{1.7}$$

for all sufficiently smooth functions f and g, where $\langle f(x,t), g(x,t)\rangle$ is the inner product given by

$$\big\langle f(x,t), g(x,t)\big\rangle = \frac{1}{\Lambda\psi}\int_\Lambda\int_\psi \bar{f}(x,t)g(x,t)dtdx,$$

where $\bar{f}$ is the complex conjugate of f, Λ is the spatial domain, and ψ is the temporal domain. The procedure we must follow requires the imposition of solvability conditions, applied through the Fredholm Alternative Theorem [46]. This theorem says that for a bounded linear operator L with a problem of the form

$$Lu = f, \quad \text{and} \quad L^\dagger v = g \tag{1.8}$$

for some continuous functions f and g, one of the following holds:

- either the inhomogeneous equations (1.8) have unique solutions u and v respectively, and the corresponding homogeneous equations,

$$Lu = 0, \quad \text{and} \quad L^\dagger v = 0$$

have only the trivial solutions $u = 0$ and $v = 0$.

- or the homogeneous equations

$$Lu = 0, \quad \text{and} \quad L^\dagger v = 0,$$

have the same number of linearly independent solutions. In this case, inhomogeneous equations (1.8) have a solution if and only if f and g satisfy

$$\langle v, f \rangle = 0, \quad \text{and} \quad \langle g, u \rangle = 0, \tag{1.9}$$

for each u, v satisfying $L^\dagger v = 0$ and $Lu = 0$.

In our study in this thesis, the operator L contains differential operator and is hence unbounded. However, we can make L bounded by choosing appropriate boundary condition and restricting its domain to an appropriate function space [37]. We will not consider these functional analytic details in this thesis.

As we explained above, equation (1.5) has a non-zero solution, so it is the second of these alternatives that applies to weakly nonlinear theory. Therefore, if $LU_m = f^m_{non}$ has a solution, then

$$\langle V, f^m_{non} \rangle = \langle V, LU_m \rangle = \langle L^\dagger V, U_m \rangle = 0, \tag{1.10}$$

for any non-zero V that satisfies $L^\dagger V = 0$. This is often called the solvability condition, and having imposed this condition, (1.6) can be solved for U_m. It is equations of the form (1.10) that lead to the amplitude equations.

We do not explicitly outline the weakly nonlinear method and derivation of the solvability conditions for the parametrically forced PDE of interest here. We will give direct derivation and application of solvability conditions in Chapter 2 and Chapter 3.

1.3 Localized states in the Swift–Hohenberg equation

There have been many studies in recent years of the Swift–Hohenberg equation, which is a model for pattern-forming features introduced by Swift and Hohenberg [78], in their study of random thermal fluctuations in Boussinesq convection in the limit of an infinite domain. Additionally, it is considered as a generic model of pattern formation:

$$\partial_t u = ru - (1 + \partial_x^2)^2 u + N(u; b), \tag{1.11}$$

where $u(x, t)$ is a real scalar variable that represents the pattern-forming activity, r and b are real parameters, and $N(u; b)$ refers to nonlinear terms. There are two common choices of the nonlinear terms $N(u; b)$ that produce the essential element of finding localized states, bistability: the quadratic–cubic nonlinearity $N_{23}(u; b) = bu^2 - u^3$ and the cubic–quintic nonlinearity $N_{35}(u; b) = bu^3 - u^5$. These nonlinear terms allow a subcritical bifurcation of a small amplitude state and stability of a large amplitude state. Equations such as the Swift–Hohenberg equation have the advantage that they are simple enough to be studied analytically in detail, while having the same qualitative pattern formation features that can be observed in experiments or more realistic systems. It is a variational model in time and the steady form of the equation is conservative in space.

In the Swift–Hohenberg equation with N_{23}, a common approach is to consider a fixed b and to treat r as the primary bifurcation parameter [12]. The quadratic term allows small amplitude destabilization, while the negative cubic term gives large amplitude stability. The trivial state $u(x, t) = 0$ exists and is linearly stable for all values of b when the control parameter r is negative. The trivial solution undergoes a pattern-forming instability when it loses stability at $r = 0$, and Fourier modes e^{ikx} with wavenumber k close to one become unstable for positive r. At $r = 0$, the secondary parameter b identifies the type of criticality of the pattern-forming instability. The bifurcation diagram is supercritical if $b^2 < \frac{27}{38}$ and subcritical if $b^2 > \frac{27}{38}$. The Swift–Hohenberg equation with cubic–quintic nonlinearity N_{35}, has the same linear stability properties as the quadratic–cubic equation.

The pattern-forming pitchfork bifurcation is subcritical when b is positive.

The Swift–Hohenberg equation in both cases of quadratic–cubic and cubic–quintic nonlinearities has some important symmetries. In both cases, the model has translation symmetry and is reversible, that it is equivariant under spatial reflections $(x, u) \to (-x, u)$. The model with the N_{35} nonlinearity has in addition the symmetry $(x, u) \to (x, -u)$.

Localization mechanisms were first introduced in one dimension by Pomeau in [66], who showed that localized states require a bistability between the trivial and cellular pattern states in a subcritical bifurcation to exist. The Swift–Hohenberg equation with cubic–quintic nonlinearity was first studied by Sakaguchi and Brand in [71, 73], where they showed that stable localized solutions with a large range of lengths can be found. Sakaguchi and Brand did not discuss how the different branches of localized solutions are connected. Much of the current understanding of localized states is due to work by Burke and Knobloch [12–14]. Stationary localized states occur in the parameter region where the trivial state is stable, and so bistability is an important ingredient for the existence of localized states. In one space dimension, examples of localized states in the Swift–Hohenberg model with N_{23} nonlinearity from [11] are presented in Figure 1.4. It was found that when the domain size increases, more turns appear in the snaking curve [27]. Burke and Knobloch investigated spatially localized states in the Swift–Hohenberg equation with N_{35} nonlinearity in one spatial dimension [14], which organized in a characteristic of snakes-and-ladders structure.

Localized states also exist in the extended Swift–Hohenberg equation with more general nonlinearity $N(u; b)$ that include terms such as u_x, u_{xx}, and u_{xxx} [11]. These terms can destroy the variational structure of the Swift–Hohenberg equation; nonetheless, a snaking bifurcation diagram can still be found.

In two dimensions, localized stationary axisymmetric solutions of the Swift–Hohenberg equation were studied by Lloyd and Sandstede in [52], in which the existence of radial

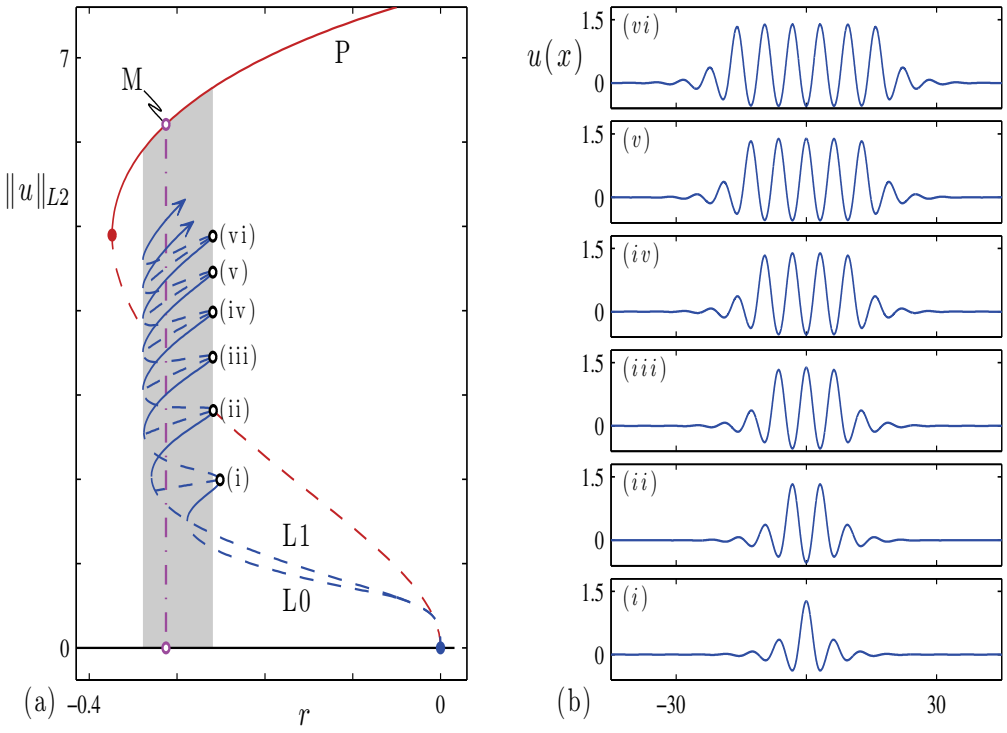

Figure 1.4: Bifurcation diagram of the Swift–Hohenberg equation with the N_{23} nonlinearity from [11] at $b = 1.8$. The shaded region is where snaking occurs. L_0 and L_1 indicate the two snaking branches. P is the periodic spatial pattern curve, which includes the Maxwell point M. The right panel (b) gives several localized solutions along the two snaking branches. Solid line presents stable branches, and dashed line presents unstable branches.

pulse, was demonstrated analytically near the pattern-forming instability of the trivial state. Their numerical investigation found snaking diagrams in the subcritical region, with localized radial structures of rings and spots.

However, in our research we study localized states in a non-variational PDE problem that we present in the next section.

1.4 The PDE model

The aim of this study is to investigate localized solutions in a PDE with parametric forcing, introduced by Rucklidge and Silber in [70] as a generic model of parametrically

forced systems such as the Faraday wave experiment. This model is not the same as the Faraday wave experiment, but it is invented in a way that the linear theory can be reduced to the Mathieu equation as in the Faraday wave experiment. There is no derivation between the PDE model and Faraday wave experiment. The model PDE is given by

$$U_t = (\mu+i\omega)U+(\alpha+i\beta)U_{xx}+(\gamma+i\delta)U_{xxxx}+Q_1U^2+Q_2|U|^2+C|U|^2U+i\Re(U)f(t), \tag{1.12}$$

where $U(x,t)$ is a complex function, $\mu < 0$ is the distance from onset of the oscillatory instability, ω, α, β, γ, and δ are real parameters, and Q_1, Q_2, and C are complex parameters. The forcing function $f(t)$ is a real 2π periodic function in time.

In this model the dispersion relation can be readily controlled, and the nonlinear terms are chosen to be simple in order that the weakly nonlinear theory and numerical solutions can be computed easily. The model shares some important features with the Faraday wave experiment but does not have a clear physical interpretation. The forcing term is chosen to be $iF\cos(2t)\Re(U)$ in order to result the Mathieu equation. The frequency and the growth rate depend on wavenumber. It has quadratic nonlinear terms, so it allows three-wave interactions. Additionally, the PDE model has a Hamiltonian limit, as does the fluid problem with low viscosity. The linearized problem reduces to the damped Mathieu equation in the same way that hydrodynamic models of the Faraday instability reduce to this equation in the inviscid limit [7] when viscusity is zero and the depth is infinety.

The model was introduced in order to understand how quasipatterns are stabilized in the Faraday wave experiment. Here, we use the same model (with different choices of parameters) to interpret the oscillons that are found in the Faraday wave experiment.

1.5 Structure of the thesis

This thesis contains five chapters, including this chapter. We begin our investigations in Chapter 2 by considering the case where the wavenumber k is zero at onset. We

start our analysis by this case because we know that localized states can be found. Analytically, in the weak forcing, weak damping, weak detuning and small amplitude limit, we do a reduction of the model PDE (1.12) to its amplitude equation, the forced complex Ginzburg–Landau equation (1.1). Furthermore, we reduce the forced complex Ginzburg–Landau equation to the Allen–Cahn equation near onset, which has exact sech localized solutions. We also extend this analysis to the strong forcing case recovering the Allen–Cahn equation directly from the model PDE without the intermediate step. We find excellent agreement between numerical localized solutions of the model PDE, localized solutions of the forced complex Ginzburg–Landau equation, and localized solutions of the Allen–Cahn equation. This is the first time that a PDE with time dependent forcing has been reduced to the Allen–Cahn equation, and its localized oscillatory solutions quantitatively studied. In this chapter the preferred wavenumber is zero, so results are directly relevant to localized patterns found in Turing systems.

In Chapter 3 we investigate the existence of localized oscillons with non-zero preferred wavenumber. This chapter includes work that is more relevant to the Faraday wave experiment, where the preferred wavenumber at onset is non-zero. The PDE model (1.12) is reduced to the coupled forced complex Ginzburg–Landau equations (1.2) in the limit of weak damping, weak detuning, weak forcing, small group velocity, and small amplitude. We find localized structures in the coupled forced complex Ginzburg–Landau equations numerically for the first time. Near onset, we reduce the coupled forced complex Ginzburg–Landau equations (1.2) asymptotically to the real Ginzburg–Landau equation, which also has exact sech localized solutions. We compare quantitatively the localized solutions from the real Ginzburg–Landau equation with oscillons that we find numerically in the PDE model.

In Chapter 4, we find examples of localized oscillons in the PDE model with cubic–quintic nonlinearity in the strong damping, strong forcing and large amplitude case. Numerical results we present in this chapter were found by time-stepping. In one spatial dimension, we find evidence for two snaking localization curves. In two dimensions, we

give examples of axisymmetric and non-axisymmetric oscillons.

We conclude and discuss future work in Chapter 5.

Chapter 2

Localized patterns with zero wavenumber

2.1 Introduction

The complex Ginzburg–Landau (CGL) equation is the normal form description of pattern forming systems close to a Hopf bifurcation with preferred wavenumber zero [20]. Adding time dependent forcing to the original problem results in a forcing term in the CGL equation, the form of which depends on the ratio between the Hopf and driving frequencies. When the Hopf frequency is half the driving frequency (the usual subharmonic parametric resonance), the resulting PDE is known as the forced complex Ginzburg–Landau (FCGL) equation [15]:

$$A_T = (\tilde{\mu} + i\nu)A + (1 + i\kappa)A_{XX} - (1 + i\rho)|A|^2 A + \Gamma\bar{A}, \tag{2.1}$$

where all parameters are real, and $\tilde{\mu}$ is the distance from the onset of the oscillatory instability, ν is the detuning between the Hopf frequency and the driving frequency, κ represents the dispersion, ρ is the nonlinear frequency correction, and Γ is the forcing amplitude. The complex amplitude, $A(X, T)$, represents the oscillation in a continuous system near a Hopf bifurcation point in one spatial dimension. In the absence of forcing,

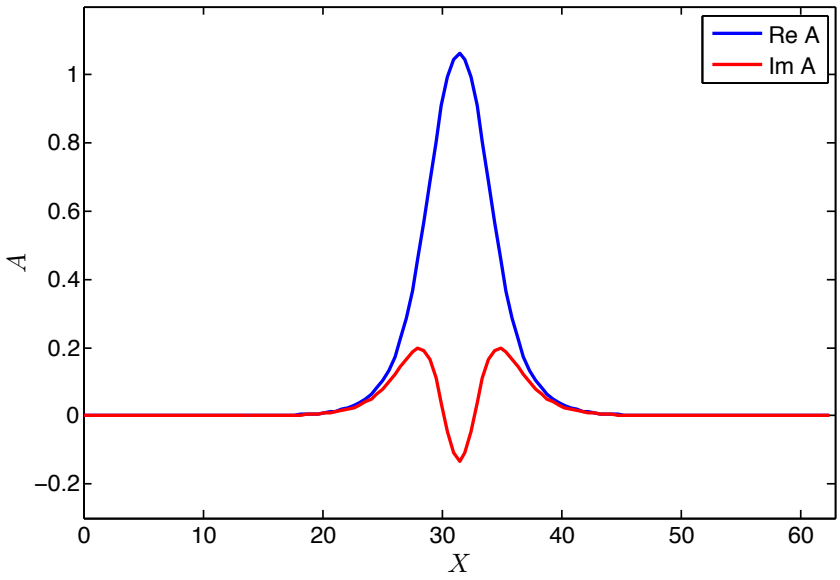

Figure 2.1: Localized solutions of the FCGL equation (2.1) with $\tilde{\mu} = -0.5$, $\rho = 2.5$, $\nu = 2$, $\kappa = -2$, and $\Gamma = 1.496$; the bifurcation point is at $\Gamma_0 = 2.06$, following [15].

the state $A = 0$ is stable, so $\tilde{\mu} < 0$. The amplitude of the response is $|A|$, and $\arg(A)$ represents the phase difference between the response and the forcing.

The FCGL equation is a valid description of the full system in the limit of weak forcing, weak damping, small amplitude oscillations and near resonance [21, 31]. This model is known to produce localized solutions in 1D [15] and in 2D [61]. It should be noted that these localized solutions have large spatial extent (in the limits mentioned above) and so are different from the oscillons observed in fluid and granular experiments. In spite of the cubic coefficient in (2.1) having negative real part, the initial bifurcation at $\Gamma = \Gamma_0$ is subcritical, the unstable branch turns around in a saddle-node bifurcation, and so there is a non-zero stable solution (the flat state) close to Γ_0. The localized solution is a homoclinic connection from the zero state back to itself (Figure 2.1). Further from Γ_0, there are fronts (heteroclinic connections) between the zero and the flat state and back.

In this chapter we simplify the PDE (1.12) by removing quadratic terms, by taking the parametric forcing to be $\cos(2t)$, where t is the fast time scale, by working in one rather than two spatial dimensions, and by removing fourth-order spatial derivatives. The

resulting model PDE is:

$$U_t = (\mu + i\omega)U + (\alpha + i\beta)U_{xx} + C|U|^2U + i\Re(U)F\cos(2t), \tag{2.2}$$

where the forcing amplitude F is real, and C is a complex parameter.

We first seek oscillon solutions of (2.2) by choosing parameter values where (2.2) can be reduced to the FCGL equation (2.1). In particular, the preferred wavenumber will be zero, and we will take F to be small, $\mu < 0$ to be small, and ω will be close to 1. We will also consider strong forcing and damping below. In the Faraday wave experiment the $k = 0$ mode is neutral and cannot be excited, which means experimental oscillons can only be seen with non-zero wavenumbers. This indicates a qualitative difference between this choice of parameters for the PDE model and the Faraday wave experiment.

Here we study equation (2.2) in two ways. First, in Section 2.2 we reduce the model PDE asymptotically to an amplitude equation of the form of the FCGL equation (2.1) by introducing a multiple scales expansion. The numerically computed localized solutions of the FCGL equation (e.g., Figure 2.1) will then be a guide to finding localized solutions in the model PDE. Second, we solve the model PDE itself numerically using Fourier spectral methods and Exponential Time Differencing (ETD2) [23]. We are able to continue the localized solutions using AUTO [6], and we make quantitative comparisons between localized solutions of the model PDE and the FCGL equation. In Sections 2.3 and 2.5 we will do reductions of the FCGL equation and the PDE to the Allen–Cahn equation [1, 34] in the weak and strong damping cases respectively; the Allen–Cahn equation has exact localized sech solutions. We give numerical results in Section 2.4 and we conclude in Section 2.6. The results of this chapter appear in [2].

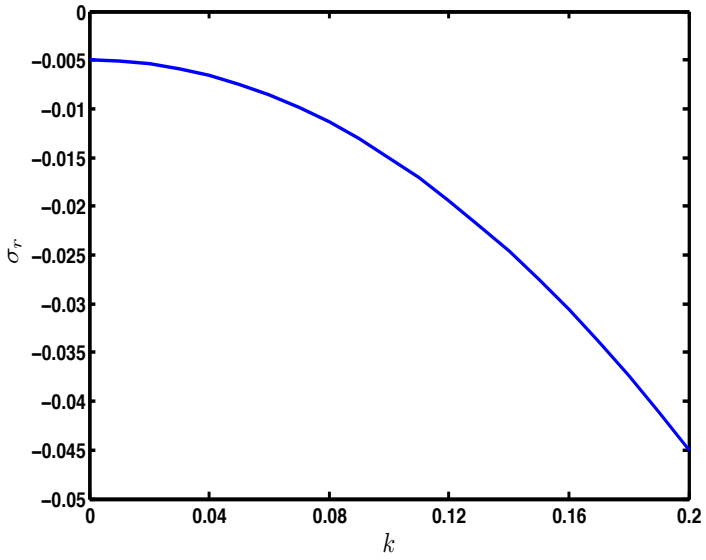

Figure 2.2: The growth rate of equation (2.2) with $\mu = -0.005$ and $\alpha = 1$.

2.2 Derivation of the amplitude equation: weak damping case

In this section we will take the weak forcing, weak damping, weak detuning and small amplitude limit of the model PDE (2.2), and derive the FCGL equation (2.1). Before taking any limits and in the absence of forcing, let us start by linearizing (2.2) about $U = 0$, and consider solutions of the form $U(x,t) = e^{\sigma t + ikx}$, where σ is the complex growth rate of a mode with wave number k. The growth rate σ is given by

$$\sigma = \mu - \alpha k^2 + i(\omega - \beta k^2), \tag{2.3}$$

where $\sigma = \sigma_r + i\sigma_i$. Figure 2.2 presents the real part of the growth rate σ_r. The forcing $F\cos(2t)$ will drive a subharmonic response with frequency 1; by choosing $\alpha > 0$ and ω close to 1, we can arrange that a mode with k close to zero will have the largest growth rate. With weak forcing we also need μ, which is negative, to be close to zero, otherwise

all modes would be damped. In this case, we are close to the Hopf bifurcation that occurs at $\mu = 0$.

We now consider the linear theory of the forced model PDE:

$$U_t = (\mu + i\omega)U + (\alpha + i\beta)U_{xx} + iRe(U)F\cos(2t), \tag{2.4}$$

This can be transformed to a Mathieu-like equation [70]. The normal expectation would be that $\cos(2t)$ would drive a subharmonic response at frequencies $+1$ and -1. However, because ω is close to 1, the leading behavior of (2.4) is

$$\frac{\partial}{\partial t}U = iU, \qquad \text{or} \qquad \ell_1 U = \left(\frac{\partial}{\partial t} - i\right)U = 0.$$

The component of U at frequency -1 cancels at leading order, while the component at frequency $+1$ dominates. Furthermore, since $\omega = 1 + \nu$ with ν small, and since the strongest response is at or close to wavenumber k where $\omega - \beta k^2 = 1$, modes with wavenumber $k = 0$ will be preferred. Therefore, the leading solution is proportional to e^{it}, and so we will seek solutions of the form $U(x,t) = Ae^{it}$, where A is a complex constant. The argument of A relates to the phase difference between the driving force and the response, and is not arbitrary. Later, we will allow A to depend on space and time.

A necessary condition for the existence of localized states is that the trivial states have at least one spatial eigenvalue with positive real part and one with negative real part. Thus, in Figure 2.3 we show the motion of the eigenvalues in the complex plane as F varies. Figure 2.3 (a) shows the spatial eigenvalue structures of the trivial state that is determined by linearizing the PDE model (2.2). When $F < F_0$ there are four eigenvalues, two there are approching zero as well as 12 others. As F continues to increase one of the pairs of eigenvalues moves towards the origin and collides at zero when $F = F_0$. The uniform flat state $A^{\pm}_{uni}$ bifurcates from the $A = 0$ state at $F = F_0$, so that this collision corresponds to the bifurcation. When $F > F_0$ the zero eigenvalues spilt along the imaginary axis.

Therefore, spatially localized states may exist everywhere in $F < F_0$. Figure 2.3 (b) presents the spatial eigenvalues of the non-trivial flat state. All these eigenvalues were computed using AUTO. In fact, AUTO computes Floquet multipliers in space at each value of F, and the spatial eigenvalues are then $log\left(\frac{\text{Floquet multipliers}}{L_x}\right)$, where L_x is the domain size.

To apply standard weakly nonlinear theory, we need the adjoint linear operator $\ell_1^\dagger$. First we define an inner product between two functions $f(t)$ and $g(t)$ by

$$\left\langle f(t), g(t) \right\rangle = \frac{1}{2\pi}\int_0^{2\pi} \bar{f}(t)g(t)dt, \tag{2.5}$$

where $\bar{f}$ is the complex conjugate of f. With this inner product, the adjoint operator $\ell_1^\dagger$, defined by $\left\langle f, \ell_1 g \right\rangle = \left\langle \ell_1^\dagger f, g \right\rangle$, is given by

$$\ell_1^\dagger = i - \frac{d}{dt}.$$

The adjoint eigenfunction is then $U^\dagger = e^{it}$. We take the inner product of (2.4) with this adjoint eigenfunction:

$$\begin{aligned} 0 &= \left\langle U^\dagger, \ell_1 U \right\rangle + \left\langle U^\dagger, (\mu + i\nu)U + iRe(U)F\cos(2t) \right\rangle \\ &= 0 + \frac{1}{2\pi}\int_0^{2\pi} (\mu + i\nu)Ue^{-it} + \frac{iF}{4}(U + \bar{U})(e^{it} + e^{-3it})dt. \end{aligned}$$

We write $U = \sum_{j=-\infty}^{+\infty} U_j e^{ijt}$, and $\bar{U} = \sum_{j=-\infty}^{+\infty} \bar{U}_j e^{-ijt}$, so

$$\begin{aligned} 0 = &\frac{1}{2\pi}\int_0^{2\pi} (\mu + i\nu)\sum_{j=-\infty}^{+\infty} U_j e^{i(j-1)t} \\ &+ \frac{iF}{4}\left(\sum_{j=-\infty}^{+\infty} U_j e^{i(j+1)t} + U_j e^{i(j-3)t} + \bar{U}_j e^{i(-j+1)t} + \bar{U}_j e^{i(-j-3)t}\right)dt \\ = &(\mu + i\nu)U_1 + \frac{iF}{4}\left(U_{-1} + U_3 + \bar{U}_1 + \bar{U}_{-3}\right). \end{aligned}$$

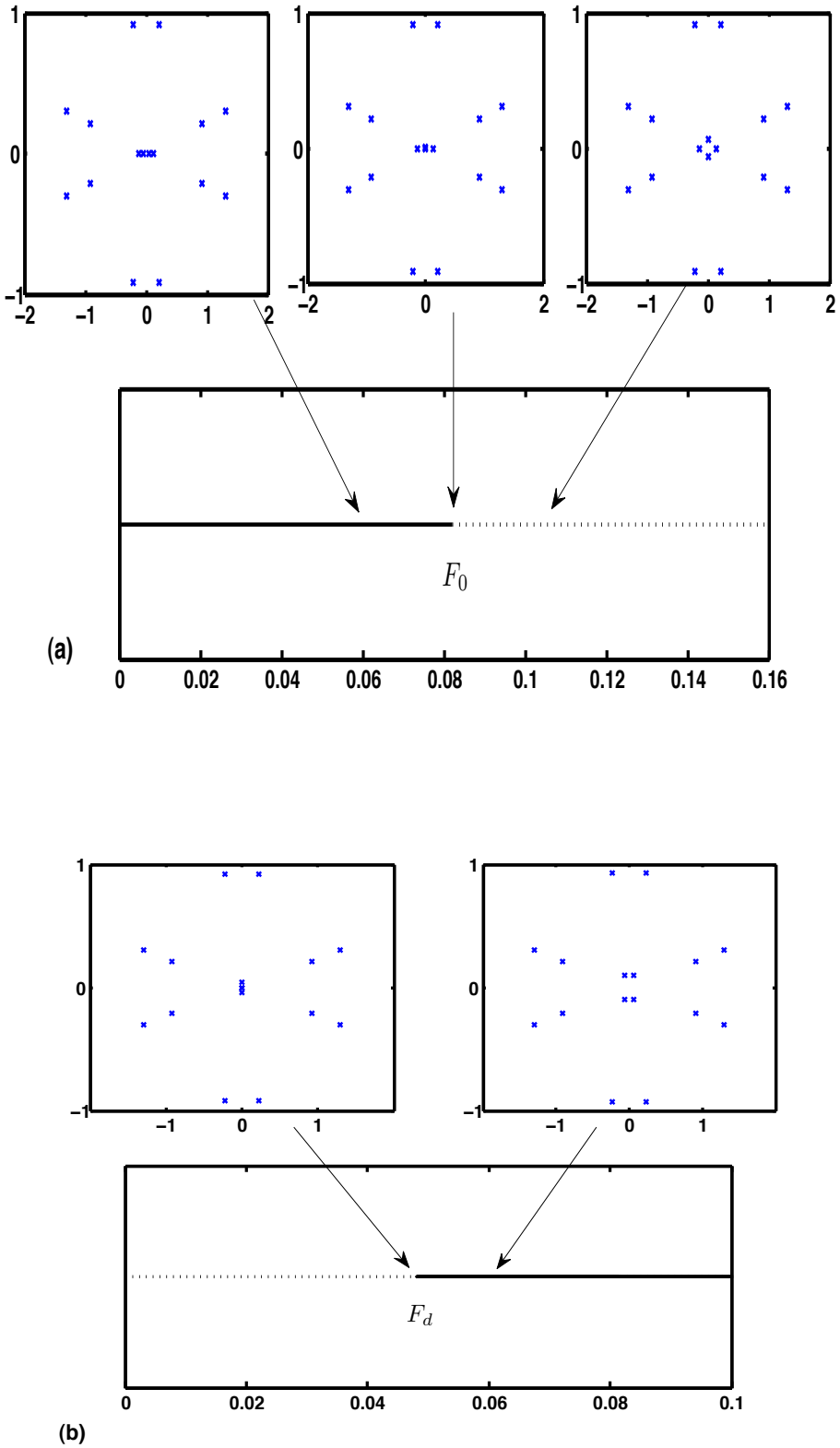

Figure 2.3: Temporal stability of (a) the zero and (b) the non-zero flat solutions as a function of the forcing amplitude F. Solid (dotted) lines represent stable (unstable) solutions in time. The insets represent the spatial eigenvalues in the complex plane, which do not govern temporal stability.

Since the frequency $+1$ component of U dominates at onset, as discussed above, we retain only U_1 and $\bar{U}_1$, which satisfy

$$\begin{bmatrix} \mu + i\nu & \frac{iF}{4} \\ -\frac{iF}{4} & \mu - i\nu \end{bmatrix} \begin{bmatrix} U_1 \\ \bar{U}_1 \end{bmatrix} = \begin{bmatrix} 0 \\ 0 \end{bmatrix}$$

This system has a non-zero solution when its determinant is zero; this gives the critical forcing amplitude $F_0 = 4\sqrt{\mu^2 + \nu^2}$. This equation also fixes the phase of U_1.

To perform the weakly nonlinear calculation, we introduce a small parameter ϵ and make the substitutions: $\omega = 1 + \epsilon^2\nu$, $F \longrightarrow \epsilon^2 F$, $\mu \longrightarrow \epsilon^2\mu$, and expand the solution U in powers of ϵ as

$$U = \epsilon U_1 + \epsilon^2 U_2 + \epsilon^3 U_3 + ..., \tag{2.6}$$

where U_1, U_2, U_3, ... are $O(1)$ complex functions.
At $O(\epsilon)$, we get $\ell_1 U_1 = (\frac{\partial}{\partial t} - i)U_1 = 0$, which has solutions of the form

$$U_1 = A(X, T)e^{it},$$

where the amplitude A is $O(1)$, and X and T are slow space and time variables: $T = \epsilon^2 t$, and $X = \epsilon x$. At $O(\epsilon^2)$, we have $U_2(x, t) = 0$. At $O(\epsilon^3)$, equation (2.2) is reduced to

$$\ell_1 U_3 + \frac{\partial U_1}{\partial T} = (\mu + i\nu)U_1 + (\alpha + i\beta)\frac{\partial^2 U_1}{\partial X^2} + C|U_1|^2 U_1 + iF\cos(2t)Re(U_1),$$

We take the inner product with $U_1^\dagger$, and use $\left\langle U_1^\dagger, \ell_1 U_3 \right\rangle = 0$ to find the amplitude equation for a long-scale modulation:

$$A_T = (\mu + i\nu)A + (\alpha + i\beta)A_{XX} + C|A|^2 A + \frac{iF}{4}\bar{A}. \tag{2.7}$$

We can do a rescaling of the equation (2.7) in order to bring it to the standard FCGL form by rotating $A \longrightarrow Ae^{i\frac{\pi}{4}}$, which removes the i in front of the $\bar{A}$ term but does not affect

any other term. With this, the amplitude equation of the model PDE reads

$$A_T = (\mu + i\nu)A + (\alpha + i\beta)A_{XX} + C|A|^2A + \Gamma\bar{A}, \tag{2.8}$$

where $\Gamma = \frac{F}{4}$. A similar calculation in two dimensions yields the same equation but with A_{XX} replaced by $A_{XX} + A_{YY}$.

One can see that the amplitude equation (2.8) takes the form of the FCGL equation (2.1). We are now in a position to use the results from [15], where they find localized solutions of (2.1), to look for localized solutions of the model PDE (2.2). The stationary homogeneous solutions of (2.8), which we call the flat states, can easily be computed. These satisfy:

$$0 = (\mu + i\nu)A + C|A|^2A + \Gamma\bar{A}.$$

To solve this steady problem we look for solutions of the form $A = Re^{i\phi}$, where R is real and ϕ is the phase. Dividing by $Re^{i\phi}$ results in:

$$0 = (\mu + i\nu) + CR^2 + \Gamma e^{-2i\phi}. \tag{2.9}$$

We can then separate the real and imaginary parts and eliminate ϕ by using $\sin^2\phi + \cos^2\phi = 1$ to get a fourth order polynomial:

$$(C_r^2 + C_i^2)R^4 + 2(\mu C_r + \nu C_i)R^2 - \Gamma^2 + \mu^2 + \nu^2 = 0, \tag{2.10}$$

where $C = C_r + iC_i$. This can be solved for R^2, from which ϕ can be determined using (2.9).

Examination of the polynomial (2.10) shows that when the forcing amplitude Γ reaches $\Gamma_0 = \sqrt{\mu^2 + \nu^2}$, a subcritical bifurcation occurs provided that $\mu C_r + \nu C_i < 0$. A flat state A^-_{uni} is created, which turns into the A^+_{uni} state at $\Gamma_d = \sqrt{-\frac{(\mu C_r + \nu C_i)^2}{(C_r^2 + C_i^2)} + \mu^2 + \nu^2}$, when a saddle-node bifurcation occurs. We will reduce (2.8) further in Section 2.3 by assuming

we are close to onset, and finding explicit expressions for localized solutions.

2.3 Reduction to the Allen–Cahn equation: weak damping case

The FCGL equation (2.8) can be reduced to the Allen–Cahn equation [15, Appendix A] by setting $\Gamma = \Gamma_0 + \epsilon_1^2\lambda$, where $\Gamma_0 = \sqrt{\mu^2+\nu^2}$ is the critical forcing amplitude, λ is the bifurcation parameter, and ϵ_1 is a new small parameter that controls the distance to onset. We expand A in powers of ϵ_1 as

$$A(X,T) = \epsilon_1 A_1(X,T) + \epsilon_1^2 A_2(X,T) + \epsilon_1^3 A_3(X,T) + ...,$$

where A_1, A_2, A_3 are $O(1)$ complex functions. We further scale $\frac{\partial}{\partial T}$ to be $O(\epsilon_1^2)$ and $\frac{\partial}{\partial X}$ to be $O(\epsilon_1)$.

At $O(\epsilon_1)$ we get

$$0 = (\mu + i\nu)A_1 + \sqrt{\mu^2+\nu^2}\bar{A}_1,$$

which defines a linear operator

$$\begin{bmatrix} \mu+i\nu & \sqrt{\mu^2+\nu^2} \\ \sqrt{\mu^2+\nu^2} & \mu-i\nu \end{bmatrix} \begin{bmatrix} A_1 \\ \bar{A}_1 \end{bmatrix} = \begin{bmatrix} 0 \\ 0 \end{bmatrix}$$

The solution is $A_1 = B(X,T)e^{i\phi_1}$, where B is real, and the phase ϕ_1 is fixed by $e^{-2i\phi_1} = -\frac{\mu+i\nu}{\sqrt{\mu^2+\nu^2}}$. This gives

$$\phi_1 = \tan^{-1}\left(\frac{\mu+\sqrt{\mu^2-\nu^2}}{\nu}\right),$$

At $O(\epsilon_1^3)$, we have

$$B_T e^{i\phi_1} = (\mu+i\nu)A_3 + (\alpha+i\beta)B_{XX}e^{i\phi_1} + CB^3e^{i\phi_1} + \lambda Be^{-i\phi_1} + \Gamma_0\bar{A}_3. \qquad (2.11)$$

We take the complex conjugate of (2.11) and multiply this by $e^{-i\phi_1}$, and then add (2.11) multiplied by $e^{i\phi_1}$ to eliminate A_3. With this, equation (2.8) reduces to the Allen–Cahn equation

$$B_T = \frac{-\lambda\sqrt{\mu^2+\nu^2}}{\mu}B + \frac{(\alpha\mu+\beta\nu)}{\mu}B_{XX} + \frac{\mu C_r + \nu C_i}{\mu}B^3. \tag{2.12}$$

We can readily find localized solutions of (2.12) in terms of hyperbolic functions. This leads to an approximate oscillon solution of (2.8) of the form

$$A = \sqrt{\frac{2(\Gamma-\Gamma_0)\sqrt{\mu^2+\nu^2}}{\mu C_r+\nu C_i}}\operatorname{sech}\left(\sqrt{\frac{(\Gamma-\Gamma_0)\sqrt{\mu^2+\nu^2}}{(\alpha\mu+\beta\nu)}}X\right)e^{i\phi_1}, \tag{2.13}$$

provided $\Gamma < \Gamma_0$, $\mu < 0$, $\mu C_r + \nu C_i < 0$, and $\alpha\mu + \beta\nu < 0$. Note that in the PDE (2.2) we have the assumption $U_1 = \epsilon A e^{it}$, therefore the spatially localized oscillon is given approximately by

$$U_{loc} = \sqrt{\frac{(F-F_0)\sqrt{\mu^2+\nu^2}}{2(\mu C_r+\nu C_i)}}\operatorname{sech}\left(\sqrt{\frac{(F-F_0)\sqrt{\mu^2+\nu^2}}{4(\alpha\mu+\beta\nu)}}x\right)e^{i(t+\phi_1)}, \tag{2.14}$$

again provided $F < F_0$. We compare the approximate solution U_{loc} with a numerical solution of the PDE below, as a dotted line in Figure 2.9(a).

2.4 Numerical results: weak damping case

In this section, we present numerical solutions of (2.1) (in the form written in (2.8)) and (2.2), using the known [15] localized solutions of (2.1) to help find similar solutions of (2.2), and comparing the bifurcation diagrams of the two cases.

We use both time-stepping methods and continuation on both PDEs. For time-stepping, we use a pseudospectral method, using FFTs with up to 1280 Fourier modes, and the exponential time differencing method ETD2 [23], which has the advantage of solving the non-time dependent linear parts of the PDEs exactly. We treat the forcing term ($\Gamma\bar{A}$ and

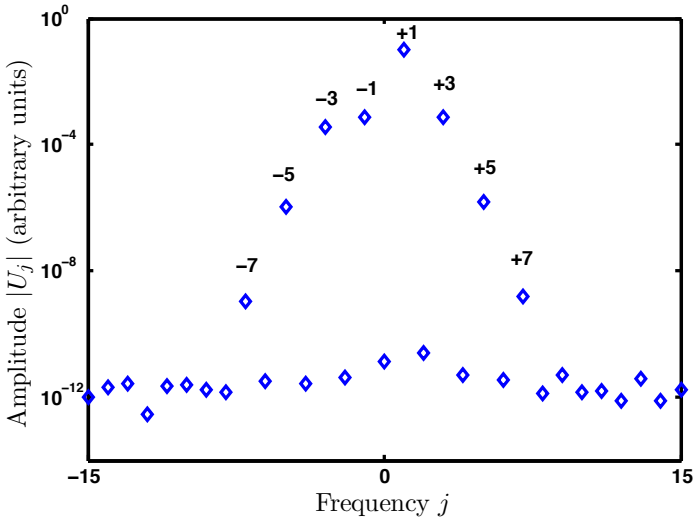

Figure 2.4: The truncated Fourier series in time of a localized solution of the PDE (2.2), showing that e^{it}, with frequency $+1$, is the most important mode, that frequencies -3, -1, and $+3$ have similar importance, and that higher frequency modes have amplitudes at least a factor of 100 smaller. The parameter values are $\mu = -0.005$, $\alpha = 1$, $\beta = -2$, $\nu = 2$, $F = 0.0579$, and $C = -1 - 2.5i$.

$Re(U)\cos(2t)$) with the nonlinear terms.

For continuation, we use AUTO [6] (see Appendix A), treating x as the time-like independent variable, to find steady solutions of the FCGL (2.8). For the PDE (2.2), we represent solutions with a truncated Fourier series in time with the frequencies -3, -1, 1 and 3 (see Figure 2.4). The choice of these frequencies comes from the forcing $Re(e^{it})\cos(2t)$ in the PDE, taking $U = e^{it}$ as the basic solution, as described above.

Following [15] we will take illustrative parameter values for the amplitude equation (2.8): $\mu = -0.5$, $\alpha = 1$, $\beta = -2$, and $C = -1 - 2.5i$, and solve the equation on domains of size $L_X = 20\pi$. For (2.2), we use $\epsilon = 0.1$, which implies $\mu = -0.005$, $F = 0.04\Gamma$, $\omega = 1.02$, $L_x = 200\pi$, and use the same α, β, and C. We show examples of localized solutions in the FCGL equation and the PDE (2.2) in Figure 2.5, demonstrating the

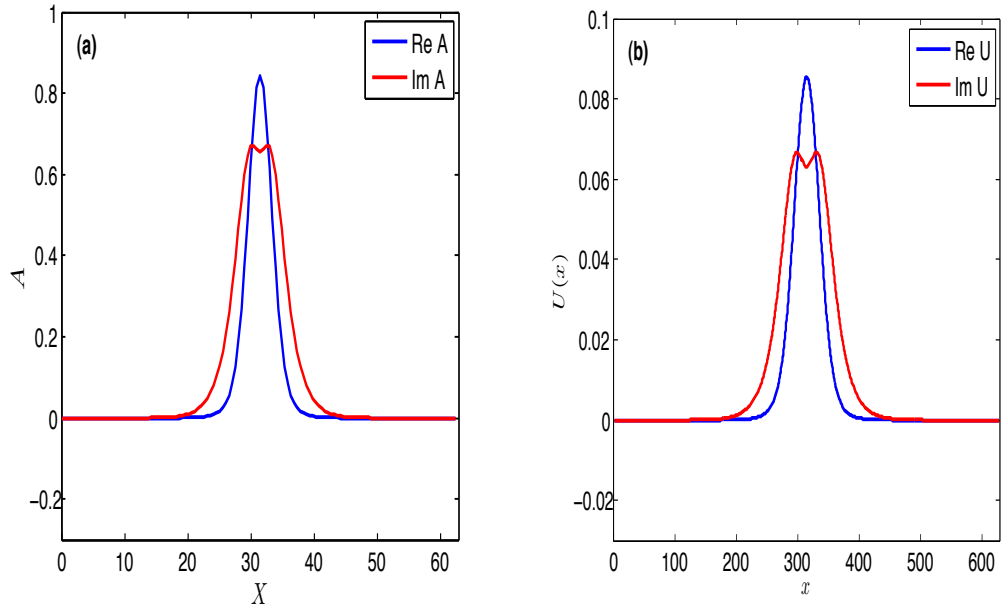

Figure 2.5: (a) Example of a localized solution to the FCGL equation (2.7) with $\mu = -0.5$, and $F = 5.984$. (b) Example of a localized solution to the PDE model (2.2) with $\mu = -0.5\epsilon^2$, and $F = 5.984\epsilon^2$, where $\epsilon = 0.1$. In both models $\alpha = 1$, $\beta = -2$, and $\nu = 2$, and $C = -1 - 2.5i$. Note the factor of ϵ in the scalings of the two axes.

quantitative agreement as expected between the two.

In all bifurcation diagrams we present solutions in terms of their norms

$$N = \sqrt{\frac{2}{L_x}\int_0^{L_x} |U|^2\, dx},$$

We computed (following [15]) the location of these stable localized solutions in the (ν,Γ) parameter plane, shown in green in Figure 2.6. In this figure one can see that the region of localized solutions starts where $\mu C_r + \nu C_i = 0$, when the primary bifurcation changes from supercritical to subcritical [29, 45], and gets wider as ν increases. We also show the bistability region of the amplitude equation between the primary (Γ_0) and the saddle-node (Γ_d) bifurcations.

Part of the difficulty of computing localized solutions in the PDE comes from finding

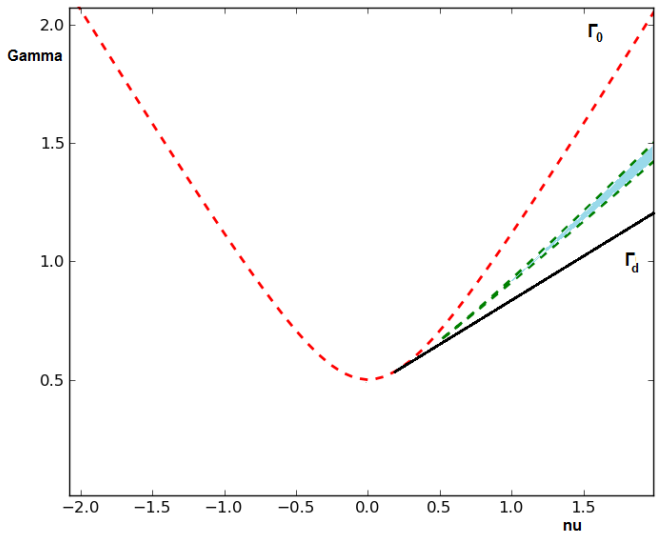

Figure 2.6: The (ν, Γ)-parameter plane for FCGL equation (2.8), $\mu = -0.5$, $\alpha = 1$, $\beta = -2$, and $C = -1 - 2.5i$, recomputed following [15]. Stable localized solutions exist in the shaded green region. The dashed red line is the primary pitchfork bifurcation at $\Gamma_0 = \sqrt{\mu^2 + \nu^2}$, and the solid black line is the saddle-node bifurcation at Γ_d.

parameter values where these are stable. In the FCGL equation with $\nu = 2$, stable localized solutions occur between $\Gamma_1^* = 1.4272$ and $\Gamma_2^* = 1.5069$. In the PDE with parameter values as above, we therefore estimate that the stable localized solutions should exist between $F_1^* = 0.04\Gamma_1^* = 0.0573$ and $F_2^* = 0.0600$. We found by time-stepping a stable oscillatory spatially localized solution in the PDE model (2.2) at $F = 0.058$ and used this as a starting point for continuation with AUTO. We found stable localized solutions between saddle-node bifurcations, at $F_1^* = 0.05688$ and $F_2^* = 0.06001$, which compares well with the prediction from the FCGL equation. In addition, the bistability region was determined by time-stepping to be between $F_d = 0.04817$ and $F_0 = 0.08165$. As ν is varied, the grey shaded region in Figure 2.7 shows the region where stable localized solutions exist in the PDE.

As the branch of localized solutions is continued the central flat part gets wider as the parameter Γ snakes back and forth (see Figure 2.8 and 2.9). This was first described as

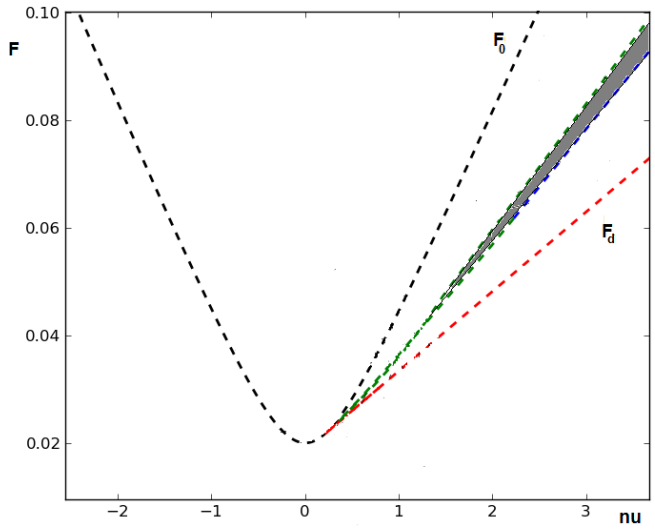

Figure 2.7: The (ν, F)-parameter plane of the PDE model (2.2) with $\mu = -0.005$, $\alpha = 1$, $\beta = -2$, and $C = -1 - 2.5i$. Stable localized solutions exist in the shaded grey region. The dashed black line is the primary pitchfork bifurcation and the dashed red line is the saddle-node bifurcation at F_d.

homoclinic snaking by [44], and later described as collapsed snaking [58]. Figure 2.8 presents the snaking regions of the PDE model and the FCGL equation. In this figure we rescale the PDE, so we can plot the bifurcation diagrams of the amplitude equation and the PDE model in top of each other. The agreement is excellent. Examples of localized solutions are given in Figure 2.9 (a)-(f) as we go along the localization curve. Our comparison between results from the FCGL equation (2.8) in Figure 2.6 and results from the model PDE (2.2) in Figure 2.7 shows excellent agreement.

Note the decaying spatial oscillations close to the flat state in Figure 2.9 (c)-(f): it is these that provide the pinning necessary to have parameter intervals of localized solutions. These parameter intervals become narrower as the localized flat state becomes wider (see Figure 2.8) since the oscillations decay in space, in contrast with the localized solutions found in the subcritical Swift–Hohenberg equation [13]. Figure 2.10 shows an example of an oscillon in space and time for a period of 2π.

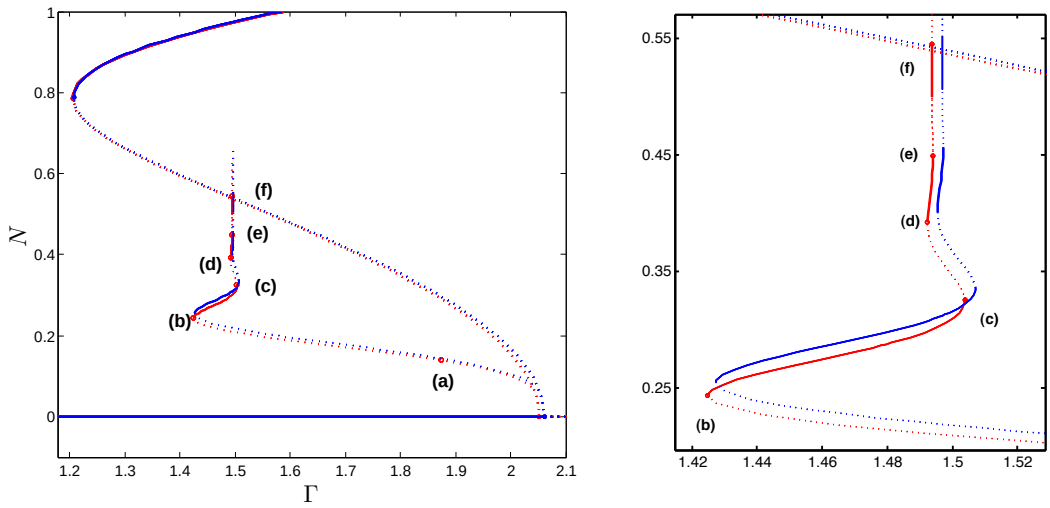

Figure 2.8: The red curves correspond to bifurcation diagram of the PDE model and the blue curves correspond to the FCGL equation. Solid (dashed) lines correspond to stable (unstable) solutions. For the PDE we use $F = 4\epsilon^2\Gamma$. Parameters are otherwise as in Figure 2.5. Example solutions at the points labeled (a)-(f) are in Figure 2.9. Bifurcation point in the FCGL is $\Gamma_0 = 2.06$, and in the PDE is $\Gamma_0 = 2.05$.

In this study so far our calculations have been based on assuming weak damping and weak forcing. Next, we study the PDE in the strong forcing case.

2.5 Reduction of the PDE to the Allen–Cahn equation: strong damping case

In the strong damping, strong forcing case, the linear part of the PDE is not solved approximately by $U_1 = e^{it}$. Rather, a Mathieu equation must be solved numerically to get the eigenfunction [70]. In this case, weakly nonlinear calculations lead to the Allen–Cahn equation directly, without the intermediate step of the FCGL equation (2.1) with its $\Gamma\bar{A}$ forcing. The advantages of reducing the PDE to the Allen–Cahn equation are that localized solutions in this equation are known analytically, and that demonstrates directly the existence of localized solutions in the PDE model.

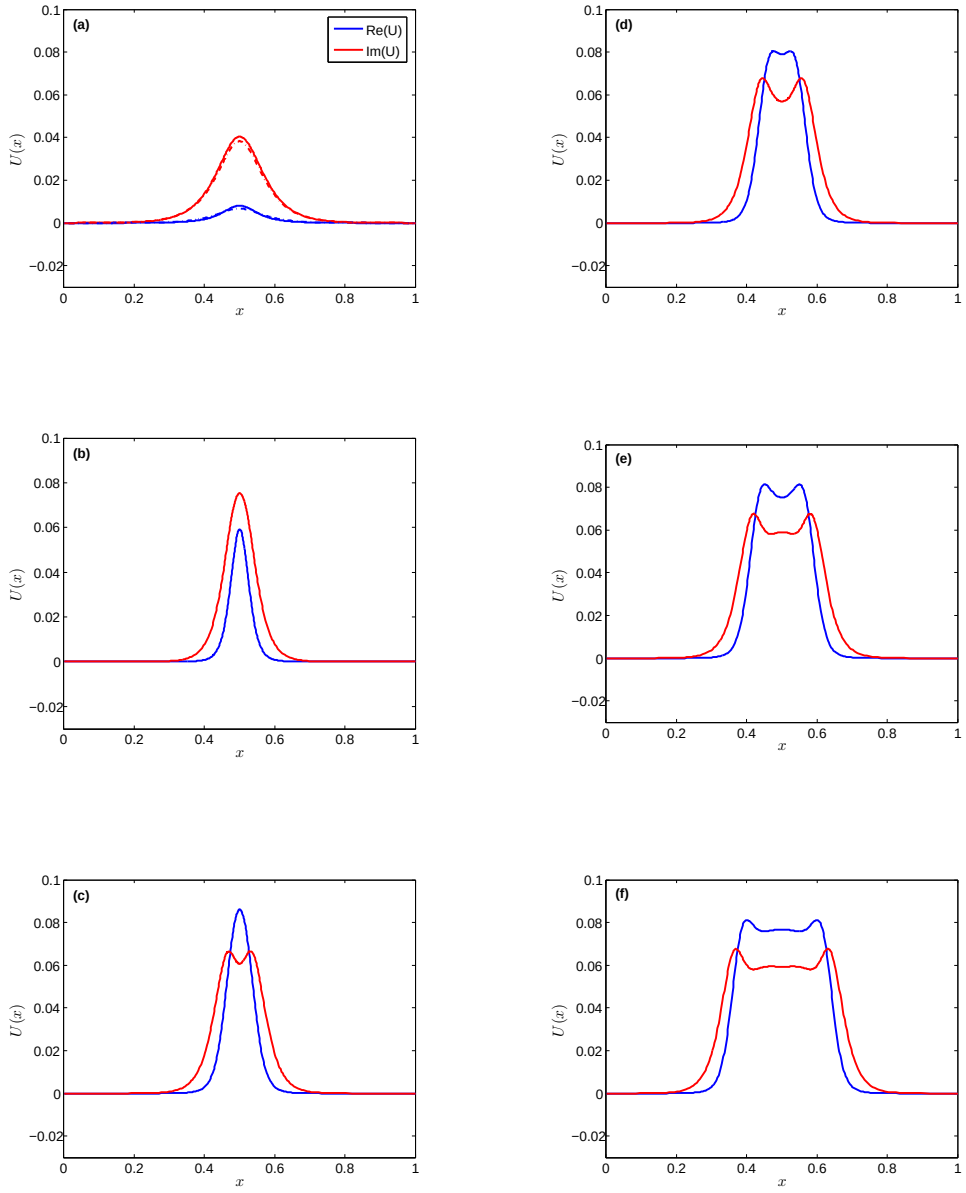

Figure 2.9: Examples of solutions to (2.2) equation at $t = 0$ along the localized branch with $\mu = -0.005$, $\alpha = 1$, $\beta = -2$, $\nu = 2$, and $C = -1 - 2.5i$. Bistability region is between $F_0 = 0.08165$ and $F_d = 0.048173$, and localized oscillons branch is between ${F_1}^* = 0.05688$ and ${F_2}^* = 0.06001$. (a) $F = 0.07499$. (b) $F = 0.05699$. (c)$F = 0.06015$. (d) $F = 0.05961$. (e) $F = 0.05976$. (f) $F = 0.05975$. Dot lines represent the real (blue) and imaginary (red) parts of U_{loc}.

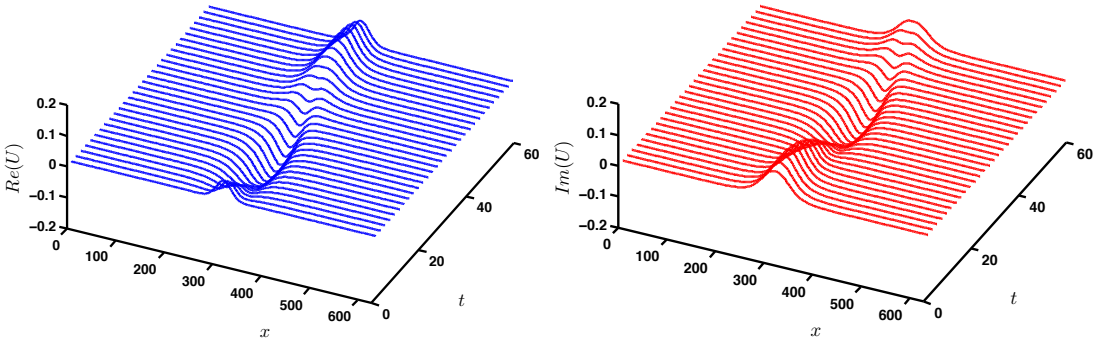

Figure 2.10: Example of oscillon in space and time for one period 2π with $\mu = -0.005$, $\alpha = 1$, $\beta = -2$, $\nu = 2$, $F = 0.0579$, and $C = -1 - 2.5i$.

We write the solution as $U = u + iv$, where $u(x,t)$ and $v(x,t)$ are real functions. Thus, equation (2.2) is written in terms of real and imaginary parts of U as

$$\begin{aligned}\frac{\partial u}{\partial t} &= \left(\mu + \alpha\frac{\partial^2}{\partial x^2}\right)u - \left(\omega + \beta\frac{\partial^2}{\partial x^2}\right)v + C_r(u^2+v^2)u - C_i(u^2+v^2)v,\\ \frac{\partial v}{\partial t} &= \left(\omega + \beta\frac{\partial^2}{\partial x^2}\right)u + \left(\mu + \alpha\frac{\partial^2}{\partial x^2}\right)v + C_r(u^2+v^2)v + C_i(u^2+v^2)u + f(t)u.\end{aligned} \tag{2.15}$$

We begin our analysis by linearizing (2.15) about $u = 0$ and $v = 0$. We write the periodic forcing function as $f(t) = f_c(t)(1 + \epsilon_1^2\lambda)$, where $f_c(t) = F_c\cos(2t)$. Here, F_c is the critical forcing amplitude, which must be determined numerically, and is where the trivial solution loses stability. We seek a critical eigenfunction of the form

$$U = p_1(t) + iq_1(t), \tag{2.16}$$

where $p_1(t)$ and $q_1(t)$ are real 2π-periodic functions. Note that in writing $u + iv$ in this form, we are taking the critical wavenumber to be zero. The analysis follows that presented in [70], but in the current work the spatial scaling and the chosen solution are different, again because the critical wavenumber is zero. Substituting into (2.15) at onset

leads to

$$\begin{aligned}\left[\frac{\partial}{\partial t}-\mu\right]p_1 &= -\omega q_1,\\ \left[\frac{\partial}{\partial t}-\mu\right]q_1 &= \omega p_1 + f_c(t)p_1,\end{aligned} \tag{2.17}$$

which can be combined to give a damped Mathieu equation

$$\left[\frac{d}{dt}-\mu\right]^2 p_1 + \left(\omega^2 + f_c(t)\omega\right)p_1 = 0,$$

or

$$\ddot{p}_1 - 2\mu\dot{p}_1 + \left(\mu^2+\omega^2+f_c(t)\omega\right)p_1 = Lp = 0, \tag{2.18}$$

defining a linear operator

$$L = \frac{\partial^2}{\partial t^2} - 2\mu\frac{\partial}{\partial t} + (\mu^2+\omega^2+\omega f_c(t))$$

The critical forcing function $f_c(t) = F_c\cos(2t)$ is determined by the condition that (2.18) should have a non-zero solution $p_1(t)$, from which $q_1(t)$ is found by solving the top line in (2.17). Using the inner product (2.5), we have the adjoint linear operator, given by

$$L^\dagger = \frac{\partial^2}{\partial t^2} + 2\mu\frac{\partial}{\partial t} + (\mu^2+\omega^2+\omega f_c(t)).$$

The adjoint equation is $L^\dagger p_1^\dagger = 0$, where $p_1^\dagger$ is the adjoint eigenfunction, which is computed numerically. In order to reduce the model PDE (2.2) to the Allen–Cahn equation, we expand solutions in powers of ϵ_1 as

$$\begin{aligned}u &= \epsilon_1 u_1 + \epsilon_1^2 u_2 + \epsilon_1^3 u_3 + ...,\\ v &= \epsilon_1 v_1 + \epsilon_1^2 v_2 + \epsilon_1^3 v_3 + ...,\end{aligned} \tag{2.19}$$

where $\epsilon_1 \ll 1$ and u_1, u_2, u_3, ..., v_1, v_2, v_3, ... are $O(1)$ real functions. We introduce the slow time variable $T = \epsilon_1^2 t$ and the slow space variable $X = \epsilon_1 x$. Substituting equation (2.19) into (2.15), the associated equations at each power of ϵ_1 are as follows. At $O(\epsilon_1)$,

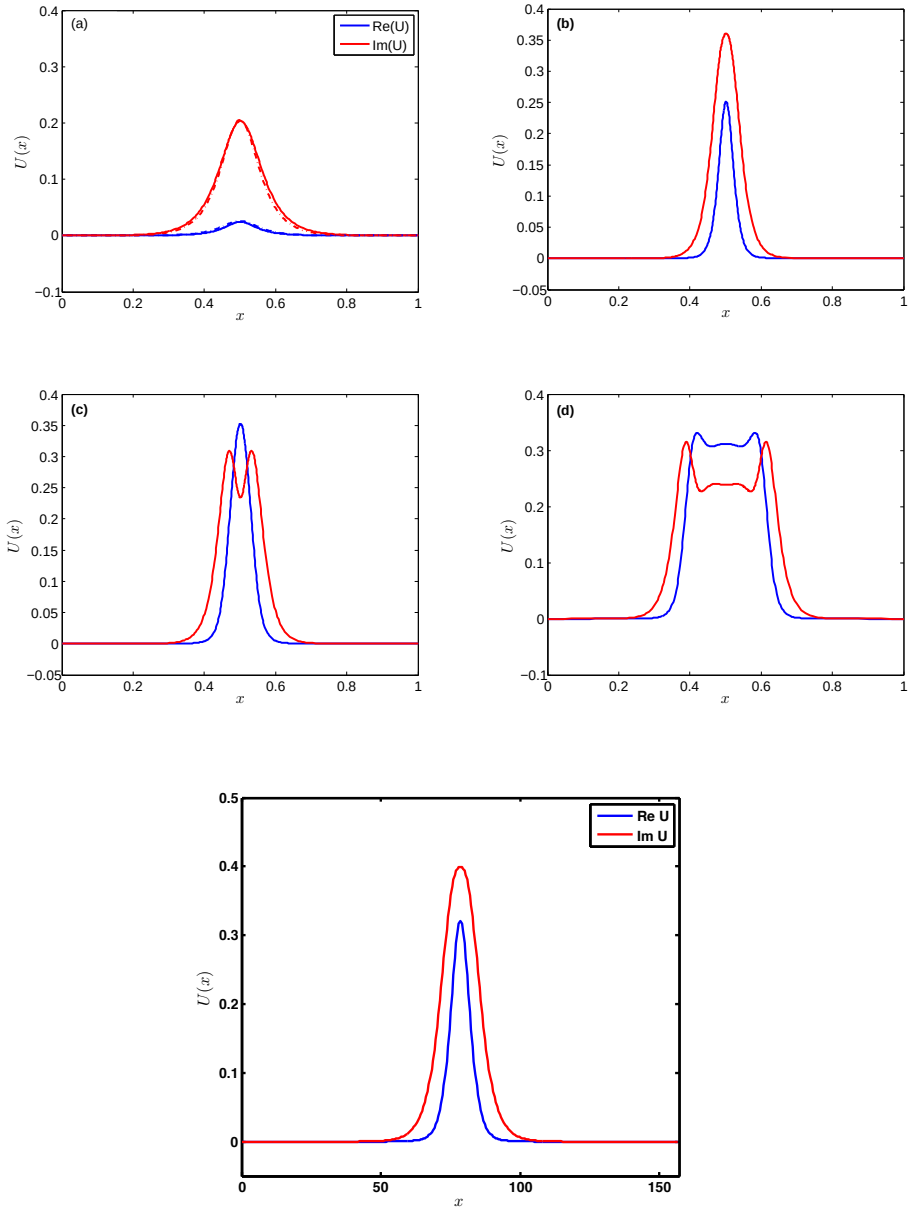

Figure 2.11: Examples of solutions to (2.2) in the strong damping limit with $\epsilon = 0.5$, $F = 2.304$, $\mu = -0.125$, $\alpha = 1$, $\beta = -2$, $\nu = 2$, $\omega = 1 + \nu\epsilon^2$, and $C = -1 - 2.5i$. The bistability region is between $F_0 = 2.3083$ and $F_d = 1.2228$. Dotted lines in (a) represent the real (blue) and imaginary (red) parts of the analytic solution U_{loc}. The last panel is a stable solution obtained by time-stepping the PDE (2.2) at $F = 1.5$, between (b) and (c).

the linear argument above arises, and we have $u_1 + iv_1 = B(X,T)(p_1 + iq_1)$, where $p_1 + iq_1$ is the critical eigenfunction, normalized so that $\langle p_1 + iq_1, p_1 + iq_1 \rangle = 1$, and B is a real function of X and T. Note that the phase of the response is determined by the critical eigenfunction. At $O(\epsilon_1^2)$, the linear problem arises, so there is no interesting terms appear at this order of ϵ_1. At $O(\epsilon_1^3)$, the problem is written as

$$\begin{aligned}
\left(\frac{\partial}{\partial t} - \mu\right) u_3 + \frac{\partial u_1}{\partial T} &= -\omega v_3 + \alpha \frac{\partial^2 u_1}{\partial X^2} - \beta \frac{\partial^2 v_1}{\partial X^2} + C_r(u_1^2 + v_1^2)u_1 - C_i(u_1^2 + v_1^2)v_1, \\
\left(\frac{\partial}{\partial t} - \mu\right) v_3 + \frac{\partial v_1}{\partial T} &= \omega u_3 + f_c(t)u_3 + \lambda f_c(t)u_1 + \alpha \frac{\partial^2 v_1}{\partial X^2} + \beta \frac{\partial^2 u_1}{\partial X^2} + C_r(u_1^2 + v_1^2)v_1 \\
&\quad + C_i(u_1^2 + v_1^2)u_1.
\end{aligned}$$

Eliminating v_3, we find

$$\begin{aligned}
Lu_3 = &- \left(\frac{\partial}{\partial t} - \mu\right) \frac{\partial u_1}{\partial T} + \omega \frac{\partial v_1}{\partial T} \\
&+ \left(\frac{\partial}{\partial t} - \mu\right) \left(\alpha \frac{\partial^2 u_1}{\partial X^2} - \beta \frac{\partial^2 v_1}{\partial X^2}\right) \\
&- \omega \left(\alpha \frac{\partial^2 v_1}{\partial X^2} + \beta \frac{\partial^2 u_1}{\partial X^2}\right) - \omega \lambda f_c(t) u_1 \\
&- \omega \left(C_r \left(u_1^2 + v_1^2\right) v_1 + C_i \left(u_1^2 + v_1^2\right) u_1\right) \\
&+ \left(\frac{\partial}{\partial t} - \mu\right) \left(C_r \left(u_1^2 + v_1^2\right) u_1 - C_i \left(u_1^2 + v_1^2\right) v_1\right).
\end{aligned} \tag{2.20}$$

We apply the solvability condition to equation (2.20) $\langle p_1^\dagger, Lu_3 \rangle = 0$. We substitute the solution $u_1 = Bp_1$, and $v_1 = Bq_1$ into equation (2.20), and then we take the inner product between $p_1^\dagger$ and this equation. Note that we use $\left(\frac{\partial}{\partial t} - \mu\right) p_1 = -\omega q_1$, so the equation can

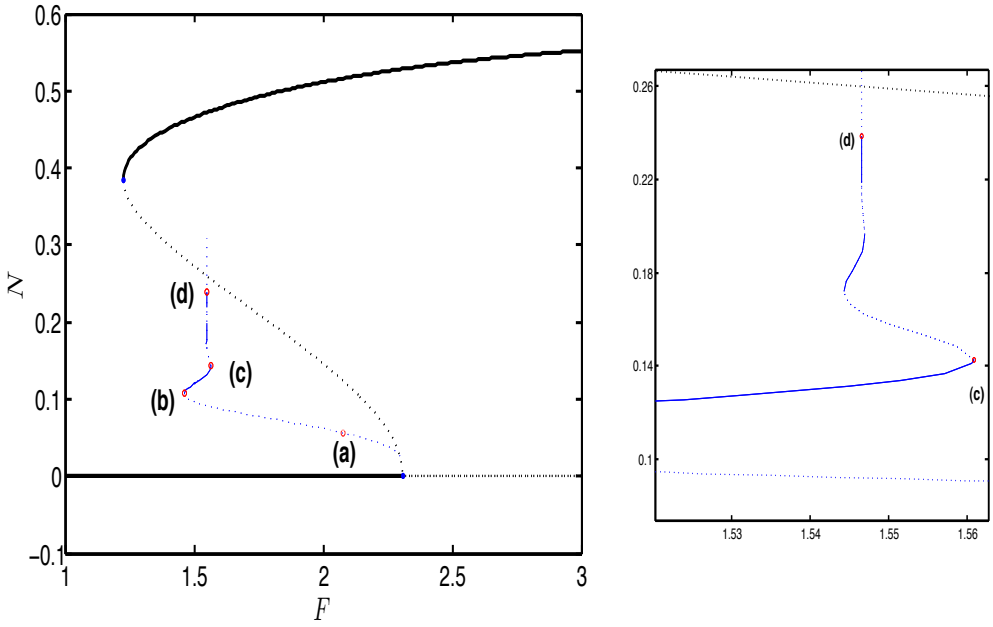

Figure 2.12: Bifurcation diagram of the PDE with strong forcing and strong damping black lines represent the zero and flat states, and blue lines represent oscillons. The parameters as in Figure 2.11. Example solution at the points labelled (a)-(d) are in Figure 2.11.

be then written as

$$\begin{aligned}\left\langle p_1^\dagger, 2\left(\frac{\partial}{\partial t}-\mu\right)p_1\right\rangle\frac{\partial B}{\partial T} = &-\left\langle p_1^\dagger, \omega f_c(t) p_1\right\rangle \lambda B \\ &+\left\langle p_1^\dagger, \left(\left(\frac{\partial}{\partial t}-\mu\right)(\alpha p_1-\beta q_1)-\omega(\alpha q_1+\beta p_1)\right)\frac{\partial^2 B}{\partial X^2}\right\rangle \\ &+\Big\langle p_1^\dagger, -\omega\left(C_r\left(p_1^2+q_1^2\right)q_1+C_i\left(p_1^2+q_1^2\right)p_1\right) \\ &\quad+\left(\frac{\partial}{\partial t}-\mu\right)\left(C_r\left(p_1^2+q_1^2\right)p_1-C_i\left(p_1^2+q_1^2\right)q_1\right)\Big\rangle B^3,\end{aligned} \tag{2.21}$$

We find coefficients of the above equation by computing the inner products numerically. Therefore, the PDE is reduced to the Allen–Cahn equation as

$$B_T = 1.5687\lambda B + 11.1591 B_{XX} + 9.4717 B^3, \tag{2.22}$$

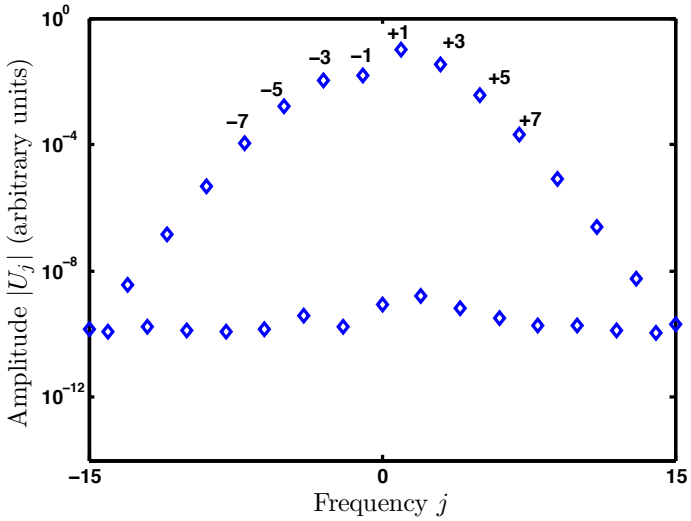

Figure 2.13: The truncated Fourier series in time of a localized solution of the PDE (2.2), showing that even with strong forcing, the modes $+1$, $+3$, -1, and -3 dominate. The parameter values are the same as in Figure 2.11.

for the parameter values in Figure 2.11 (a). Note that $U = \epsilon_1 U_1$, $X = \epsilon_1 x$, and $\epsilon_1^2 \lambda = \frac{F}{F_0} - 1$, so that the spatially localized solution takes the form

$$U_{loc} = \sqrt{\frac{-3.1374(\frac{F}{F_0} - 1)}{9.4717}} \operatorname{sech}\left(\sqrt{\frac{-1.5687(\frac{F}{F_0} - 1)}{11.1591}} x\right) (p_1(t) + i q_1(t)) \,. \qquad (2.23)$$

Thus, we have found approximate examples of localized solutions of the PDE, which are qualitatively similar to those found in the weak damping case. Figure 2.11 (a) shows the comparison between the numerical solution and U_{loc}. This solution is continued using AUTO to compute a bifurcation diagram in Figure 2.12 and further example solutions are shown in Figure 2.11 (b)-(d), again qualitatively similar to the weak damping case. These solutions represent the truncated PDE with -3, -1, $+1$, $+3$ Fourier modes, which continued to dominate the modes that have been discarded (see Figure 2.13). Figure 2.11 (e) is a time-stepping example of a stable localized solution of the PDE.

2.6 Conclusion

In the present study we examine the possible existence of spatially localized structures in the model PDE (2.2) with time dependent parametric forcing. Since bistability is known to lead to the formation of localized solutions, we consider subcritical bifurcations from the zero state. The localized solutions we find are time dependent, unlike most previous work on this class of problems; they oscillate with half the frequency of the driving force. In the weak damping, weak forcing limit, the solutions and bifurcations of the PDE are accurately described by its amplitude equation, the forced complex Ginzburg-Landau (FCGL) equation. Our work uses results in [15], where localized solutions are observed in the FCGL equation in 1D. We reduce the FCGL equation to the Allen–Cahn equation to find an asymptotically exact spatially localized solution of the PDE analytically, close to onset.

By continuing the numerical solution of the PDE model (2.2) that we take from time-stepping as an initial condition, we found the branch of localized states. The stability of this branch was determined by time-stepping, and the region where stable localized solutions occur was found. The saddle-node bifurcations on the snaking curve arise from pinning associated with the decaying spatial oscillations on either edge of the flat state.

The numerical examples we give in this chapter indicate how localized solutions exist in 1D, and show excellent agreement between the PDE model and the FCGL equation. The agreement remains qualitatively good even with strong damping and strong forcing. In the strong damping limit, we reduce the PDE directly to the Allen–Cahn equation analytically, close to onset. By continuing the approximate solution, examples of stable localized oscillons are observed numerically.

In the current work the preferred wavenumber is zero, so our results are directly relevant to localized patterns found in Turing systems, such as those found in [80, 86]. In contrast, in the Faraday wave experiment, the preferred wavenumber is non-zero, and so this work is not directly relevant to the oscillons that are observed there. Our interest next is to find

and analyze spatially localized oscillons with non-zero wave number in the PDE model, both in 1D and in 2D. This will indicate how localized solutions might be studied in (for example) the Zhang–Viñals model [93], and how the weakly nonlinear calculations of [77] might be extended to the oscillons observed in the Faraday wave experiment.

Chapter 3

Localized patterns with non-zero wavenumber

3.1 Introduction

In the Faraday wave experiment, the preferred wavenumber is away from zero as we discused in Chapter 1. Consequently, in this chapter we will investigate the existence of localized oscillons that arise with non-zero preferred wavenumber. Our aim is to find and analyze spatially localized oscillons with non-zero wavenumber in the PDE model (1.12) theoretically and numerically in 1D. The approach will be similar to that in Chapter 2, though more complicated. Although we will work with a model PDE, our approach will show how localized solutions might be studied in PDEs more directly connected to the Faraday wave experiment, such as the Zhang–Viñals model [93] or the Navier–Stokes equations [77], and how weakly nonlinear calculations from the Navier–Stokes equations might be extended to the oscillons observed in the Faraday wave experiment.

We simplify the PDE as in Chapter 2 by removing quadratic terms, and by taking the parametric forcing to be $\cos(2t)$, where t is the fast time scale. In contrast to Chapter 2, here we will retain the fourth-order spatial derivatives in the PDE model (1.12) with parametric forcing. The extra term $((\gamma + i\delta)U_{xxxx})$ is needed because we require more

control over the dispersion relation. The resulting model PDE is then

$$U_t = (\mu + i\omega)U + (\alpha + i\beta)U_{xx} + (\gamma + i\delta)U_{xxxx} + C|U|^2U + i\Re(U)F\cos(2t), \quad (3.1)$$

where $U(x,t)$ is a complex function, $\mu < 0$ is the distance from onset of the oscillatory instability, ω, α, β, γ, δ and F are real parameters, and C is a complex parameter as defined in Chapter 2.

In this case we can model waves with a slowly varying envelope in one spatial dimension by looking at solutions of the form

$$U(x,t) = A(X,T)e^{i(t+x)} + B(X,T)e^{i(t-x)}, \quad (3.2)$$

where X and T are slow scales, and x and t are scaled so that the wave has critical wavenumber $k_c = 1$ and critical frequency $\Omega_c = 1$. In order to cover the symmetries of the PDE model, we include both the left- and right-travelling waves but the time dependence will be e^{it} only, without e^{-it}. In section 3.2.1, we explain in detail how the solution of the linear operator, that we will define later, involves e^{it} only. The $+1$ frequency will dominate at leading order because of our choice of dispersion relation. Since the analysis at this stage of our research study is complicated, we will consider the one-dimensional case rather than having A and B depend on another long-scale Y, although we consider two-dimensional patterns numerically in Chapter 4.

In this chapter we will do an asymptotic reduction of the model PDE (3.1) to the coupled forced complex Ginzburg–Landau (coupled FCGL) equations in the limit of weak damping, weak detuning, weak forcing, small group velocity, and small amplitude, and we will study the properties of the coupled FCGL equations. Some numerical examples of spatially localized oscillons in the coupled FCGL equations will be given. We will also investigate the effect of changing the group velocity. Furthermore, we will reduce the coupled FCGL equations to the real Ginzburg–Landau equation in a further limit of weak

forcing and weak amplitude close to onset, which is known to have exact localized sech solutions. Throughout, we will use weakly nonlinear theory by introducing a multiple scale expansion to do the reduction to the amplitude equations as in Chapter 2. Finally, we give numerical examples of oscillons in the PDE model.

3.2 Derivation of the coupled forced complex Ginzburg–Landau (FCGL) equation

In this section we will study the PDE model (3.1) in the limit of weak damping, weak detuning, weak forcing and small amplitude in order to derive its amplitude equation. In addition, we will need to assume that the group velocity is small. We start with linearizing (3.1) about zero, and as before we consider solutions of the form $U(x,t) = e^{\sigma t + ikx}$, where σ is the complex growth rate of a mode with wavenumber k. Without taking any limits and without considering the forcing, the growth rate is given by the following expression

$$\sigma = \mu - \alpha k^2 + \gamma k^4 + i(\omega - \beta k^2 + \delta k^4), \tag{3.3}$$

where $\sigma = \sigma_r + i\sigma_i$, so σ_r gives the damping rate of modes with wavenumber k, and σ_i gives the frequency of oscillation:

$$\Omega(k) = \sigma_i = \omega - \beta k^2 + \delta k^4.$$

We will also need the group velocity of the waves, defined by

$$v_g = \frac{d\Omega(k)}{dk} = -2\beta k + 4\delta k^3.$$

We will choose parameters so that we are in a weak damping, weak detuning, and small group velocity limit for modes with wavenumber $k = 1$. Specifically, in order to find spatially localized oscillons and to do the reduction to the amplitude model, we will

impose the following:

- All waves have to be damped, so that we need $\sigma_r(k) < 0$, for all k.
- The growth rate $\sigma_r(\pm 1)$ is close to zero.
- Waves with $k \simeq \pm 1$ are most weakly damped, so $\frac{d\sigma_r}{dk} = 0$ at $k = \pm 1$
- Waves with $k \simeq \pm 1$ are driven subharmonically by $\cos(2t)$, so $\sigma_i(\pm 1)$ is close to 1. Note that $\sigma_i(\pm 1)$ could be close to -1 but not both $+1$ and -1.
- The group velocity v_g at $k \simeq \pm 1$ is small.
- The forcing $F\cos(2t)$ is weak.

To have all waves damped we choose $\mu < 0$, $\alpha < 0$, and $\gamma < 0$. Choosing $\alpha < 0$ allows a non-monotonic growth rate; and $\sigma_r < 0$ requires $\alpha > -2\sqrt{\mu\gamma}$. We also need to make the growth rate σ_r to be close to zero when $k = k_c = 1$. Therefore, we introduce a new parameter ρ, so we have

$$\sigma_r(k = 1) = \mu - \alpha + \gamma = \epsilon^2\rho,$$

where $0 < \epsilon \ll 1$ and $\rho < 0$. Figure 3.1 shows the real part of the growth rate where the dissipation ρ can be determind at $k = 1$. It indicates that the damping rate is $O(\epsilon^2)$. The growth rate σ_r achieves a maximum when the wavenumber k is one, so that

$$\frac{d\sigma_r}{dk}(k = 1) = -2\alpha + 4\gamma = 0,$$

which gives the condition $\alpha = 2\gamma$, and so $\mu = \frac{\alpha}{2} + \epsilon^2\rho$.

The frequency of the oscillation $\Omega(k_c)$ is close to 1 at $k = 1$, so we can write

$$\Omega(k = 1) = \omega - \beta + \delta = 1 + \epsilon^2\nu,$$

where ν is the detuning. Figure 3.2 shows the dispersion relation $\Omega(k)$.

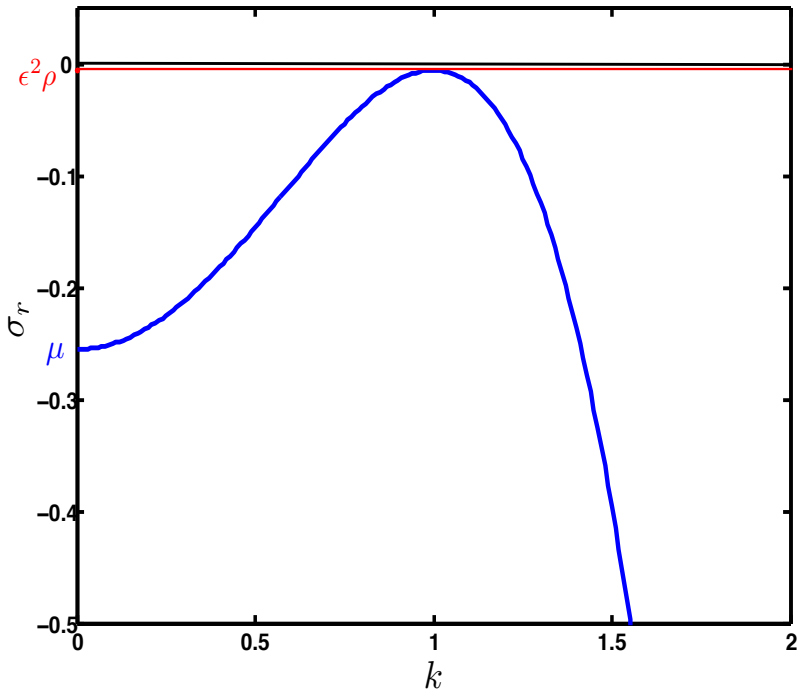

Figure 3.1: The growth rate of equation (3.1) with $\mu = -0.255$, $\alpha = -0.5$, and $\gamma = -0.25$. Here $\sigma_r(k=1) = \epsilon^2\rho = \mu - \alpha + \gamma = -0.005$.

To scale the group velocity to be $O(\epsilon)$, we calculate the maximum of the frequency of the oscillation at $k = +1$ or $k = -1$:

$$\frac{d\sigma_i}{dk} = -2k\beta + 4\delta k^3 = \epsilon v_g,$$

which for $k = +1$ gives $\delta = \frac{2\beta+\epsilon v_g}{4}$. The group velocity at $k = -1$ is $-\epsilon v_g$.

To perform the weakly nonlinear theory, we assume that the forcing is weak, and so we scale the forcing amplitude with ϵ as

$$F \to \epsilon^2 F, \quad \text{or} \quad F = 4\epsilon^2\Gamma.$$

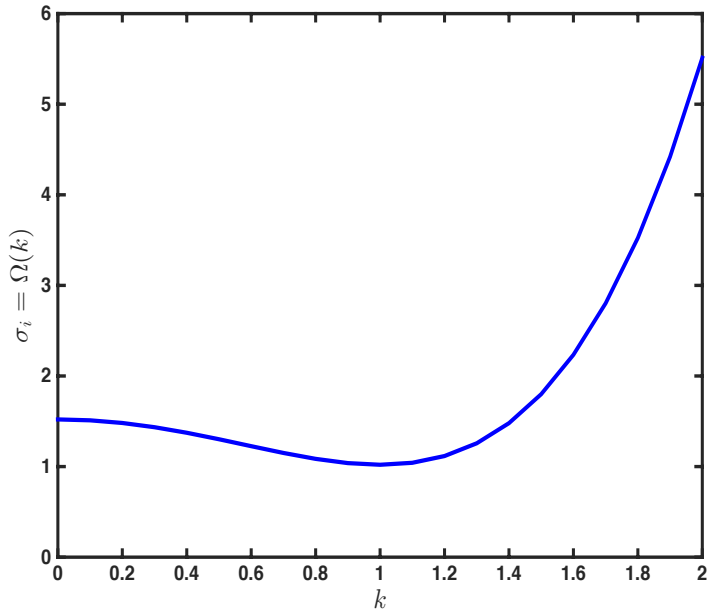

Figure 3.2: The dispersion relation $\sigma_i(k)$ of the linear theory of (3.1) equation with $\omega = 1 + \beta - \delta + \epsilon^2\nu = 1.52$, $\beta = 1$, and $\delta = 0.4995$, $\nu = 2$, and $\epsilon = 0.1$.

We relate the parameters in the PDE model with the parameters in the amplitude equations of the PDE model in a way that we can connect examples of localized oscillons in both equations. In table 3.1 all PDE parameters are defined in terms of parameters that will appear in the coupled FCGL equations.

3.2.1 Linear theory

With the parameters as in table 3.1, the linear theory of the PDE (3.1) at leading order is given by

$$U_t = \left(\frac{\alpha}{2} + i\left(\frac{\beta}{2} + 1\right)\right) U + (\alpha + i\beta)\, U_{xx} + \left(\frac{\alpha}{2} + i\frac{\beta}{2}\right) U_{xxxx}, \tag{3.4}$$

The PDE model (3.1)	The coupled FCGL (3.16)
μ, ω, α, β, γ, δ, and F	ρ, ν, α, β, v_g, and Γ
$\mu = \alpha - \gamma + \epsilon^2\rho = \frac{\alpha}{2} + \epsilon^2\rho$	$\rho = \frac{\mu-\alpha+\gamma}{\epsilon^2}$
$\gamma = \frac{\alpha}{2}$	
$\delta = \frac{2\beta+\epsilon v_g}{4}$	$v_g = \frac{-2\beta+4\delta}{\epsilon}$
$\omega = 1 + \frac{\beta}{2} - \frac{\epsilon v_g}{4} + \epsilon^2\nu$	$\nu = \frac{\omega-1-\beta+\delta}{\epsilon^2}$
$F = 4\epsilon^2\Gamma$	$\Gamma = \frac{F}{4\epsilon^2}$

Table 3.1: Relationships between parameters of the PDE model and the coupled FCGL equations. Note these relationships depend on the choice of ϵ. The parameters α and β are the same in both models.

which defines a linear operator L as

$$LU = \left[-\frac{\partial}{\partial t} + \left(\frac{\alpha}{2} + i\left(\frac{\beta}{2} + 1\right)\right) + (\alpha + i\beta)\frac{\partial^2}{\partial x^2} + \left(\frac{\alpha}{2} + i\frac{\beta}{2}\right)\frac{\partial^4}{\partial x^4}\right] U,$$

or we can write it as

$$LU = \left(-\frac{\partial}{\partial t} + i\right) U + \left(\frac{\alpha}{2} + i\frac{\beta}{2}\right)\left(1 + \frac{\partial^2}{\partial x^2}\right)^2 U.$$

Note that the term $\left(1 + \frac{\partial^2}{\partial x^2}\right)^2$ is similar to a term that appears in the classic pattern-forming PDE, the Swift-Hohenberg equation [78]. To find all solutions, we substitute $U = e^{\sigma t + ikx}$ into the above equation to get

$$-\sigma + i + \left(\frac{\alpha}{2} + i\frac{\beta}{2}\right)\left(1 - k^2\right)^2 = 0,$$

which becomes

$$\sigma = i + \left(\frac{\alpha}{2} + i\frac{\beta}{2}\right)\left(1 - k^2\right)^2.$$

We assume that our problem has periodic boundary conditions. The periodic boundary condition implies that $k \in \mathbb{R}$. Furthermore, we require $\sigma_r = 0$ since we are considering neutral modes. The real and imaginary parts of this equation give

$$k = \pm 1 \quad \text{and} \quad \sigma = i.$$

Therefore, $LU = 0$ implies that neutral modes are a linear combinations of $U(x,t) = e^{i(t+x)}$ and $U(x,t) = e^{i(t-x)}$.

3.2.2 Weakly nonlinear theory

In order to apply the standard weakly nonlinear theory, we need the adjoint linear operator $L^\dagger$. Therefore, we define an inner product between two functions $f(x,t)$ and $g(x,t)$ by

$$\big\langle f(x,t), g(x,t) \big\rangle = \frac{1}{4\pi^2} \int_0^{2\pi} \int_0^{2\pi} \bar{f}(x,t) g(x,t) \quad dt \quad dx, \tag{3.5}$$

where $\bar{f}$ is the complex conjugate of f. We will do integration by parts since we have periodic boundary conditions. The adjoint linear operator $L^\dagger$ is defined with the above inner product by

$$\begin{aligned}
\big\langle f(x,t), Lg(x,t) \big\rangle &= \frac{1}{4\pi^2} \int_0^{2\pi} \int_0^{2\pi} \bar{f} \left(-g_t + \left(\frac{\alpha}{2} + i \left(1 + \frac{\beta}{2} \right) \right) g \right) \quad dt \quad dx \\
&\quad + \frac{1}{4\pi^2} \int_0^{2\pi} \int_0^{2\pi} \bar{f} \left((\alpha + i\beta) g_{xx} + \left(\frac{\alpha}{2} + i\frac{\beta}{2} \right) g_{xxxx} \right) \quad dt \quad dx, \\
&= \frac{1}{4\pi^2} \int_0^{2\pi} \int_0^{2\pi} \left(\bar{f}_t + \left(\frac{\alpha}{2} + i \left(1 + \frac{\beta}{2} \right) \right) \bar{f} \right) g \quad dt \quad dx \\
&\quad + \frac{1}{4\pi^2} \int_0^{2\pi} \int_0^{2\pi} \left((\alpha + i\beta) \bar{f}_{xx} + \left(\frac{\alpha}{2} + i\frac{\beta}{2} \right) \bar{f}_{xxxx} \right) g \quad dt \quad dx, \\
&= \big\langle L^\dagger f(x,t), g(x,t) \big\rangle,
\end{aligned} \tag{3.6}$$

and so

$$L^\dagger f = \left(\frac{\partial}{\partial t} - i + \left(\frac{\alpha}{2} - i\frac{\beta}{2} \right) \left(1 + \frac{\partial^2}{\partial x^2} \right)^2 \right) f.$$

This adjoint linear operator changes the sign of $\frac{\partial}{\partial t}$ term and takes the complex conjugate of other terms of L. The adjoint eigenfunctions are given by solving $L^\dagger f = 0$; the solutions are linear combinations of $e^{i(t\pm x)}$.

We expand U in powers of the small parameter ϵ as in Chapter 2:

$$U = \epsilon U_1 + \epsilon^2 U_2 + \epsilon^3 U_3 + ..., \tag{3.7}$$

where U_1, U_2, U_3, ... are $O(1)$ complex functions. Recall that

$$\begin{aligned}
\mu &= \frac{\alpha}{2} + \epsilon^2 \rho, \\
\gamma &= \frac{\alpha}{2}, \\
\omega &= 1 + \frac{\beta}{2} - \epsilon \frac{v_g}{4} + \epsilon^2 \nu, \\
\delta &= \frac{\beta}{2} + \frac{\epsilon v_g}{4}, \\
F &= 4\epsilon^2 \Gamma.
\end{aligned}$$

We will derive solutions U_1, U_2, U_3, ..., at each order of ϵ.

At $O(\epsilon)$, the linear theory arises and the linear operator defined above acts on U_1 as

$$LU_1 = 0.$$

The solution U_1 takes the form

$$U_1 = A(X,T)e^{i(t+x)} + B(X,T)e^{i(t-x)}, \tag{3.8}$$

where the amplitudes A and B are functions of X and T, the long and slow scale modulations of space and time variables:

$$T = \epsilon^2 t, \quad \text{and} \quad X = \epsilon x.$$

The multiple scale expansions below will determine the evolution equations for $A(X,T)$ and $B(X,T)$.

At second order in ϵ, we get $LU_2 = 0$. Note that $\frac{\partial^2 U_1}{\partial x \partial X}$ term cancels with $\frac{\partial^4 U_1}{\partial x^3 \partial X}$ term. We would have had a $\frac{\partial^4 U_1}{\partial x^3 \partial X}$ as a forcing term at $O(\epsilon^2)$ if we had not ensured that the group velocity is $O(\epsilon)$.

At third order in ϵ, we get

$$\begin{aligned}\frac{\partial U_3}{\partial t} + \frac{\partial U_1}{\partial T} = &\left(\frac{\alpha}{2} + i\left(1 + \frac{\beta}{2}\right)\right) U_3 + (\alpha + i\beta)\frac{\partial^2 U_3}{\partial x^2} \\ &+ \left(\frac{\alpha}{2} + i\frac{\beta}{2}\right)\frac{\partial^4 U_3}{\partial x^4} + (\rho + i\nu)U_1 + (\alpha + i\beta)\frac{\partial^2 U_1}{\partial X^2} \\ &+ 6\left(\frac{\alpha}{2} + i\frac{\beta}{2}\right)\frac{\partial^4 U_1}{\partial x^2 \partial X^2} + iv_g\frac{\partial^4 U_1}{\partial x^3 \partial X} \\ &+ 4i\Gamma\cos(2t)Re(U_1) + C|U_1|^2 U_1,\end{aligned} \tag{3.9}$$

which becomes

$$\begin{aligned}\frac{\partial U_1}{\partial T} = &LU_3 + (\rho + i\nu)U_1 + (\alpha + i\beta)\frac{\partial^2 U_1}{\partial X^2} \\ &+ 6\left(\frac{\alpha}{2} + i\frac{\beta}{2}\right)\frac{\partial^4 U_1}{\partial x^2 \partial X^2} + iv_g\frac{\partial^4 U_1}{\partial x^3 \partial X} \\ &+ 4i\Gamma\cos(2t)Re(U_1) + C|U_1|^2 U_1.\end{aligned} \tag{3.10}$$

The linear operator L is singular so we must apply a solvability condition: we take the inner product between the adjoint eigenfunction $e^{i(t+x)}$ and equation (3.10), which gives

$$\begin{aligned}\left\langle e^{i(t+x)}, \frac{\partial U_1}{\partial T}\right\rangle = &\left\langle e^{i(t+x)}, LU_3\right\rangle + (\rho + i\nu)\left\langle e^{i(t+x)}, U_1\right\rangle + (\alpha + i\beta)\left\langle e^{i(t+x)}, \frac{\partial^2 U_1}{\partial X^2}\right\rangle \\ &+ \left\langle e^{i(t+x)}, 6\left(\frac{\alpha}{2} + i\frac{\beta}{2}\right)\frac{\partial^4 U_1}{\partial x^2 \partial X^2}\right\rangle + iv_g\left\langle e^{i(t+x)}, \frac{\partial^4 U_1}{\partial x^3 \partial X}\right\rangle \\ &+ 4i\Gamma\left\langle e^{i(t+x)}, \cos(2t)Re(U_1)\right\rangle + C\left\langle e^{i(t+x)}, |U_1|^2 U_1\right\rangle.\end{aligned} \tag{3.11}$$

We have

$$\left\langle e^{i(t+x)}, LU_3 \right\rangle = \left\langle L^\dagger e^{i(t+x)}, U_3 \right\rangle = 0,$$

so U_3 is removed, and equation (3.11) becomes an equation in U_1:

$$\begin{aligned}\left\langle e^{i(t+x)}, \frac{\partial U_1}{\partial T} \right\rangle &= (\rho + i\nu) \left\langle e^{i(t+x)}, U_1 \right\rangle + (\alpha + i\beta) \left\langle e^{i(t+x)}, \frac{\partial^2 U_1}{\partial X^2} \right\rangle \\ &+ \left\langle e^{i(t+x)}, 6\left(\frac{\alpha}{2} + i\frac{\beta}{2}\right) \frac{\partial^4 U_1}{\partial x^2 \partial X^2} \right\rangle + i v_g \left\langle e^{i(t+x)}, \frac{\partial^4 U_1}{\partial x^3 \partial X} \right\rangle \\ &+ 4i\Gamma \left\langle e^{i(t+x)}, \cos(2t) Re(U_1) \right\rangle + C \left\langle e^{i(t+x)}, |U_1|^2 U_1 \right\rangle .\end{aligned} \tag{3.12}$$

Substituting the solution U_1 leads to

$$\begin{aligned}&\left\langle e^{i(t+x)}, \frac{\partial}{\partial T}\left(Ae^{i(t+x)} + Be^{i(t-x)}\right) \right\rangle \\ &= (\rho + i\nu) \left\langle e^{i(t+x)}, \left(Ae^{i(t+x)} + Be^{i(t-x)}\right) \right\rangle + (\alpha + i\beta) \left\langle e^{i(t+x)}, \frac{\partial^2}{\partial X^2}\left(Ae^{i(t+x)}\right.\right. \\ &\left.\left. + Be^{i(t-x)}\right) \right\rangle + \left\langle e^{i(t+x)}, 6\left(\frac{\alpha}{2} + i\frac{\beta}{2}\right) \frac{\partial^4}{\partial x^2 \partial X^2}\left(Ae^{i(t+x)} + Be^{i(t-x)}\right) \right\rangle \\ &+ i v_g \left\langle e^{i(t+x)}, \frac{\partial^4}{\partial x^3 \partial X}\left(Ae^{i(t+x)} + Be^{i(t-x)}\right) \right\rangle \\ &+ 4i\Gamma \left\langle e^{i(t+x)}, \frac{1}{2}\cos(2t)\left(Ae^{i(x+t)} + Be^{i(t-x)} + \bar{A}e^{-i(t+x)} + \bar{B}e^{-i(t-x)}\right) \right\rangle \\ &+ C \left\langle e^{i(t+x)}, \left(|A|^2 + A\bar{B}e^{2ix} + \bar{A}Be^{-2ix} + |B|^2\right)\left(Ae^{i(t+x)} + Be^{i(t-x)}\right) \right\rangle.\end{aligned} \tag{3.13}$$

The left hand side of (3.13) is

$$\begin{aligned}\left\langle e^{i(t+x)}, \frac{\partial}{\partial T}\left(Ae^{ix} + Be^{-ix}\right)e^{it} \right\rangle &= \frac{1}{4\pi^2}\int_0^{2\pi}\int_0^{2\pi} e^{-ix}\frac{\partial}{\partial T}\left(Ae^{ix} + Be^{-ix}\right) dt \quad dx \\ &= \frac{\partial A}{\partial T}.\end{aligned} \tag{3.14}$$

We compute the right hand side of (3.13) in three parts. The first five lines are:

$$\begin{aligned}
&\left((\rho+i\nu)+(\alpha+i\beta)\frac{\partial^2}{\partial X^2}-6\left(\frac{\alpha}{2}+i\frac{\beta}{2}\right)\frac{\partial^2}{\partial X^2}\right)\left\langle e^{i(t+x)},\left(Ae^{i(t+x)}+Be^{i(t-x)}\right)\right\rangle\\
&+iv_g\left\langle e^{i(t+x)},\frac{\partial^4}{\partial X\partial x^3}\left(Ae^{i(t+x)}+Be^{i(t-x)}\right)\right\rangle\\
&=\frac{1}{4\pi^2}\int_0^{2\pi}\int_0^{2\pi}e^{-ix}\Big((\rho+i\nu)+(\alpha+i\beta)\frac{\partial^2}{\partial X^2}\\
&\quad-6\left(\frac{\alpha}{2}+i\frac{\beta}{2}\right)\frac{\partial^2}{\partial X^2}+v_g\frac{\partial}{\partial X}\Big)Ae^{ix}dt\quad dx\\
&=\left((\rho+i\nu)-2(\alpha+i\beta)\frac{\partial^2}{\partial X^2}+v_g\frac{\partial}{\partial X}\right)A.
\end{aligned}$$

The forcing term is:

$$\begin{aligned}
&4i\Gamma\left\langle e^{i(t+x)},\frac{1}{2}\cos(2t)(Ae^{i(t+x)}+Be^{i(t-x)}+\bar{A}e^{-i(t+x)}+\bar{B}e^{-i(t-x)})\right\rangle\\
&=\frac{4i\Gamma}{16\pi^2}\int_0^{2\pi}\int_0^{2\pi}e^{-i(t+x)}\big(\bar{A}(e^{-i(4t+2x)}+e^{-2ix})+A(e^{2it}+e^{-2it})\\
&\quad+B(e^{i(3t-x)}+e^{-i(t+x)})+\bar{B}(e^{i(t+x)}+e^{i(-3t+x)})\big)dt\quad dx\\
&=i\Gamma\bar{B}.
\end{aligned}$$

The nonlinear terms are:

$$\begin{aligned}
&C\left\langle e^{i(t+x)},\left(|A|^2+A\bar{B}e^{2ix}+\bar{A}Be^{-2ix}+|B|^2\right)\left(Ae^{i(t+x)}+Be^{i(t-x)}\right)\right\rangle\\
&=\frac{C}{4\pi^2}\int_0^{2\pi}\int_0^{2\pi}e^{-ix}\left(|A|^2+A\bar{B}e^{2ix}\quad+\bar{A}Be^{-2ix}+|B|^2\right)\left(Ae^{ix}+Be^{-ix}\right)dt\quad dx\\
&=C\left(|A|^2+2|B|^2\right)A.
\end{aligned}\tag{3.15}$$

The above equations result in the following equation for the amplitude $A(X,T)$

$$\frac{\partial A}{\partial T}=(\rho+i\nu)A-2(\alpha+i\beta)\frac{\partial^2 A}{\partial X^2}+v_g\frac{\partial A}{\partial X}+C\left(|A|^2+2|B|^2\right)A+i\Gamma\bar{B}.$$

By the symmetry $A\leftrightarrow B$, and $X\to -X$, we get the equation for B. Therefore the

amplitude equation is given by

$$\begin{aligned}\frac{\partial A}{\partial T} &= (\rho + i\nu)A - 2(\alpha + i\beta)\frac{\partial^2 A}{\partial X^2} + v_g\frac{\partial A}{\partial X} + C\left(|A|^2 + 2|B|^2\right)A + i\Gamma\bar{B},\\ \frac{\partial B}{\partial T} &= (\rho + i\nu)B - 2(\alpha + i\beta)\frac{\partial^2 B}{\partial X^2} - v_g\frac{\partial B}{\partial X} + C\left(2|A|^2 + |B|^2\right)B + i\Gamma\bar{A}.\end{aligned} \tag{3.16}$$

Thus the PDE model has been reduced to the coupled FCGL, in the weak damping, weak detuning, small group velocity and small amplitude limit. We note that the $-2\alpha\frac{\partial^2 A}{\partial X^2}$ term makes the above equations look like it might be an ill-posed problem, but recall that $\alpha < 0$.

If the group velocity were zero, which means the condition $\beta = 2\delta$ is valid, the resulting system becomes

$$\begin{aligned}\frac{\partial A}{\partial T} &= (\rho + i\nu)A - 2(\alpha + i\beta)\frac{\partial^2 A}{\partial X^2} + C(|A|^2 + 2|B|^2)A + i\Gamma\bar{B}.\\ \frac{\partial B}{\partial T} &= (\rho + i\nu)B - 2(\alpha + i\beta)\frac{\partial^2 B}{\partial X^2} + C(2|A|^2 + |B|^2)B + i\Gamma\bar{A}.\end{aligned} \tag{3.17}$$

These equations have solutions where $A = B$, representing two travelling waves sitting exactly on top of each other. In equations (3.16) the group velocity terms have different signs, which makes the envelopes travel in opposite directions. In the next section we will represent briefly a study of a related problem to equations (3.16), where the group velocity is $O(1)$ and the domain size L takes a significant role.

3.3 The effect of scaling of the group velocity in the coupled FCGL equations

In the derivation of the coupled FCGL equations in Section 3.2, we assumed that the group velocity v_g is $O(\epsilon)$; but in reality, v_g is $O(1)$. Our study reveals that the $O(\epsilon)$ assumption on the group velocity is needed to make progress. Although, in this thesis we scale the group velocity with $O(\epsilon)$, this could be avoided by following the approach in [57],

which is a study of a related problem. In [57], Martel, Knobloch and Vega investigated the possible solutions of a pair of parametrically driven weakly dissipative nonlinear Schrödinger equations with nonlocal coupling. Their work was based on studying the average of the coupled FCGL equations with the assumption that the group velocity is $O(1)$. They studied the following system

$$\begin{aligned} A_t &= i\beta A_{xx} + v_g A_x + (\rho + i\nu)A + iC_i(|A|^2 + \kappa|B|^2)A + \Gamma\bar{B}, \\ B_t &= i\beta B_{xx} - v_g B_x + (\rho + i\nu)B + iC_i(|B|^2 + \kappa|A|^2)B + \Gamma\bar{A}, \end{aligned} \tag{3.18}$$

where the wave amplitudes A and B vary slowly in both space and time, and assumed to be small. The real coefficients $\rho < 0$, ν, β, v_g and $\Gamma > 0$ measure the decay rate, detuning, dispersion, group velocity of the waves, and the amplitude of the parametric forcing. The coefficients $C_i \in \mathbb{R}$ and κ represent the nonlinear self- and cross-interaction terms, and they are assumed to satisfy $C_i(1 + \kappa) \neq 0$. With the choice $\alpha = 0$, $C_r = 0$, $\kappa = 2$, equations (3.16), and (3.18) are the same up to a change of phase.

It was assumed that dissipation, detuning and forcing amplitude are weak. The authors used a multiple scales analysis based on the domain size L, with A and B representing the amplitudes of slowly varying left- and right-travelling waves, as in (3.2). They used left-travelling and right-travelling coordinates, with each wave seeing only the average of the other. The resulting averaged equations are the nonlocal. These equations were valid close to threshold of the primary parametric instability. The averaged equations are

$$\begin{aligned} A_\tau &= i\beta A_{\eta\eta} + (\rho + i\nu)A + iC_i(|A|^2 + \kappa\langle|B|^2\rangle)A + \Gamma\langle\bar{B}\rangle, \\ B_\tau &= i\beta B_{\xi\xi} + (\rho + i\nu)B + iC_i(|B|^2 + \kappa\langle|A|^2\rangle)B + \Gamma\langle\bar{A}\rangle, \end{aligned} \tag{3.19}$$

where $\eta = x + t$, $\xi = x - t$, and $\tau = \frac{t}{L^2}$. The notation $\langle ... \rangle$ refers to an average over the spatial variable η or ξ.

Spatially uniform and non-uniform solutions with both simple and complex time-dependence were found. The spatially uniform solutions are in the form of standing

waves. The properties of the linear stability were studied in the averaged coupled equations for the trivial and of nontrivial spatially uniform states. The authors looked at the role of the domain size L, and the effect of distant side boundaries. They did not study spatially localized solutions. The approach in [57] could allow us to lift the $O(\epsilon)$ assumption on the group velocity v_g in future work.

In the next section we will examine the properties of equations (3.16), where the group velocity plays an important role in the dynamics of the equations.

3.4 Properties of the coupled FCGL equations

In our study we assume that the group velocity v_g is small, of order ϵ, which means that we can study the coupled FCGL equations without averaging. Recall that the coupled FCGL equations are:

$$\begin{aligned} A_T &= (\rho + i\nu)A - 2(\alpha + i\beta)A_{XX} + v_g A_X + C(|A|^2 + 2|B|^2)A + i\Gamma\bar{B}, \\ B_T &= (\rho + i\nu)B - 2(\alpha + i\beta)B_{XX} - v_g B_X + C(2|A|^2 + |B|^2)B + i\Gamma\bar{A}, \end{aligned} \tag{3.20}$$

where $\rho < 0$, ν, $\alpha < 0$, β, v_g and Γ are real and measure the dissipation, detuning, diffusion, dispersion, group velocity and forcing of the wave; C is the original complex cubic coefficient from (3.1). In the absence of forcing, $\Gamma = 0$, all waves decay.

Following [41] we can identify the symmetries and how they affect the structure of (3.20): (i) translation in x: since $x \to x + \phi^*$, we get

$$U(x + \phi^*, t) = A(X + \epsilon\phi^*, T)e^{i(t+x+\phi^*)} + B(X + \epsilon\phi^*, T)e^{i(t-x-\phi^*)},$$

where $A(X,T) \to A(X + \epsilon\phi^*, T)e^{i\phi^*}$, $B(X,T) \to B(X + \epsilon\phi^*, T)e^{-i\phi^*}$. If we suppress the change from X to $X + \epsilon\phi^*$, then (3.20) is equivariant under

$$A \to Ae^{i\phi^*}, \quad B \to Be^{-i\phi^*},$$

where ϕ^* is arbitrary.

(ii) reflection in x: since $x \to -x$, we write

$$U(-x,t) = A(-X,T)e^{i(t-x)} + B(-X,T)e^{i(t+x)}.$$

Equation (3.20) is equivariant under $A \to B$, $A_X \to -B_X$, and $A_{XX} \to B_{XX}$.

Amplitude equations arising from a Hopf bifurcation usually have time t translation symmetry, which manifests as equivariance under phase shifts of the amplitudes. However, the underlying PDE is non-autonomous, and so rotating A and B by a common phase is not a symmetry of (3.20). Indeed the $\cos(2t)$ term in (3.1) spoils the t translation symmetry of the original problem. Equations (3.20) do have T translation symmetry, but this is an artifact of the truncation at cubic order.

The equations (3.20) have solutions made up from travelling waves, standing waves, and amplitude-modulated waves. Travelling waves move from place to place with constant speed, and transport energy. Standing waves refer to waves that remain in a constant position. They can arise as a result of interference between two waves traveling in opposite directions, and the phase of a standing wave does not depend on position. When the amplitude of the wave is modulated, the variation in the amplitude is called the envelope of the wave. Modulated waves can vary with space and time.

The parametric forcing provides an interesting coupling between the two travelling waves with amplitudes A and B. The coupling terms in the coupled FCGL equations make it impossible to find pure travelling waves (i.e. $A \neq 0$, $B = 0$ is not a solution of (3.20)). Solutions of (3.20) can have A and B of unequal amplitude. A special class of solutions is at small and equal amplitudes, with travelling waves combining to form standing waves. Indeed, standing waves are typically seen in the Faraday wave experiment. The equations also have spatially uniform and nonuniform solutions. In the next sections we will analyze the zero and non-zero flat solutions of the coupled FCGL equations (3.20).

3.4.1 The zero solution

Here we will study the zero state of the coupled FCGL equations, $A = B = 0$. The stability of the zero state under small perturbations with complex growth rate s and wavenumber q can be studied by examining the dispersion relation, which relates the growth rate $s \in \mathbb{C}$ of a Fourier mode $e^{\pm iqX}$ with wavenumber $q \in \mathbb{R}$, so that the amplitudes A and B take the form

$$A = \hat{A}e^{sT+iqX}, \quad \text{and} \quad B = \hat{B}e^{\bar{s}T-iqX},$$

where $|\hat{A}| \ll 0$ and $|\hat{B}| \ll 0$ for $\hat{A}$, $\hat{B} \in \mathbb{C}$. Substituting these solutions into equation (3.20), linearizing and taking the complex conjugate of the second equation for B gives (dropping hats):

$$\begin{aligned} sA &= (\rho + i\nu)A + 2(\alpha + i\beta)q^2A + iv_gqA + i\Gamma\bar{B}. \\ s\bar{B} &= (\rho - i\nu)\bar{B} + 2(\alpha - i\beta)q^2\bar{B} - iv_gq\bar{B} - i\Gamma A. \end{aligned} \tag{3.21}$$

Note that we chose $\hat{B}e^{\bar{s}T-iqX}$ in order that the exponential term cancel. We can write equations (3.21) as

$$\begin{bmatrix} \rho + i\nu + 2(\alpha + i\beta)q^2 + iv_gq - s & i\Gamma \\ -i\Gamma & \rho - i\nu + 2(\alpha - i\beta)q^2 - iv_gq - s \end{bmatrix} \begin{bmatrix} A \\ \bar{B} \end{bmatrix} = \begin{bmatrix} 0 \\ 0 \end{bmatrix}.$$

There is a nontrivial solution only when the determinant of the above matrix is zero, so

$$\big(s - (\rho + i\nu) - 2(\alpha + i\beta)q^2 - iv_gq\big)\big(s - (\rho - i\nu) - 2(\alpha - i\beta)q^2 + iv_gq\big) = \Gamma^2. \tag{3.22}$$

We are interested in locating the bifurcations at which zero solutions is neutrally stable, so the real part of s is zero. We will show in addition that s must be real. This is not easy to see directly from (3.22), so we consider first the case where $q = 0$, and s is pure

imaginary, so $s = is_i$.

The determinant in this case is

$$(is_i - (\rho + i\nu))\,(is_i - (\rho - i\nu)) - \Gamma^2 = 0.$$

The real and imaginary parts of the above equation give
Re: $\rho^2 + \nu^2 - s_i^2 = \Gamma^2$.
Im: $2s_i\rho = 0 \longrightarrow s_i = 0 \quad \text{or} \quad \rho = 0$.
Since $\rho < 0$, this gives $s_i = 0$, and

$$\rho^2 + \nu^2 = \Gamma^2.$$

Next, we consider $q \neq 0$ with s still purely imaginary; so equation (3.22) becomes

$$\big((\rho + 2\alpha q^2) + i(\nu + 2\beta q^2 + v_g q - s_i)\big)\,\big((\rho + 2\alpha q^2) - i(\nu + 2\beta q^2 + v_g q + s_i\big) = \Gamma^2.$$

The real and imaginary parts of the above equation are
Re: $(\rho + 2\alpha q^2)^2 + 2v_g(\nu^2 + 2\beta q^2)q + (v_g q)^2 - s_i^2 = \Gamma^2$.
Im: $2s_i(\rho + 2\alpha q^2) = 0 \longrightarrow s_i = 0, \quad$ since $\quad (\rho + 2\alpha q^2) \neq 0$, with $\rho < 0$ and $\alpha < 0$.
Therefore, we have a neutral stability condition ($s = 0$):

$$(\rho + 2\alpha q^2)^2 + (\nu + 2\beta q^2 + v_g q)^2 = \Gamma^2. \tag{3.23}$$

Figure 3.3 shows solutions of this equation in the $(q - \Gamma)$ plane. The stability of the zero state changes when $\Gamma = \Gamma_c$, the minimum of the neutral stability curve, and the non-zero flat state is created with $q = q_c$. This corresponds to a uniform pattern in the PDE (3.1) with wavenumber $1 + \epsilon q$. The critical wavenumber q_c can be computed by solving a cubic equation in q at the minimum of the neutral stability curve (3.23), which is given by

$$2\alpha q(2\rho + 2\alpha q^2) + (\nu + 2\beta q^2 + v_g q)(4\beta q + v_g) = 0. \tag{3.24}$$

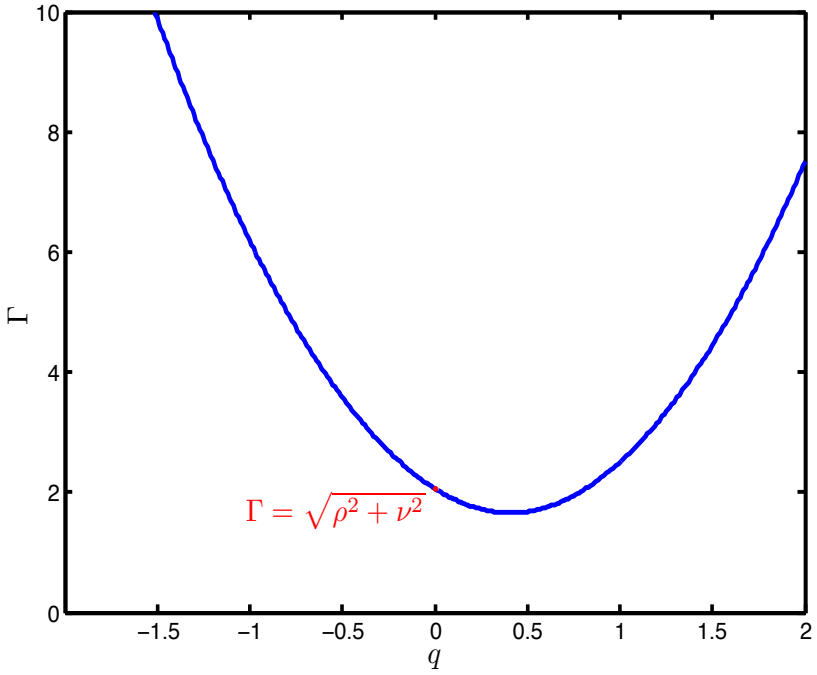

Figure 3.3: The linear theory of the zero state of the coupled FCGL equations (3.23) with $\rho = -0.5$, $\nu = 2$, $\alpha = -0.5$, $\beta = 1$, and $v_g = -2$. The blue line is the neutral stability curve, so above this curve modes grow, while below it modes decay.

The wavenumber q_c is positive if $\nu v_g < 0$ and negative if $\nu v_g > 0$.

3.4.2 Non-zero homogeneous solutions

We study the non-zero flat state, which represents a spatially uniform steady pattern in A and B with wavenumber 0 (so $U(x)$ has wavenumber 1). In section 3.4.3 below we consider the case of patterns with wavenumber $1 + \epsilon q$. With $q = 0$, the pattern satisfies the following:

$$\begin{aligned} 0 &= (\rho + i\nu)A + C(|A|^2 + 2|B|^2)A + i\Gamma\bar{B}. \\ 0 &= (\rho + i\nu)B + C(2|A|^2 + |B|^2)B + i\Gamma\bar{A}. \end{aligned} \tag{3.25}$$

In order to solve this steady system we consider solutions of the form $A = R_0 e^{i\phi_1}$ and $B = R_0 e^{i\phi_2}$, where R_0 is real, and ϕ_1 and ϕ_2 are different phases. We expect these equal amplitude solutions because of the $A \leftrightarrow B$ symmetry, but they are not necessarily the only solutions that can be found.

Substituting the steady uniform solutions into equations (3.25) gives

$$\begin{aligned} 0 &= (\rho + i\nu)R_0 e^{i\phi_1} + 3CR_0^3 e^{i\phi_1} + i\Gamma R_0 e^{-i\phi_2}. \\ 0 &= (\rho + i\nu)R_0 e^{i\phi_2} + 3CR_0^3 e^{i\phi_2} + i\Gamma R_0 e^{-i\phi_1}. \end{aligned}$$

In the above equations, $R_0 = 0$ is a solution. For $R_0 \neq 0$, we divide the system by R_0, so we have

$$\begin{aligned} 0 &= (\rho + i\nu)e^{i\phi_1} + 3CR_0^2 e^{i\phi_1} + i\Gamma e^{-i\phi_2}. \\ 0 &= (\rho + i\nu)e^{i\phi_2} + 3CR_0^2 e^{i\phi_2} + i\Gamma e^{-i\phi_1}. \end{aligned}$$

Dividing the first equation by $e^{i\phi_1}$ and the second equation by $e^{i\phi_2}$ results in the same equation

$$0 = (\rho + i\nu) + 3CR_0^2 + i\Gamma e^{-i\Phi}, \tag{3.26}$$

where $\Phi = \phi_1 + \phi_2$. This is similar to equation (2.9). Now we can separate the real and imaginary parts as

$$\begin{aligned} 0 &= \rho + 3C_r R_0^2 + \Gamma \sin\Phi. \\ 0 &= \nu + 3C_i R_0^2 + \Gamma \cos\Phi, \end{aligned} \tag{3.27}$$

where $C = C_r + iC_i$.

Eliminating Φ by using the equality $\cos^2\Phi + \sin^2\Phi = 1$ gives the following polynomial

$$9(C_r^2 + C_i^2)R_0^4 + 6(\rho C_r + \nu C_i)R_0^2 + \rho^2 + \nu^2 - \Gamma^2 = 0. \tag{3.28}$$

This equation can be solved for R_0^2. Moreover, we can solve equation (3.27) for Φ, which leads to

$$\tan\Phi = \frac{\rho + 3C_r R_0^2}{\nu + 3C_i R_0^2}.$$

We compute the discriminant of (3.28) (a degree-2 polynomial in R_0^2) in order to determine a saddle-node bifurcation. The discriminant of (3.28) is given by

$$\Delta = 36(\rho C_r + \nu C_i)^2 - 36(\rho^2 + \nu^2 - \Gamma^2)(C_r^2 + C_i^2).$$

Studying the polynomial (3.28) shows that the critical forcing amplitude is $\sqrt{\rho^2+\nu^2}$, and a subcritical bifurcation occurs if $\rho C_r + \nu C_i < 0$. The non-zero flat states A_{uni}^- and B_{uni}^- are created, which become A_{uni}^+ and B_{uni}^+ at a saddle-node bifurcation ($\Delta = 0$) when $\Gamma = \Gamma_d$, where

$$\Gamma_d = \sqrt{\rho^2 + \nu^2 - \frac{(\rho C_r + \nu C_i)^2}{C_r^2 + C_i^2}}.$$

A supercritical bifurcation occurs when $\rho C_r + \nu C_i > 0$.

3.4.3 Steady states with constant amplitude

Now we can look at steady uniform amplitude states of the form $A = R_0 e^{i(qX+\phi_1)}$, and $B = R_0 e^{i(-qX+\phi_2)}$, where R_0 and q are real, and ϕ_1 and ϕ_2 are the phases. These represent uniform patterns with wavenumber $1 + \epsilon q$ in $U(x)$. We substitute these solutions into equations (3.20)

$$\begin{aligned}
0 &= (\rho + i\nu)R_0 e^{i(qX+\phi_1)} + 2(\alpha + i\beta)q^2 R_0 e^{i(qX+\phi_1)} + iv_g q R_0 e^{i(qX+\phi_1)} \\
&\quad + 3CR_0^3 e^{i(qX+\phi_1)} + i\Gamma R_0 e^{i(qX-\phi_2)}. \\
0 &= (\rho + i\nu)R_0 e^{i(-qX+\phi_2)} + 2(\alpha + i\beta)q^2 R_0 e^{i(-qX+\phi_2)} + iv_g q R_0 e^{i(-qX+\phi_2)} \\
&\quad + 3CR_0^3 e^{i(-qX+\phi_2)} + i\Gamma R_0 e^{-i(qX+\phi_1)}.
\end{aligned}$$

In the above equations, $R_0 = 0$ is a solution. For $R_0 \neq 0$, we divide the system by R_0 as before and by $e^{i(qX+\phi_1)}$ (top equation) and $e^{i(-qX+\phi_2)}$ (bottom equation) to get a single equation:

$$0 = (\rho + i\nu) + 2(\alpha + i\beta)q^2 + iv_g q + 3CR_0^2 + i\Gamma e^{-i\Phi},$$

where $\Phi = \phi_1 + \phi_2$. The real and imaginary parts of the above equation are

$$\begin{aligned} \text{Re:} \quad & 0 = \rho + 2\alpha q^2 + 3C_r R_0^2 + \Gamma \sin\Phi. \\ \text{Im:} \quad & 0 = \nu + 2\beta q^2 + v_g q + 3C_i R_0^2 + \Gamma \cos\Phi. \end{aligned} \tag{3.29}$$

We eliminate Φ once again by using the equality $\cos^2\Phi + \sin^2\Phi = 1$ to give the following polynomial for R_0:

$$\begin{aligned} 0 = {} & 9(C_r^2 + C_i^2)R_0^4 + 6\left((\rho + 2\alpha q^2)C_r + (\nu + v_g q + 2\beta q^2)C_i\right)R_0^2 + (\rho + 2\alpha q^2)^2 \\ & + (\nu + v_g q + 2\beta q^2)^2 - \Gamma^2. \end{aligned} \tag{3.30}$$

This equation can be solved for R_0^2. Solving equations (3.29) for Φ gives

$$\tan\Phi = \frac{\rho + 2\alpha q^2 + 3C_r R_0^2}{\nu + v_g q + 2\beta q^2 + 3C_i R_0^2}.$$

The discriminant of (3.30), as a polynomial in R_0^2, is given by

$$\begin{aligned} \Delta = {} & 36\left((\rho + 2\alpha q^2)C_r + (\nu + v_g q + 2\beta q^2)C_i\right)^2 - 36\big((\rho + 2\alpha q^2)^2 + (\nu + v_g q + 2\beta q^2)^2 \\ & - \Gamma^2\big)(C_r^2 + C_i^2). \end{aligned}$$

Examination of the polynomial (3.30) shows that when the forcing amplitude Γ reaches $\sqrt{(\rho + 2\alpha q^2)^2 + (\nu + v_g q + 2\beta q^2)^2}$, a subcritical bifurcation occurs provided that $(\rho + 2\alpha q^2)C_r + (\nu + v_g q + 2\beta q^2)C_i < 0$. Spatially oscillatory states A_{sp}^- and B_{sp}^- are created, which turns into the A_{sp}^+ and B_{sp}^+ states at a saddle-node ($\Delta = 0$) bifurcation at $\Gamma = \Gamma_d$,

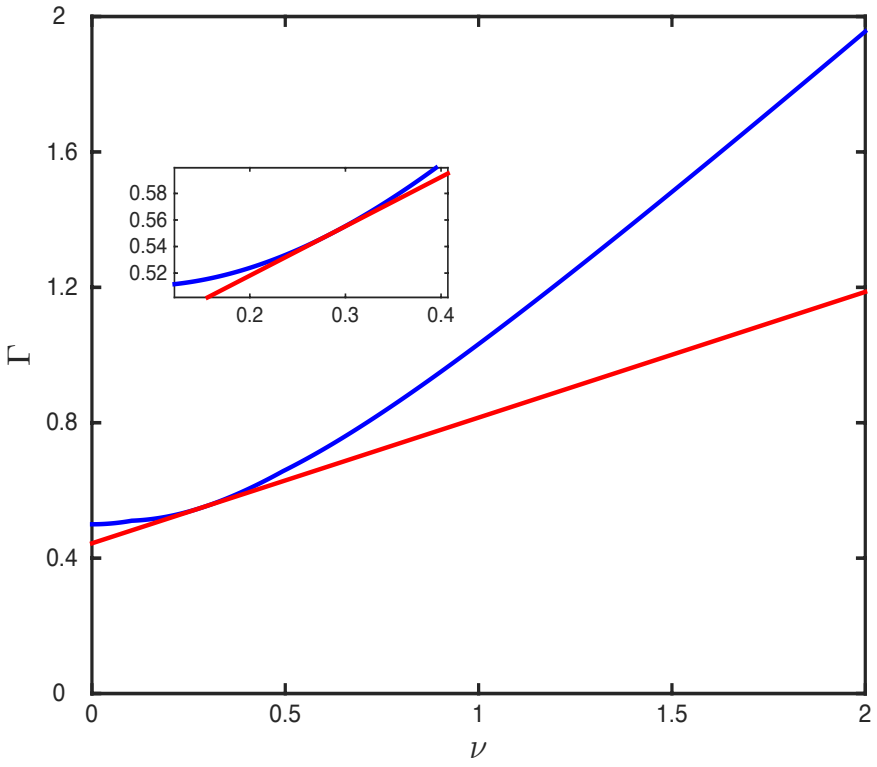

Figure 3.4: The $(\nu - \Gamma)$ parameter plane of the coupled FCGL equations (3.23) with $\rho = -0.5$, $\alpha = -0.5$, $\beta = 1$, and $v_g = -1$. The blue line is the the primary pitchfork bifurcation at Γ_c, and the red line is the saddle-node bifurcation at Γ_d

with

$$\Gamma_d = \sqrt{(\rho + 2\alpha q^2)^2 + (\nu + v_g q + 2\beta q^2)^2 - \frac{\left((\rho + 2\alpha q^2)C_r + (\nu + v_g q + 2\beta q^2)C_i\right)^2}{C_r^2 + C_i^2}}. \tag{3.31}$$

Putting $q = 0$ in the above expression recovers the results from section 3.4.2. Figure 3.4 shows equations (3.23) and (3.31) in the $(\nu - \Gamma)$ parameter plane of the coupled FCGL equations for $\nu > 0$. It also shows a close up of the intersection point, where the primary bifurcation changes from supercritical to subcritical at $(\rho + 2\alpha q^2)C_r + (\nu + v_g q + 2\beta q^2)C_i = 0$ with $\nu = 0.284$ (see Figure 3.5). Localized solutions can be found in the bistability region between Γ_c and Γ_d. Our investigation reveals that for $\nu < 0$ two preferred wavenumbers can be detected. However, in this section we study the case when

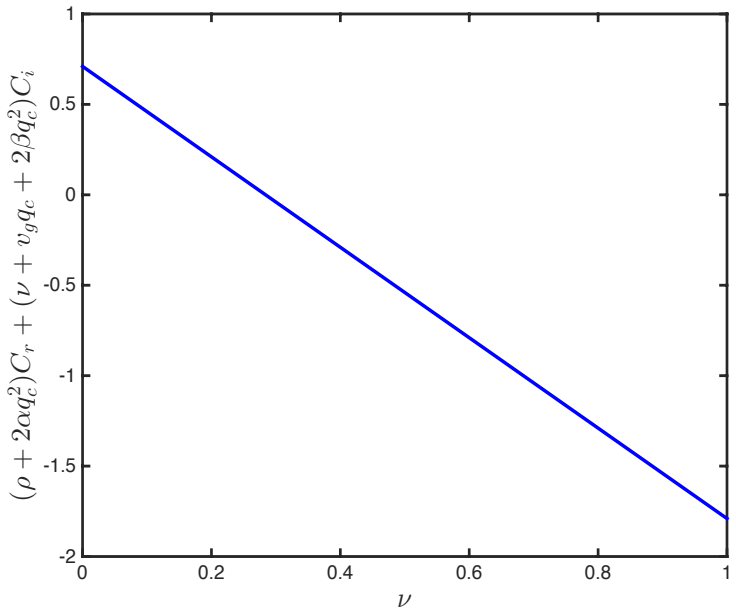

Figure 3.5: The point where the primary bifurcation of the coupled FCGL equations (3.23) changes from supercritical to subcritical with $\rho = -0.5$, $\alpha = -0.5$, $\beta = 1$, and $v_g = -1$, $q_c = 0.1$.

$\nu > 0$, and we leave the $\nu < 0$ case for future work.

3.4.4 Localized solutions

Without further simplifications (see section 3.5) analytic expansions for localized solutions of the coupled FCGL equations (3.20) are not possible. In this section we will present some numerical examples of stable spatially localized oscillons in the coupled FCGL equations found by using the time-stepping method. We use a pseudospectral method as in Chapter 2 with 128 Fourier modes.

We will take the following parameter values $\rho = -0.5$, $\nu = 2$, $\alpha = -0.5$, $\beta = 1$, and $C = -1 - 2.5i$. We solve the coupled equations on a domain size $L_X = 20\pi$. With group velocity $v_g = 0$, localized solutions have A and B the same, but otherwise A and B are unequal.

Figure 3.6 shows an example of a localized oscillon in the coupled FCGL equations with $v_g = -0.2$. As we increase the magnitude of the group velocity v_g, so that $v_g = -0.75$ (Figure 3.7), we can see that A and B start to move apart. Note that in Figure 3.6 and Figure 3.7 we fixed Γ to be $\Gamma = 1.462$. Figure 3.8 presents localized oscillons with $v_g = -1$, with $\Gamma = 1.4$ and $\Gamma = 1.438$. Solutions of the coupled FCGL equations are constant in time T as shown in Figure 3.9.

3.5 Reduction to the real Ginzburg–Landau equation

In this section we will reduce the coupled FCGL equations to the real Ginzburg–Landau equation close to the subcritical bifurcation from the zero solution to the flat state. The reduction from the coupled FCGL equations to the real Ginzburg–Landau equation was done by Riecke [67], in the supercritical case. Therefore, we take the complex conjugate of the second equation of (3.20), so the coupled FCGL equations become

$$\begin{aligned} \frac{\partial A}{\partial T} &= D_1 A + D_2 \frac{\partial^2 A}{\partial X^2} + v_g \frac{\partial A}{\partial X} + C(|A|^2 + 2|B|^2)A + i\Gamma \bar{B}. \\ \frac{\partial \bar{B}}{\partial T} &= \bar{D}_1 \bar{B} + \bar{D}_2 \frac{\partial \bar{B}}{\partial X^2} - v_g \frac{\partial \bar{B}}{\partial X} + \bar{C}(2|A|^2 + |B|^2)\bar{B} - i\Gamma A, \end{aligned} \tag{3.32}$$

For simplicity, we write $D_1 = \rho + i\nu$, and $D_2 = -2(\alpha + i\beta)$. In order to reduce the coupled FCGL equation to the real Ginzburg–Landau equation, we apply weakly nonlinear theory close to onset. The real Ginzburg–Landau equation has an exact sech solution, which can be used as a starting point to find spatially localized solutions in the PDE model.

We begin the analysis by scaling the forcing Γ as

$$\Gamma \to \Gamma_c \left(1 + \epsilon_2^2 \Gamma_2\right),$$

where $0 < \epsilon_2 \ll 1$, and Γ_c is the critical forcing at critical wavenumber q_c as shown in Figure 3.3, Γ_2 is the new bifurcation parameter. We expand the solution in powers of the

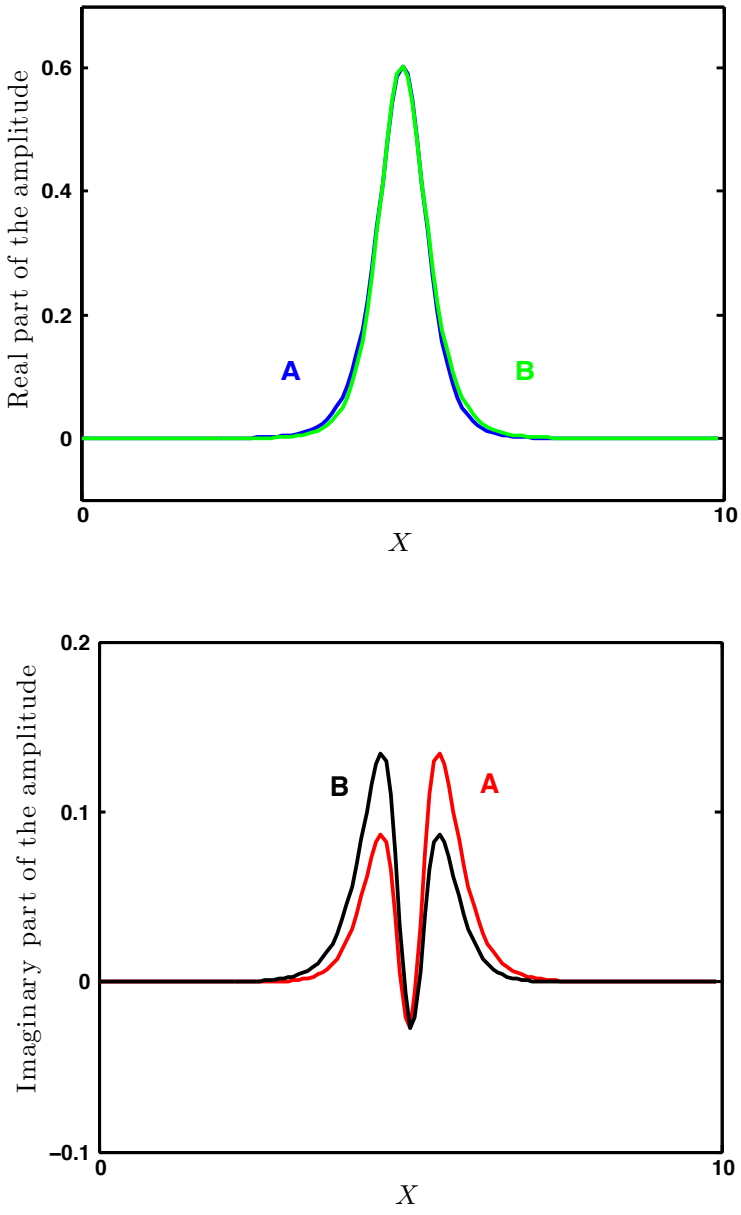

Figure 3.6: Solutions to the coupled FCGL equations (3.20) with $L_X = 20\pi$, $\rho = -0.5$, $\nu = 2$, $\alpha = -0.5$, $\beta = 1$, $v_g = -0.2$, $\Gamma = 1.462$, and $C = -1 - 2.5i$. For this choice of parameters, $\Gamma_c = 2.04$, $\Gamma_d = 1.21$. See Figure 3.10 for solutions of the PDE (3.1) at similar parameter values.

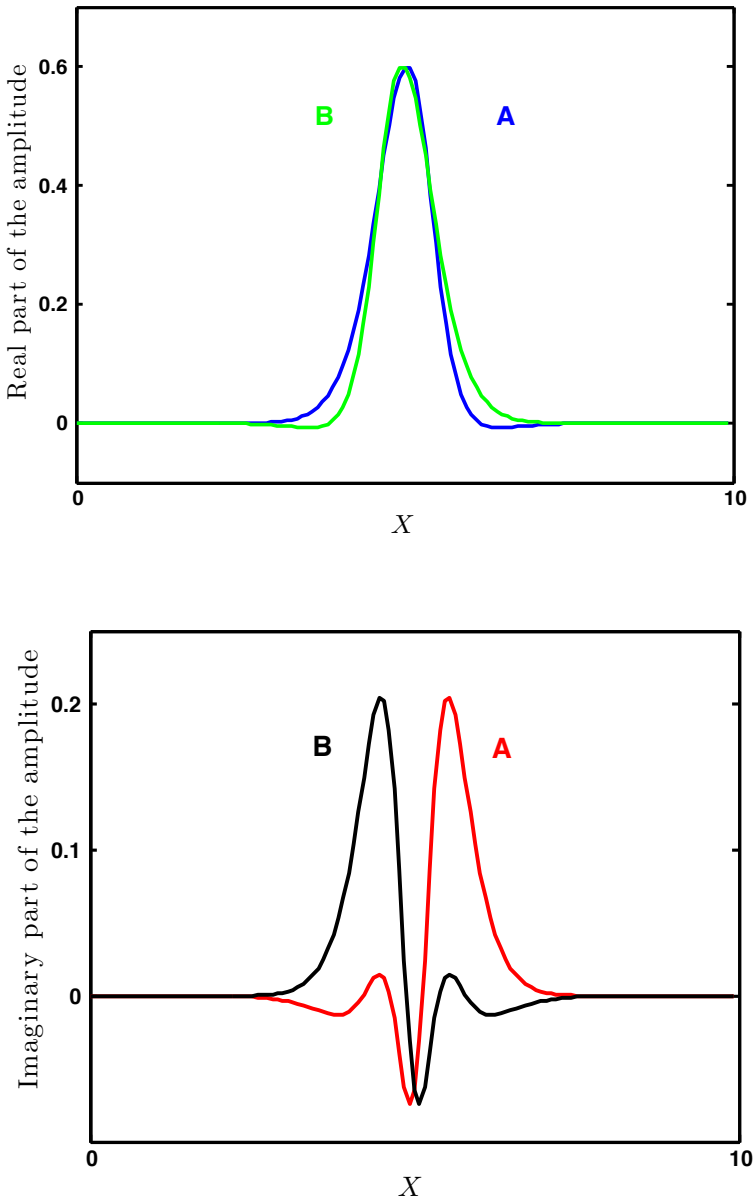

Figure 3.7: Solutions to the coupled FCGL equations (3.20). All parameters are the same as those in Figure 3.6 except the group velocity $v_g = -0.75$.

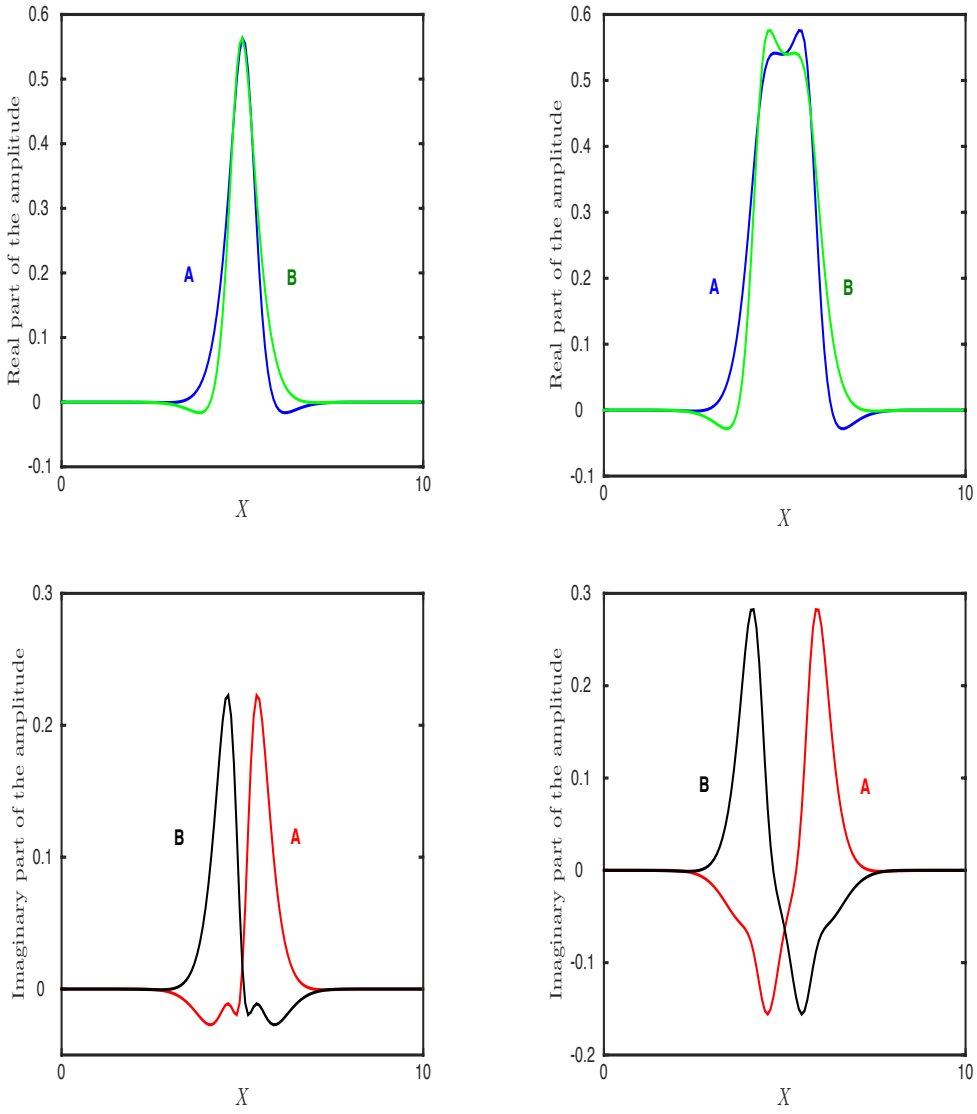

Figure 3.8: Examples of solutions to (3.20) with the same parameter values as in Figure 3.6, and $v_g = -1$. The left column is at $\Gamma = 1.4$, whereas the right column is with $\Gamma = 1.438$. We did not find stable oscillons where $\Gamma < 1.4$. The values of Γ_c and Γ_d are $\Gamma_c = 1.95$ and $\Gamma_d = 1.21$.

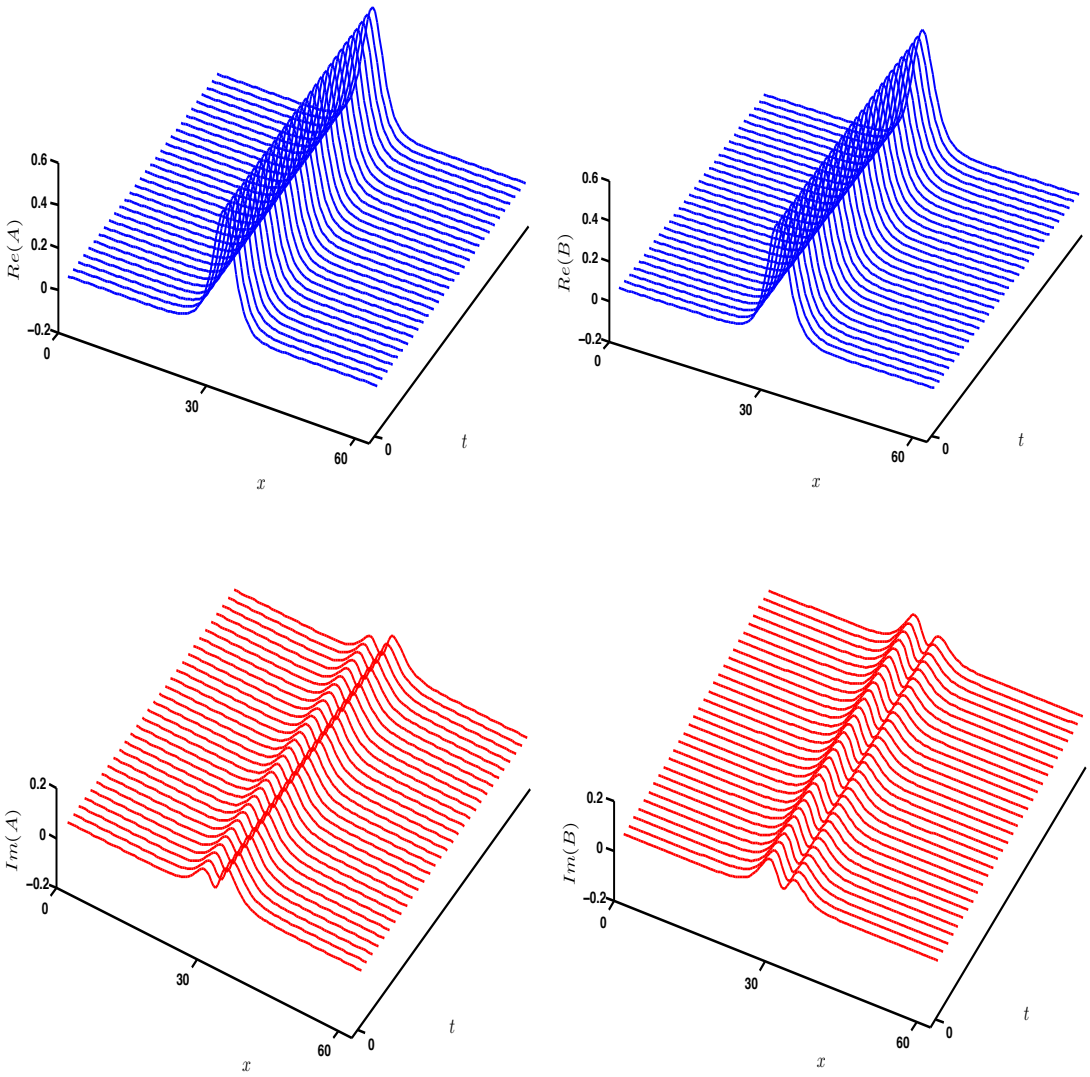

Figure 3.9: Example of solutions to (3.20) in space and time for one period of time $T = [0, 2\pi]$, which shows that the solutions are constant in time with $\Gamma = 1.4$. Other parameter values are the same as in Figure 3.6. The left column represents the amplitude A, whereas the right column represents the amplitude B.

new small parameter ϵ_2 as follows

$$\begin{bmatrix} A \\ \bar{B} \end{bmatrix} = \begin{bmatrix} \epsilon_2 A_1 + \epsilon_2^2 A_2 + \epsilon_2^3 A_3 + ... \\ \epsilon_2 \bar{B}_1 + \epsilon_2^2 \bar{B}_2 + \epsilon_2^3 \bar{B}_3 + ... \end{bmatrix}.$$

From section 3.4.1, the growth rate is real with frequency zero (locked to the forcing), so

$$\frac{\partial}{\partial T} \to \epsilon_2^2 \frac{\partial}{\partial \tilde{T}},$$

and the preferred wavenumber $q_c \neq 0$, so

$$\frac{\partial}{\partial X} \to \frac{\partial}{\partial X} + \epsilon_2 \frac{\partial}{\partial \tilde{X}}.$$

where $\tilde{X}$ and $\tilde{T}$ are very long and slow scales.

At $O(\epsilon_2)$, we have

$$\begin{aligned} 0 &= D_1 A_1 + D_2 \frac{\partial^2 A_1}{\partial X^2} + v_g \frac{\partial A_1}{\partial X} + i\Gamma_c \bar{B}_1, \\ 0 &= \bar{D}_1 \bar{B}_1 + \bar{D}_2 \frac{\partial \bar{B}_1}{\partial X^2} - v_g \frac{\partial \bar{B}_1}{\partial X} - i\Gamma_c A_1. \end{aligned}$$

We can solve the above system by assuming that

$$A_1 = \tilde{A}(\tilde{X}, \tilde{T}) e^{iq_c X}, \quad \text{and} \quad B_1 = \tilde{B}(\tilde{X}, \tilde{T}) e^{-iq_c X}.$$

At this order of ϵ_2 and by dropping tildes, the coupled FCGL equations become

$$\begin{aligned} 0 &= D_1 A - D_2 q_c^2 A + i v_g q_c A + i\Gamma_c \bar{B}, \\ 0 &= \bar{D}_1 \bar{B} - \bar{D}_2 q_c^2 \bar{B} - i v_g q_c \bar{B} - i\Gamma_c A. \end{aligned} \tag{3.33}$$

Or we can write the system as (see section 3.4.1)

$$\begin{bmatrix} D_1 + iv_g q_c - D_2 q_c^2 & i\Gamma_c \\ -i\Gamma_c & \bar{D}_1 - iv_g q_c - \bar{D}_2 q_c^2 \end{bmatrix} \begin{bmatrix} A \\ \bar{B} \end{bmatrix} = \begin{bmatrix} 0 \\ 0 \end{bmatrix}.$$

Since the determinant is zero (same as before), we get

$$\left(D_1 + iv_g q_c - D_2 q_c^2\right)\left(\bar{D}_1 - iv_g q_c - \bar{D}_2 q_c^2\right) - \Gamma_c^2 = 0. \tag{3.34}$$

We separate the real and imaginary parts of this equation. The real part of (3.34) is given by

$$|D_1|^2 + |D_2|^2 q_c^4 - 2v_g D_{2i} q_c^3 - \left(2\left(D_{2i}D_{1i} + D_{2r}D_{1r}\right) - v_g^2\right) q_c^2 + 2D_{1i} v_g q_c - \Gamma_c^2 = 0,$$

where $D_1 = D_{1r} + iD_{1i} = \rho + i\nu$ and $D_2 = D_{2r} + iD_{2i} = -2(\alpha + i\beta)$. We can solve this quartic equation in q_c. The forcing $\Gamma = \Gamma_c$ is the minimum at q_c as shown in Figure 3.3. Recall that the wavenumber q_c is positive if $D_{1i}v_g < 0$ and negative if $D_{1i}v_g > 0$, as in section 3.4.1.

From the first equation of (3.33) we get

$$\bar{B} = -\left(\frac{D_1 + iv_g q_c - D_2 q_c^2}{i\Gamma_c}\right) A, \tag{3.35}$$

By applying (3.34) or equivalently applying (3.23) from section 3.4.1, we get

$$\left|\frac{D_1 + iv_g q_c - D_2 q_c^2}{i\Gamma_c}\right|^2 = \frac{(D_1 + iv_g q_c - D_2 q_c^2)(\bar{D}_1 - iv_g q_c - \bar{D}_2 q_c^2)}{\Gamma_c^2} = 1.$$

Therefore, we can write

$$\bar{B} = Ae^{i\phi},$$

where ϕ is real, and

$$e^{i\phi} = -\left(\frac{D_1 + iv_g q_c - D_2 q_c^2}{i\Gamma_c}\right). \tag{3.36}$$

At $O(\epsilon_2^2)$, equations (3.32) become

$$\begin{aligned} 0 &= D_1 A_2 + D_2 \frac{\partial^2 A_2}{\partial X^2} + v_g \frac{\partial A_2}{\partial X} + i\Gamma_c \bar{B}_2 + v_g \frac{\partial A}{\partial \tilde{X}} e^{iq_c X} + 2iD_2 q \frac{\partial A}{\partial \tilde{X}} e^{iq_c X}. \\ 0 &= \bar{D}_1 \bar{B}_2 + \bar{D}_2 \frac{\partial^2 \bar{B}_2}{\partial X^2} - v_g \frac{\partial \bar{B}_2}{\partial X} - i\Gamma_c A_2 - v_g \frac{\partial \bar{B}}{\partial \tilde{X}} e^{iq_c X} + 2i\bar{D}_2 q_c \frac{\partial \bar{B}}{\partial \tilde{X}} e^{iq_c X}. \end{aligned} \tag{3.37}$$

At this stage we might need to define a linear operator in order to impose the solvability condition. We chose to do the weakly nonlinear theory here without studying the linear operator, but by using a quicker method that we show next. We solve this system effectively by setting

$$A_2 \to A_2 e^{iq_c X} \quad \text{and} \quad \bar{B}_2 \to \bar{B}_2 e^{iq_c X},$$

to focus attention on $e^{iq_c X}$ component of (3.37), the only component to have an inhomogeneous part, and for which the linear operator is singular. Substituting these expressions for A_2, $\bar{B}_2$, and $\bar{B}$ into the above equations leads to the following

$$\begin{bmatrix} D_1 + iv_g q_c - D_2 q_c^2 & i\Gamma_c \\ -i\Gamma_c & \bar{D}_1 - iv_g q_c - \bar{D}_2 q_c^2 \end{bmatrix} \begin{bmatrix} A_2 \\ \bar{B}_2 \end{bmatrix} + \begin{bmatrix} v_g + 2iq_c D_2 \\ \left(-v_g + 2iq_c \bar{D}_2\right) e^{i\phi} \end{bmatrix} \frac{\partial A}{\partial \tilde{X}} = \begin{bmatrix} 0 \\ 0 \end{bmatrix}, \tag{3.38}$$

where $e^{i\phi} = -\left(\frac{D_1 + iv_g q_c - D_2 q_c^2}{i\Gamma_c}\right)$. We know that the determinant of the square matrix is zero since it is a singular matrix. We write

$$\begin{aligned} 0 &= (D_1 + iv_g q_c - D_2 q_c^2) A_2 + i\Gamma_c \bar{B}_2 + (v_g + 2iq_c D_2) \frac{\partial A}{\partial \tilde{X}}. \\ 0 &= (\bar{D}_1 - iv_g q_c - \bar{D}_2 q_c^2) \bar{B}_2 - i\Gamma_c A_2 - \left(\frac{(-v_g + 2iq_c \bar{D}_2)(D_1 + iv_g q_c - D_2 q_c^2)}{i\Gamma_c}\right) \frac{\partial A}{\partial \tilde{X}}. \end{aligned} \tag{3.39}$$

We multiply the first equation for A by $i\Gamma_c$ and the second equation for $\bar{B}$ by $(D_1+iv_gq_c-D_2q_c^2)$, which is effectively the left eigenfunction of the matrix, and then add them. This is similar to applying the solvability condition. Therefore, we end up with

$$\left(i\Gamma_c(v_g+2iq_cD_2)+\frac{(v_g-2iq_c\bar{D}_2)(D_1+iv_gq_c-D_2q_c^2)^2}{i\Gamma_c}\right)\frac{\partial A}{\partial\tilde{X}}=0. \tag{3.40}$$

Since $\frac{\partial A}{\partial\tilde{X}}\neq 0$, we need

$$-(v_g+2iq_cD_2)(\bar{D}_1-iv_gq_c-\bar{D}_2q_c^2)+(v_g-2iq_c\bar{D}_2)(D_1+iv_gq_c-D_2q_c^2)=0,$$

in order to make progress. This is the same as (3.24), which is equivalent to taking $\frac{d}{dq}$ of the relationship (3.34), at the minimum q_c, (see Figure 3.3).

Since the square matrix in (3.38) is singular, the determinant is zero and zero is an eigenvalue. Thus, the left eigenvector of zero is $\begin{bmatrix}\bar{D}_1-iv_gq_c-\bar{D}_2q_c^2\\ i\Gamma_c\end{bmatrix}$.

From the top line of (3.39), we have

$$\bar{B}_2=-\left(\frac{(v_g+2iq_cD_2)}{i\Gamma_c}\frac{\partial A}{\partial\tilde{X}}+\frac{(D_1+iv_gq_c-D_2q_c^2)}{i\Gamma_c}A_2\right).$$

The solution is

$$\begin{bmatrix}A_2\\ \bar{B}_2\end{bmatrix}=\begin{bmatrix}A_2\\ -\frac{(v_g+2iq_cD_2)}{i\Gamma_c}\frac{\partial A}{\partial\tilde{X}}-\frac{(D_1+iv_gq_c-D_2q_c^2)}{i\Gamma_c}A_2\end{bmatrix}.$$

Thus, we have A_2 to be arbitrary at this order of ϵ. It is determined at higher order of ϵ but since we are not going to higher order [69], we take

$$A_2=0,\quad \text{and}\quad \bar{B}_2=-\frac{(v_g+2iq_cD_2)}{i\Gamma_c}\quad\frac{\partial A_1}{\partial\tilde{X}},$$

or, restoring the e^{iq_cX}, we have at this order of ϵ_2

$$A_2 = 0, \quad \text{and} \quad \bar{B}_2 = -\frac{(v_g + 2iq_cD_2)}{i\Gamma_c} \quad \frac{\partial A}{\partial \tilde{X}} \quad e^{iq_cX}.$$

At $O(\epsilon_2^3)$ the problem has the following structure (with $A_2 = 0$):

$$\begin{aligned}
\frac{\partial A_1}{\partial \tilde{T}} &= D_1A_3 + D_2\frac{\partial^2 A_3}{\partial X^2} + v_g\frac{\partial A_3}{\partial X} + i\Gamma_c\bar{B}_3 + D_2\frac{\partial^2 A_1}{\partial \tilde{X}^2} + i\Gamma_c\Gamma_2\bar{B}_1 \\
&\quad + C(|A_1|^2 + 2|B_1|^2)A_1, \\
\frac{\partial \bar{B}_1}{\partial \tilde{T}} &= \bar{D}_1\bar{B}_3 + \bar{D}_2\frac{\partial^2 \bar{B}_3}{\partial X^2} - v_g\frac{\partial \bar{B}_3}{\partial X} - i\Gamma_cA_3 + 2\bar{D}_2\frac{\partial^2}{\partial X\partial \tilde{X}}\bar{B}_2 - v_g\frac{\partial \bar{B}_2}{\partial \tilde{X}} \\
&\quad + \bar{D}_2\frac{\partial^2 \bar{B}_1}{\partial \tilde{X}^2} - i\Gamma_c\Gamma_2A_1 + \bar{C}(2|A_1|^2 + |B_1|^2)B_1.
\end{aligned} \tag{3.41}$$

We write A_3 and $\bar{B}_3$ as Fourier modes with spatial dependence e^{iq_cX}:

$$A_3 \to A_3e^{iq_cX} \quad \text{and} \quad \bar{B}_3 \to \bar{B}_3e^{iq_cX}.$$

As at $O(\epsilon_2^2)$, we multiply the first equation for A by $i\Gamma_c$ and the second equation for $\bar{B}$ by $(D_1 + iv_gq_c - D_2q_c^2)$, and then add them. The coupled FCGL equations (3.41) become

$$\begin{aligned}
i\Gamma_c\frac{\partial A_1}{\partial \tilde{T}} + \left(D_1 + iv_gq_c - D_2q_c^2\right)\frac{\partial \bar{B}_1}{\partial \tilde{T}} &= i\Gamma_cD_2\frac{\partial^2 A_1}{\partial \tilde{X}^2} - \Gamma_c^2\Gamma_2\bar{B}_1 + i\Gamma_cC\left(|A_1|^2 + 2|B_1|^2\right)A_1 \\
&\quad + 2\left(D_1 + iv_gq_c - D_2q_c^2\right)\bar{D}_2\frac{\partial^2}{\partial X\partial \tilde{X}}\bar{B}_2 \\
&\quad - \left(D_1 + iv_gq_c - D_2q_c^2\right)\left(v_g\frac{\partial \bar{B}_2}{\partial \tilde{X}} - \bar{D}_2\frac{\partial^2 \bar{B}_1}{\partial \tilde{X}^2}\right) \\
&\quad - i\Gamma_c\Gamma_2\left(D_1 + iv_gq_c - D_2q_c^2\right)A_1 \\
&\quad + \bar{C}\left(D_1 + iv_gq_c - D_2q_c^2\right)\left(2|A_1|^2 + |B_1|^2\right)B_1.
\end{aligned} \tag{3.42}$$

Substituting A_1, B_1, B_2 into the above equation, dividing by the common factor of e^{iq_cX},

and dropping tilde in A_1 and B_1 gives

$$\begin{aligned}\left(i\Gamma_c - \frac{(D_1 + iv_g q_c - D_2 q_c^2)^2}{i\Gamma_c}\right)\frac{\partial A}{\partial \tilde{T}} &= -2i\Gamma_c\Gamma_2\left(D_1 + iv_g q_c - D_2 q_c^2\right)A \\ &+ \left(i\Gamma_c D_2 - \frac{\bar{D}_2\left(D_1 + iv_g q_c - D_2 q_c^2\right)^2}{i\Gamma_c}\right)\frac{\partial^2 A}{\partial \tilde{X}^2} \\ &- \left(\frac{2q_c\bar{D}_2(D_1 + iv_g q_c - D_2 q_c^2)(v_g + 2iq_c D_2)}{\Gamma_c}\right. \\ &\left. - \frac{v_g(D_1 + iv_g q_c - D_2 q_c^2)(v_g + 2iq_c D_2)}{i\Gamma_c}\right)\frac{\partial^2 A}{\partial \tilde{X}^2} \\ &+ 3\left(i\Gamma_c C - \frac{(D_1 + iv_g q_c - D_2 q_c^2)^2\bar{C}}{i\Gamma_c}\right)|A|^2 A. \end{aligned} \tag{3.43}$$

Using $D_1 + iv_g q_c - D_2 q_c^2 = -i\Gamma_c e^{i\phi}$, leads to

$$\begin{aligned}\left(i\Gamma_c - i\Gamma_c e^{2i\phi}\right)\frac{\partial A}{\partial \tilde{T}} &= -2\Gamma_c^2\Gamma_2 e^{i\phi}A + \left(i\Gamma_c D_2 - i\Gamma_c\bar{D}_2 e^{2i\phi}\right)\frac{\partial^2 A}{\partial \tilde{X}^2} \\ &+ \left(2iq_c\bar{D}_2(v_g + 2iq_c D_2) + v_g(v_g + 2iq_c D_2)\right)\frac{\partial^2 A}{\partial \tilde{X}^2}e^{i\phi} \\ &+ 3\left(i\Gamma_c C - i\Gamma_c e^{2i\phi}\bar{C}\right)|A|^2 A.\end{aligned}$$

Applying the relationships (3.34), and (3.36) to the parameter value in the left hand side gives

$$\frac{-\Gamma^2 - (D_1 + iv_g q_c - D_2 q_c^2)^2}{i\Gamma_c} = \frac{-(D_1 + iv_g q_c - D_2 q_c^2)(\bar{D}_1 + D_1 - (\bar{D}_2 + D_2)q_c^2)}{i\Gamma_c}.$$

Therefore, we multiply all terms in (3.43) by

$$\frac{-i\Gamma_c}{(D_1 + iv_g q_c - D_2 q_c^2)(\bar{D}_1 + D_1 - (\bar{D}_2 + D_2)q_c^2)}.$$

Accordingly, equation (3.41) reduces to the real Ginzburg–Landau equation

$$\frac{\partial A}{\partial \tilde{T}} = \frac{1}{\bar{D}_1 + D_1 - (\bar{D}_2 + D_2)q_c^2}\Big[-2\Gamma_c^2\Gamma_2 A + \Big((\bar{D}_1 - iv_g q_c - \bar{D}_2 q_c^2)D_2 + (D_1 + iv_g q_c - D_2 q_c^2)\bar{D}_2 + 2iv_g\bar{D}_2 q_c - 2iv_g D_2 q_c - 4|D_2|^2 q_c^2 - v_g^2\Big)\frac{\partial^2 A}{\partial \tilde{X}^2} + 3\left((\bar{D}_1 - iv_g q_c - \bar{D}_2 q_c^2)C + (D_1 + iv_g q_c - D_2 q_c^2)\bar{C}\right)|A|^2 A\Big].$$

We return values of D_1 and D_2, so the real Ginzburg–Landau equation becomes

$$\frac{\partial A}{\partial \tilde{T}} = \frac{1}{2\rho + 4\alpha q_c^2}\Big[-2\Gamma_c^2\Gamma_2 A - 4\Big(\rho\alpha + \nu\beta + \frac{v_g^2}{4} + 3v_g\beta q_c + 6(\alpha^2 + \beta^2)q_c^2\Big)\frac{\partial^2 A}{\partial \tilde{X}^2} + 6\left(\rho + 2\alpha q_c^2\right)\Big(C_r + \frac{(\nu + v_g q_c + 2\beta q_c^2)\, C_i}{(\rho + 2\alpha q_c^2)}\Big)|A|^2 A\Big].$$

We calculate the parameters in the amplitude equation above to give the real Ginzburg–Landau equation:

$$\begin{aligned}\frac{\partial A}{\partial \tilde{T}} = {} & \frac{-\Gamma_c^2\Gamma_2}{\rho + 2\alpha q_c^2}A - \frac{4\rho\alpha + 4\nu\beta + v_g^2 + 12v_g\beta q_c + 24(\alpha^2 + \beta^2)q_c^2}{2\rho + 4\alpha q_c^2}\quad \frac{\partial^2 A}{\partial \tilde{X}^2} \\ & + 3\Big(C_r + \frac{\nu + v_g q_c + 2\beta q_c^2}{\rho + 2\alpha q_c^2}C_i\Big)|A|^2 A.\end{aligned} \tag{3.44}$$

Flat solutions of this equation are consistent with the simple constant solutions of equation (3.30). The real Ginzburg–Landau equation is known to have steady sech solutions, so we can find localized solutions of (3.41) in terms of hyperbolic functions. This leads to an approximate oscillon solution of (3.41) of the form

$$A(\tilde{X}) = \sqrt{\frac{2\Gamma_c^2\Gamma_2}{h_1}}\,\mathrm{sech}\left(\sqrt{\frac{\Gamma_c^2\Gamma_2}{h_2}}\tilde{X}\right)e^{i\phi_1}, \tag{3.45}$$

where ϕ_1 is an arbitrary phase and

$$h_1 = 3\left((\rho + 2\alpha q_c^2)C_r + (\nu + v_g q_c + 2\beta q_c^2)C_i\right),$$
$$h_2 = -2\left(\rho\alpha + \nu\beta + \frac{v_g^2}{4} + v_g\beta q_c + 6(\alpha^2+\beta^2)q_c^2\right),$$

where Γ_2, h_1 and h_2 must all have the same sign for the sech solution to exist. From the linear theory we have $\bar{B}(\tilde{X}) = A(\tilde{X})e^{i\phi}$, which gives

$$\bar{B}(\tilde{X}) = \sqrt{\frac{2\Gamma_c^2\Gamma_2}{h_1}}\text{sech}\left(\sqrt{\frac{\Gamma_c^2\Gamma_2}{h_2}}\tilde{X}\right)e^{i(\phi_1+\phi)}, \tag{3.46}$$

At leading order

$$A(X) = \epsilon_2 A_1(X) = \sqrt{\frac{2\Gamma_c(\Gamma-\Gamma_c)}{h_1}}\text{sech}\left(\sqrt{\frac{\Gamma_c(\Gamma-\Gamma_c)}{h_2}}X\right)e^{i(q_cX+\phi_1)}, \tag{3.47}$$

and

$$B(X) = \epsilon_2 B_1(X) = \sqrt{\frac{2\Gamma_c(\Gamma-\Gamma_c)}{h_1}}\text{sech}\left(\sqrt{\frac{\Gamma_c(\Gamma-\Gamma_c)}{h_2}}X\right)e^{i(q_cX+\phi_1+\phi)}, \tag{3.48}$$

provided $\Gamma < \Gamma_c$, $h_1 < 0$, and $h_2 < 0$. Note that in the PDE (3.1) we have the assumption

$$U = \epsilon U_1 = \epsilon(A(X,T)e^{ix} + B(X,T)e^{-ix})e^{it},$$

which becomes

$$U = \sqrt{\frac{2\epsilon^2\Gamma_c(\Gamma-\Gamma_c)}{h_1}}\text{sech}\left(\sqrt{\frac{\epsilon^2\Gamma_c(\Gamma-\Gamma_c)}{h_2}}x\right)\cos((1+\epsilon q_c)x + \frac{\phi}{2} + \phi_1)e^{i(t-\frac{\phi}{2})}.$$

Using table 3.1, we return all parameter values. Therefore the spatially localized oscillon

is given approximately by

$$U_{loc}(x,t) = 2\sqrt{\frac{F_c(F-F_c)}{8h_1^*}}\text{sech}\left(\sqrt{\frac{F_c(F-F_c)}{16h_2^*}}x\right)\cos((1+\epsilon q_c)x + \frac{\phi}{2} + \phi_1)e^{i(t-\frac{\phi}{2})},$$

again provided $F < F_c$, and where

$$\begin{aligned}
h_1^* &= 3\left((\mu-\alpha+\gamma+2\alpha(\epsilon q_c)^2)C_r + (\omega-\beta+\delta-1+(-2\beta+4\delta)\epsilon q_c + 2\beta(\epsilon q_c)^2)C_i\right), \\
h_2^* &= -2\Big(\alpha(\mu-\alpha+\gamma) + \beta(\omega-\beta+\delta-1) + \frac{(-2\beta+4\delta)^2}{4} + 3\beta(-2\beta+4\delta)\epsilon q_c \\
&\quad + 6(\alpha^2+\beta^2)(\epsilon q_c)^2\Big),
\end{aligned}$$

where q_c and Γ_c can be determined from (3.34), so that

$$U_{loc}(x,t) = 2\sqrt{\frac{F_c(F-F_c)}{8h_1^*}}\text{sech}\left(\sqrt{\frac{F_c(F-F_c)}{16h_2^*}}x\right)\cos(k_c x + \frac{\phi}{2} + \phi_1)e^{i(t-\frac{\phi}{2})}, \quad (3.49)$$

where h_1^* and h_2^* become (since $k_c = 1+\epsilon q_c$):

$$\begin{aligned}
h_1^* &= 3\Big((\mu-\alpha+\gamma+2\alpha(k_c-1)^2)C_r + (\omega-\beta+\delta-1+(-2\beta+4\delta)(k_c-1) \\
&\quad + 2\beta(k_c-1)^2)C_i\Big), \\
h_2^* &= -2\Big(\alpha(\mu-\alpha+\gamma) + \beta(\omega-\beta+\delta-1) + \frac{(-\beta+2\delta)^2}{+}3\beta(-2\beta+4\delta)(k_c-1) \\
&\quad + 6(\alpha^2+\beta^2)(k_c-1)^2\Big).
\end{aligned}$$

This solution U_{loc} gives an approximate solution of the model PDE (3.1) valid in the limit of weak dissipation, weak detuning, weak forcing, small group velocity, and small amplitude. In the next section we compare the approximate solution U_{loc} with a numerical solution of the PDE model.

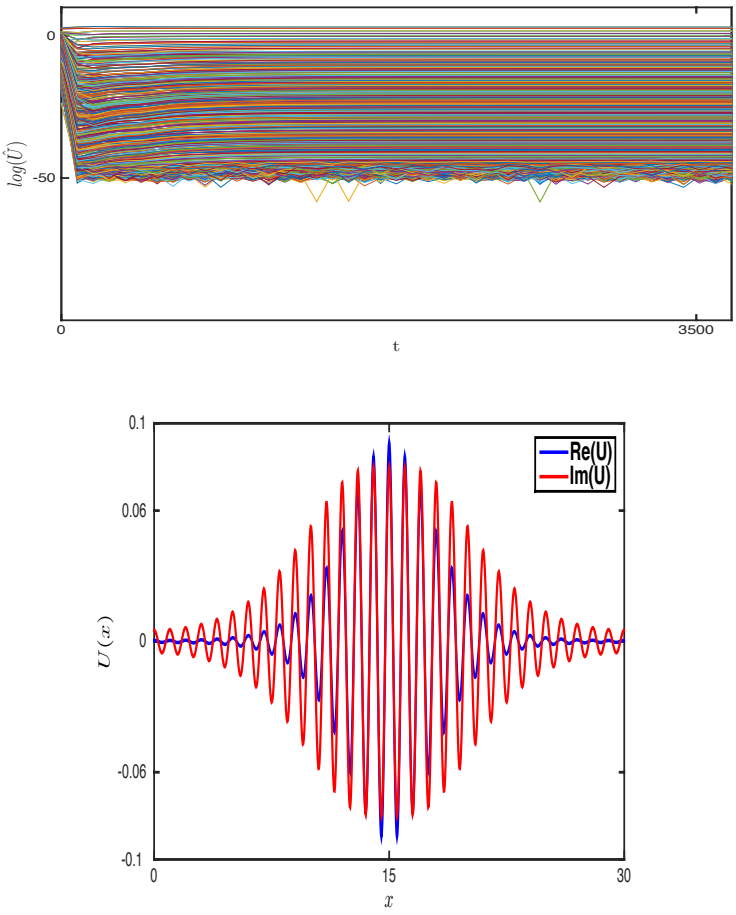

Figure 3.10: Numerical simulation of stable localized oscillon to (3.1) found by time-stepping, with $\epsilon = 0.1$, $\mu = -0.255$, $\alpha = -0.5$, $\beta = 1$, $\gamma = -0.25$, $\delta = 0.4995$, $\nu = 2$, $\omega = 1 + \beta - \delta + \epsilon^2\nu = 1.52$, $C = -1 - 2.5i$, and $F = 0.0585$. The top panel shows the time evlution of the Fourier modes, where $\hat{U}$ is the Fourier transform of U.

3.6 Numerical results

Similar to the methodology we used in Chapter 2, we present numerical simulations of the PDE model (3.1) by continuation and time-stepping. For the time-stepping we use a domain size of $L_x = 60\pi$ and $N_x = 1024$ points. The localized solution that we used as a starting point for continuation is plotted in Figure 3.10.

Using AUTO, we represent solutions by a truncated Fourier series in time with frequencies -3, -1, 1 and 3. Note that the choice of these frequencies comes from

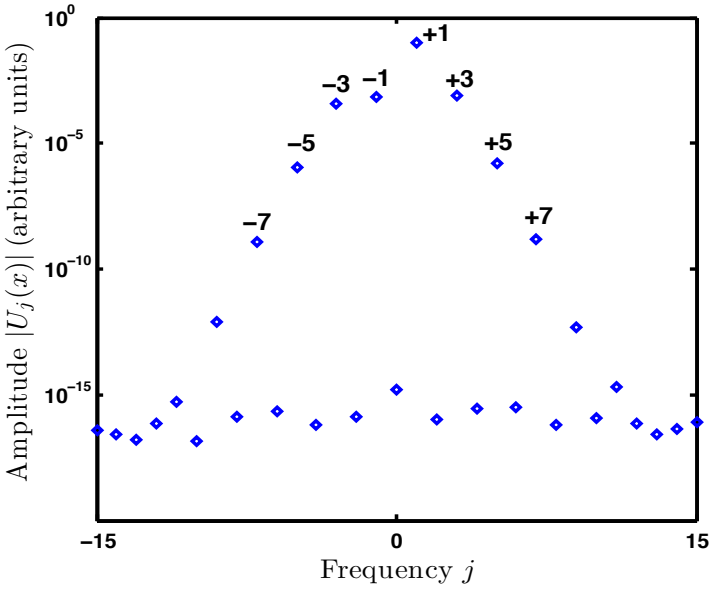

Figure 3.11: Amplitudes of the different frequencies when expanding the solution of Figure 3.10 in a Fourier series in time: frequency $+1$ is strongest, followed by frequencies -3, -1 and $+3$, as expected.

the choice of parameters: the linearized PDE at wavenumber ± 1 looks like $\frac{\partial u}{\partial t} = iu$, so the strongest Fourier component of U looks like e^{it}; then putting $u = e^{it}$ into the forcing $Re(e^{it})\cos(2t)$ generates the frequencies -3, -1, 1 and 3, as described in Chapter 2. We also checked numerically that the frequencies dominate (see Figure 3.11).

The bifurcation diagram of (3.1) as computed by AUTO is given in Figure 3.12. The transition between the stable zero state to the unstable pattern occurs at the bifurcation point $F_c = 0.08205$. The saddle-node point where unstable periodic patterns become stable periodic patterns is $F_d = 0.056$. The bistability region where we look for the branch of localized states is between F_c and F_d. The branch of localized patterns bifurcates from the branch of periodic patterns at $F_c^* = 0.07706$, which is away from F_c because of the finite domain. Stable localized patterns are located between $F_1 = 0.05695$ and $F_2 = 0.05987$, but the snaking region is small.

Examples of localized solutions along the localization curve in Figure 3.12 are given in

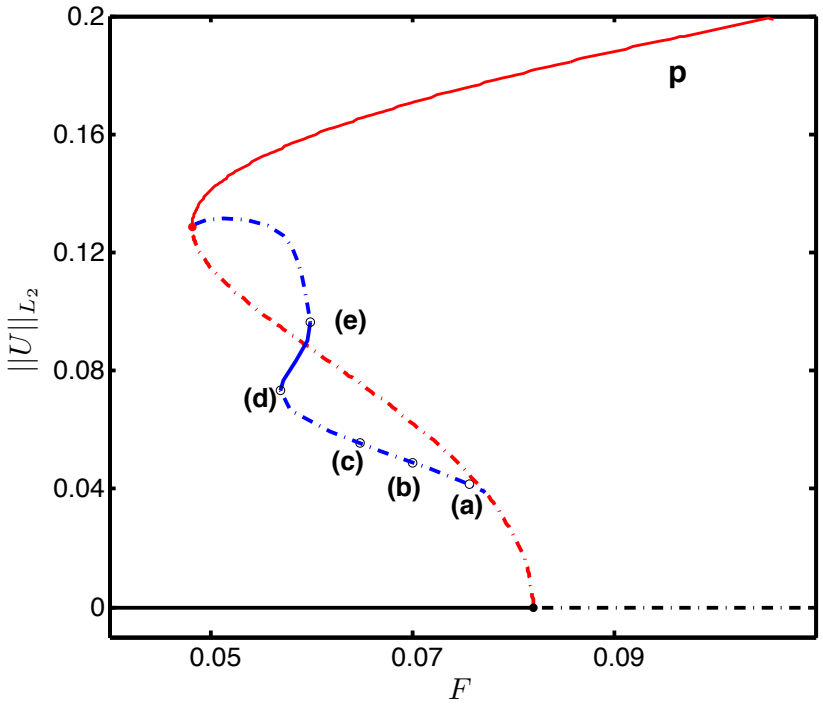

Figure 3.12: Bifurcation diagram of (3.1) in the weak damping regime with parameters as in Figure 3.10. The bistability region is between $F_c = 0.08205$ and $F_d = 0.056$. The bifurcation point $F_c^* = 0.07706$.

Figure 3.13 and 3.14 (a)-(e). Near the point F_c^* where the localized curve bifurcates, the localized solutions look like the periodic patterns: small amplitude oscillations which are not very localized (see Figure 3.13 (a)). As we go along the localization curve, the amplitude increases and the unstable oscillons become more localized (Figure 3.13 (a)-(c)). At $F_1 = 0.05695$, the localized oscillons stabilize (Figure 3.14 (d)) and then they lose stability again at $F_2 = 0.05987$ (Figure 3.14 (e)). Beyond F_c^*, the localization curve connects to the pattern branch close to the saddle-node point F_d without further snaking. The right panel of Figure 3.14 shows a typical periodic pattern.

Figure 3.15 shows the approximate solutions from (3.49), which we derived in the previous section, of the envelope equations for three different values of the forcing amplitude, starting close to the bifurcation point F_c^*. We can compare the numerical solutions of the model PDE in Figure 3.13 with the asymptotic solutions of the real

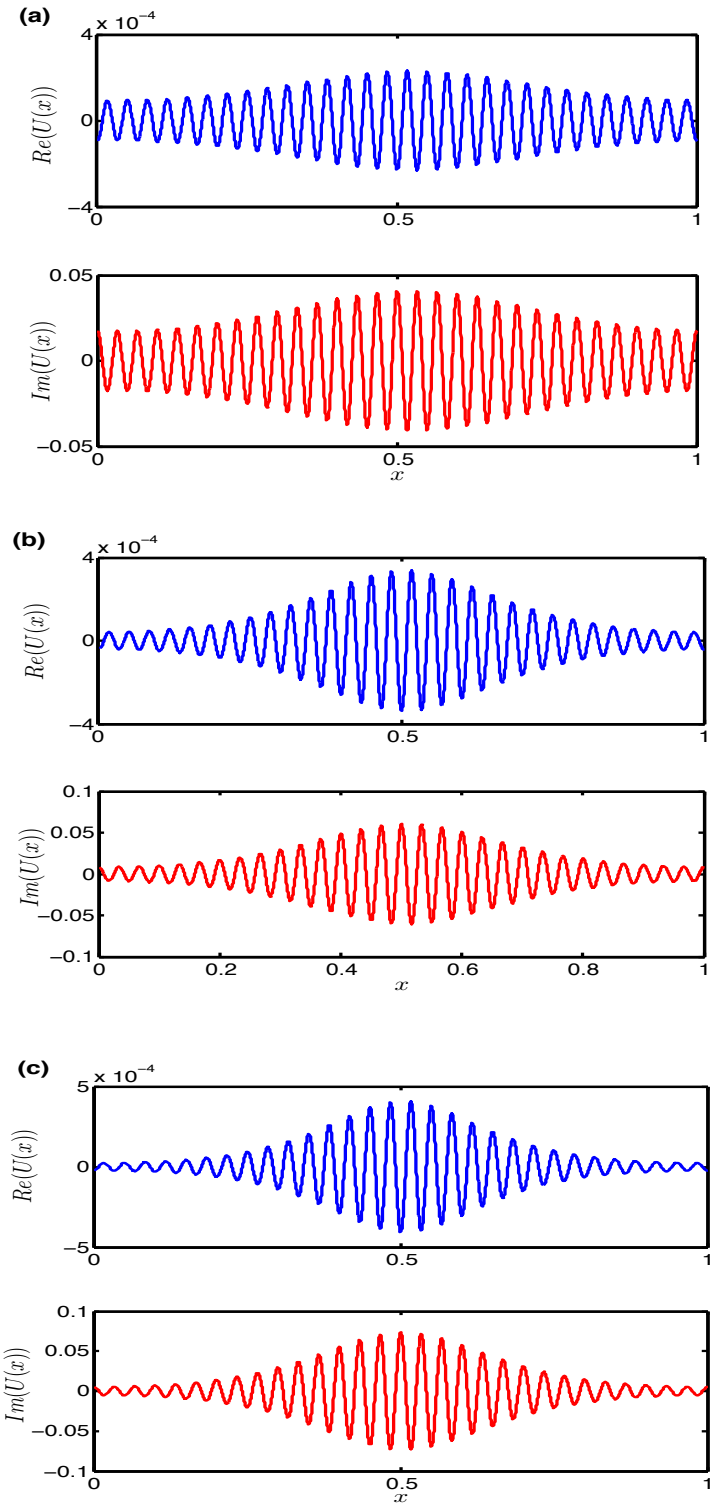

Figure 3.13: Solutions (a)-(c) along the bifurcation diagram in Figure 3.12. The blue curve represents the real part of $U(x)$, and red curve represents the imaginary part of $U(x)$. At (a) $F = 0.07569$, (b) $F = 0.07013$, and at (c) $F = 0.06486$.

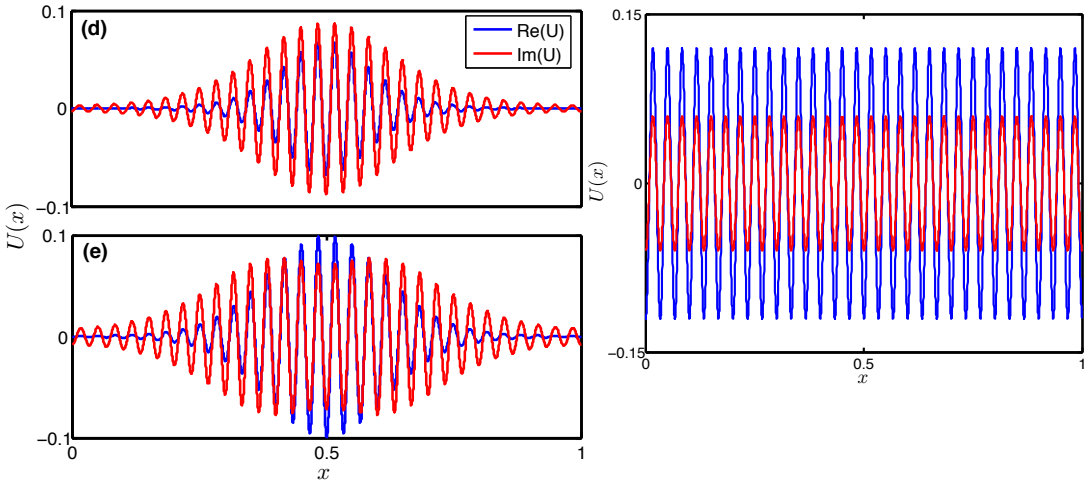

Figure 3.14: Solutions to (3.1) along the bifurcation diagram 3.12, (d) is at $F = 0.05695$ and (e) is at $F = 0.05987$. Right panel shows an example of the pattern on the upper branch.

Ginzburg–Landau equation in Figure 3.15. The difference between the two figures is because in an infinite domain the localization curve bifurcates from the zero state ($F_c^* = F_c$), while in a finite domain the bifurcation point is on the periodic branch ($F_c^* < F_c$). Solutions on the localization curve close to this bifurcation point are like spatially periodic solutions with small attenuation of the amplitude of the oscillations. As we go away from the bifurcation point, the attenuation grows until it is comparable to the amplitude of the periodic pattern and a clearly localized solution appears.

As we increase the domain size, the localization of the asymptotic solution becomes clearer. In the next section we will discuss the effect of the domain size for finding spatially periodic patterns in the model PDE (3.1).

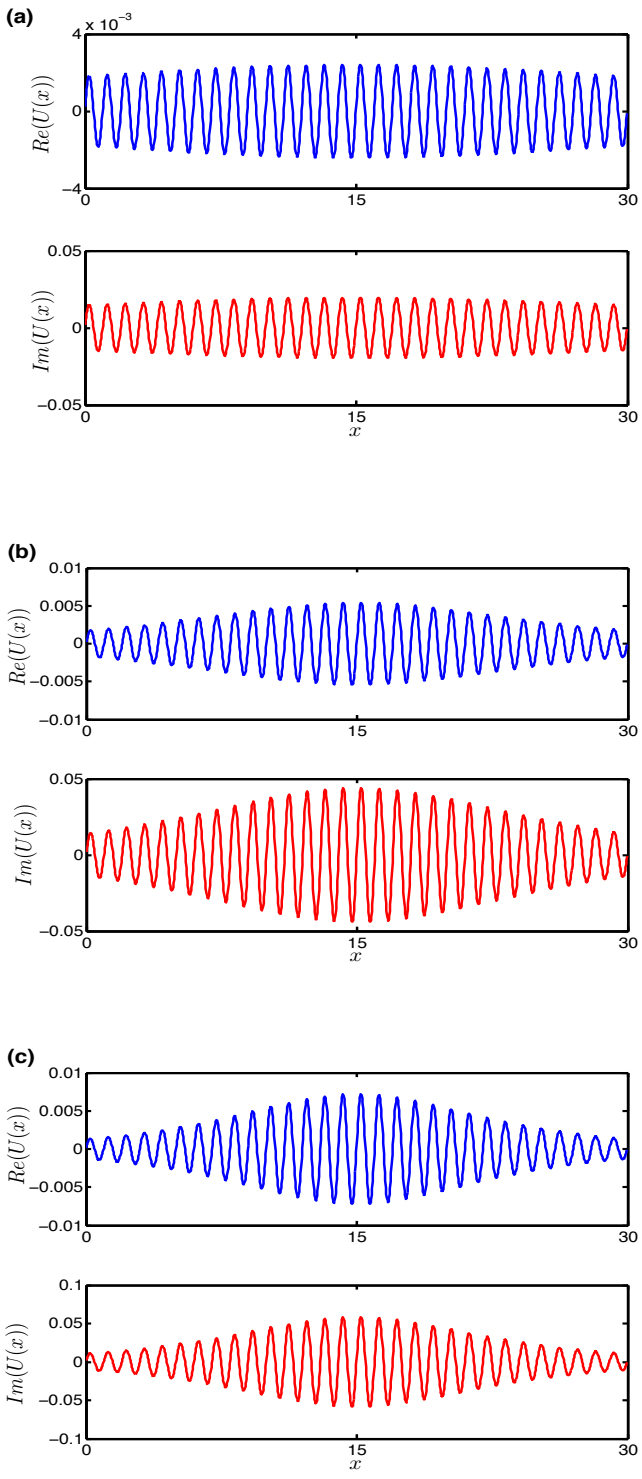

Figure 3.15: Asymptotic solutions (3.49) at the same parameter values as Figure 3.13 (a)-(c). The blue curve represents the real part of $U(x)$, and red curve represents imaginary part of $U(x)$. At (a) $F = 0.07569$, (b) $F = 0.07013$, and at (c) $F = 0.06486$.

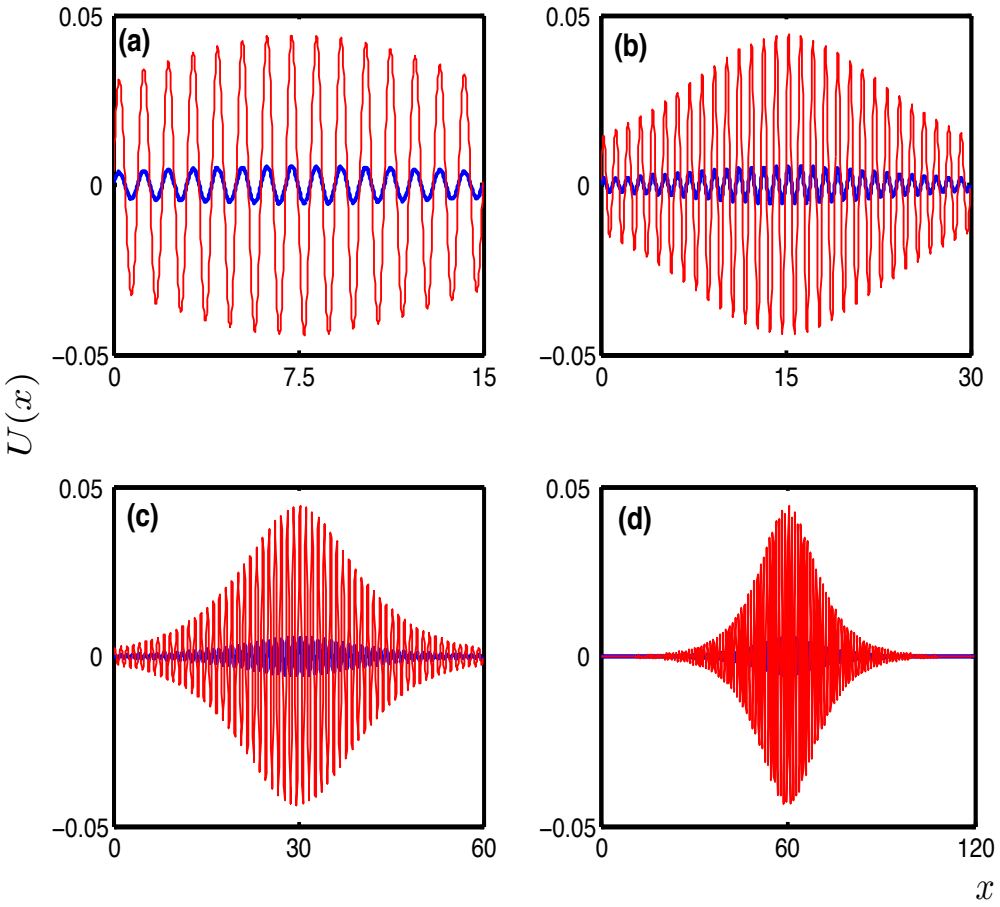

Figure 3.16: Asymptotic solution of (3.49) with the same parameter value as in Figure 3.10 at $F = 0.07013$. The size of the box increases (a) $L_x = 30\pi$, (b) $L_x = 60\pi$, (c) $L_x = 120\pi$, and (d) $L_x = 240\pi$.

3.7 The effect of the domain size

The results we simulate numerically using time-stepping and continuation methods in the previous section are in a domain with size $L_x = 60\pi$. In this section we give examples of localized oscillons with bigger domain size.

In Figure 3.16 (a)-(d) we plot the asymptotic solution (3.49) at $F = 0.07013$ for different domain sizes to show the effect of making the domain size large but still finite. Figure 3.17 (a) shows an example of a localized solution, which we found in the PDE (3.1) by

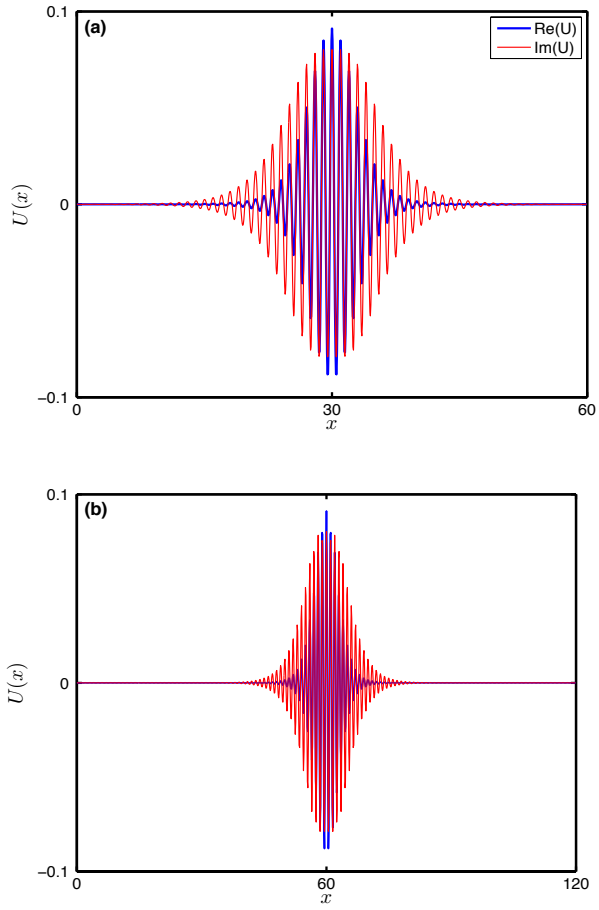

Figure 3.17: Examples of localized solutions in the PDE (3.1) with same parameters as in Figure 3.10, but different domain size. The forcing amplitude is $F = 0.05856$. The domain size in (a) is $L_x = 120\pi$. and in (b) is $L_x = 240\pi$.

time-stepping, in a box of size $L_x = 120\pi$ that is twice as big as the size of the domain in Figure 3.13 and Figure 3.14. In Figure 3.17 (b) the domain size is $L_x = 240\pi$. The time that we need to evaluate localized patterns increases as we make the domain size bigger.

Although dealing with bigger domain size is not easy, we were able to do continuation in a domain with size $L_x = 120\pi$. Figure 3.18 shows that the localization curve bifurcates at $F_c^* = 0.080829$. As expected, this point is closer to $F_c = 0.08205$ than when the domain size was $L_x = 60\pi$. Examples of localized solutions along the localization curve are given in the left panels of Figure 3.19 (a)-(c) and in Figure 3.20 (d) and (e). The right

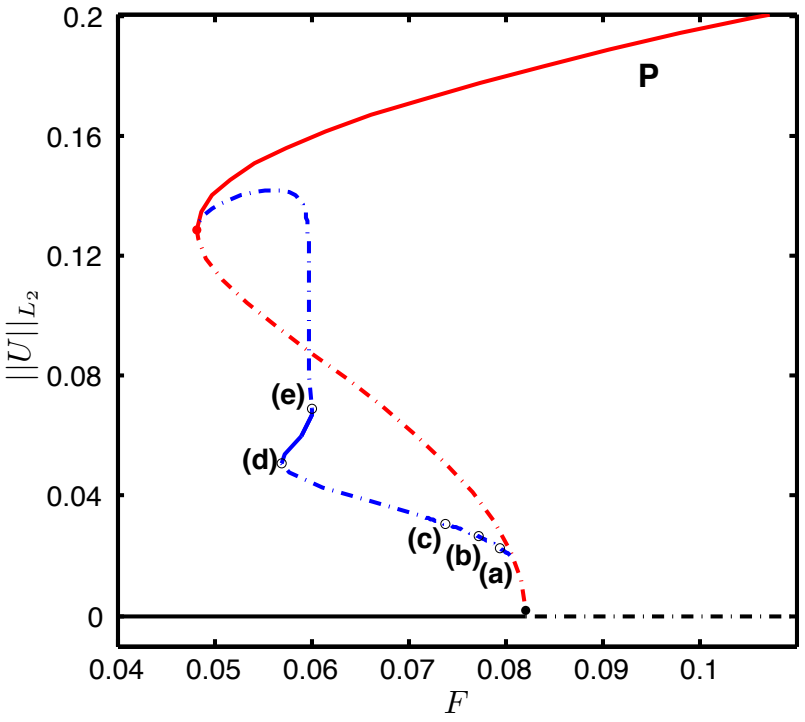

Figure 3.18: Bifurcation diagram of (3.1) in the weak damping limit in a domain size $L_x = 120\pi$ with $\epsilon = 0.1$, $\mu = -0.255$, $\alpha = -0.5$, $\beta = 1$, $\gamma = -0.25$, $\delta = 0.4995$, $\nu = 2$, $\omega = 1 + \beta - \delta + \epsilon^2\nu$, and $C = -1 - 2.5i$. The bistability region is between $F_c = 0.08246$ and $F_d = 0.056$. The bifurcation point of the localization curve is $F_c^* = 0.08027$.

panels of Figure 3.19 (a)-(c) shows solutions of (3.49). The left and right panels of Figure 3.19 are at the same value of F.

We tried to make the domain size even bigger, but we did not manage to get a bifurcation diagram for $L_x = 240\pi$ using AUTO.

3.8 Discussion

The current discussion was about constructing the PDE model (3.1) for the formation of localized states in the presence of forcing. Our aim was to show the existence of a branch of localized solutions in the bistability region by applying weakly nonlinear theory. The

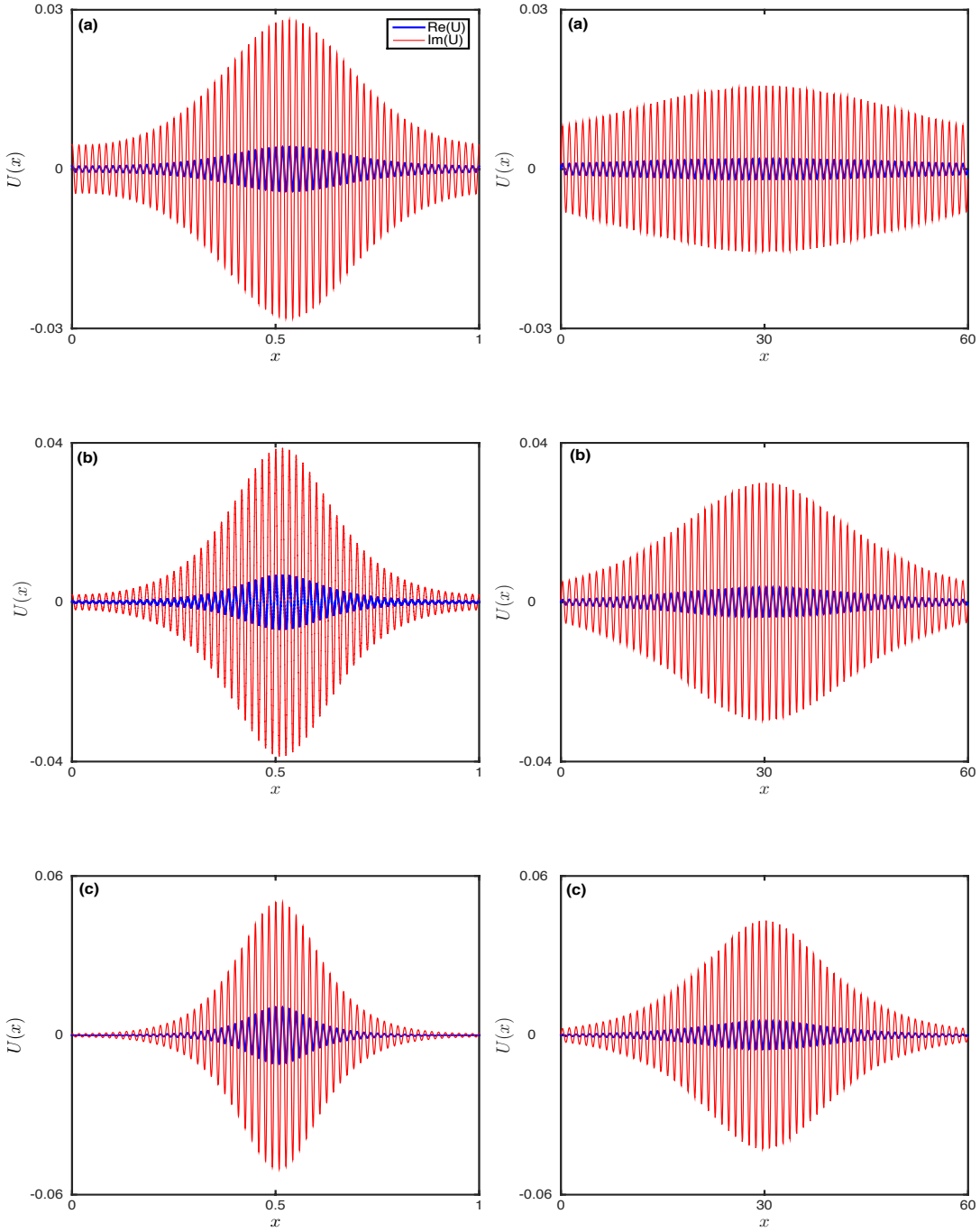

Figure 3.19: The left panels are solutions (a)-(c) along the bifurcation diagram in Figure 3.18. The right panels are Asymptotic solution (3.49). These solutions are at (a) $F = 0.07943$, (b) $F = 0.07720$, and (c) $F = 0.07389$.

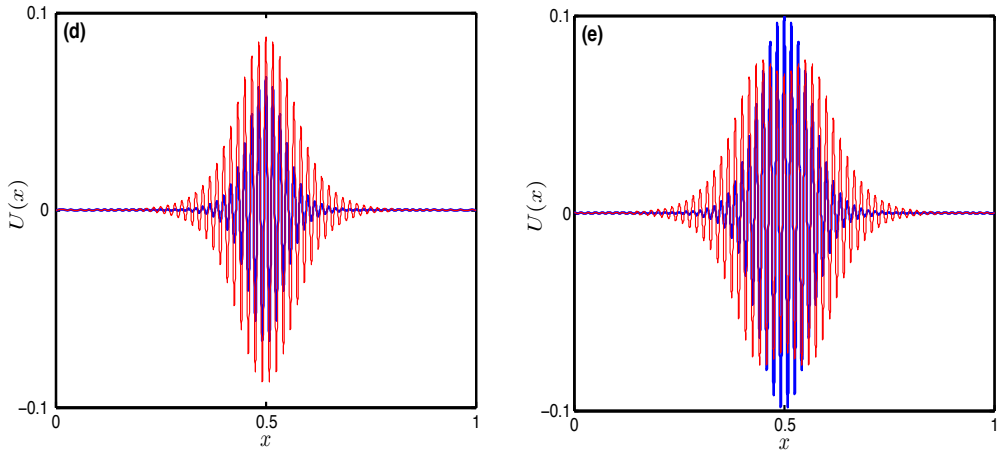

Figure 3.20: Solutions (d) and (e) along the bifurcation diagram in Figure 3.18, at (d) $F = 0.05701$, and at (e) $F = 0.06014$.

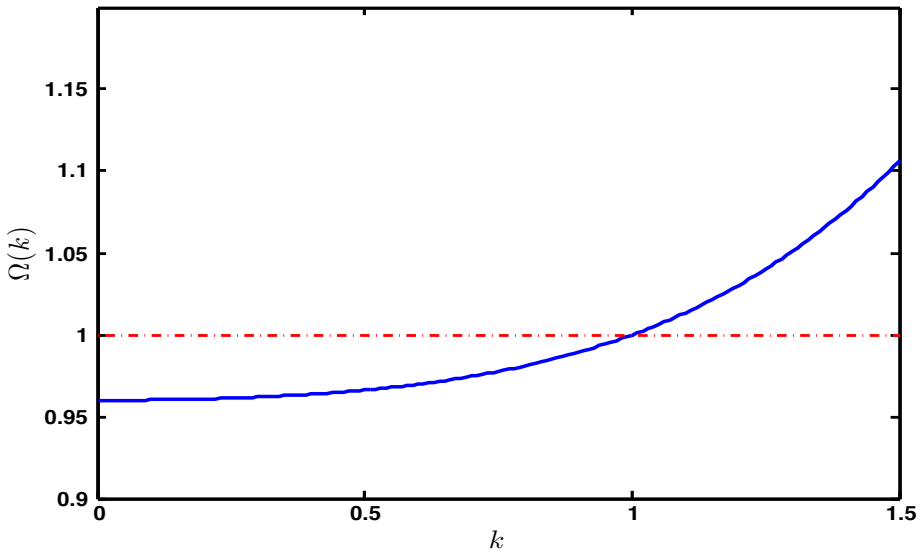

Figure 3.21: The wavenumbers of localized solutions of the PDE model (3.1) with $\beta = -0.02$, $\delta = 0.02$, $\omega = 0.96$, and $v_g = 0.4$. Note that $\Omega(k)$ is close to 1 over a wide range of k.

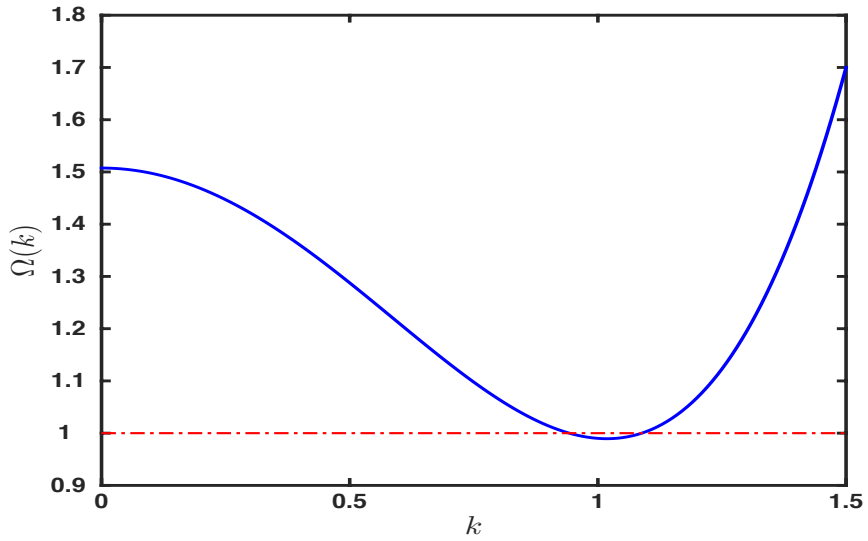

Figure 3.22: The wavenumbers of localized solutions in the PDE (3.1) with $\nu = -1$, $\beta = 1$, $\delta = 0.4825$, $\omega = 1 + \beta - \delta + (\epsilon^2\nu) = 1.5075$, $\epsilon = 0.1$. Note that $\Omega(k) = 1$ is close to 1 at two distinct wavenumbers.

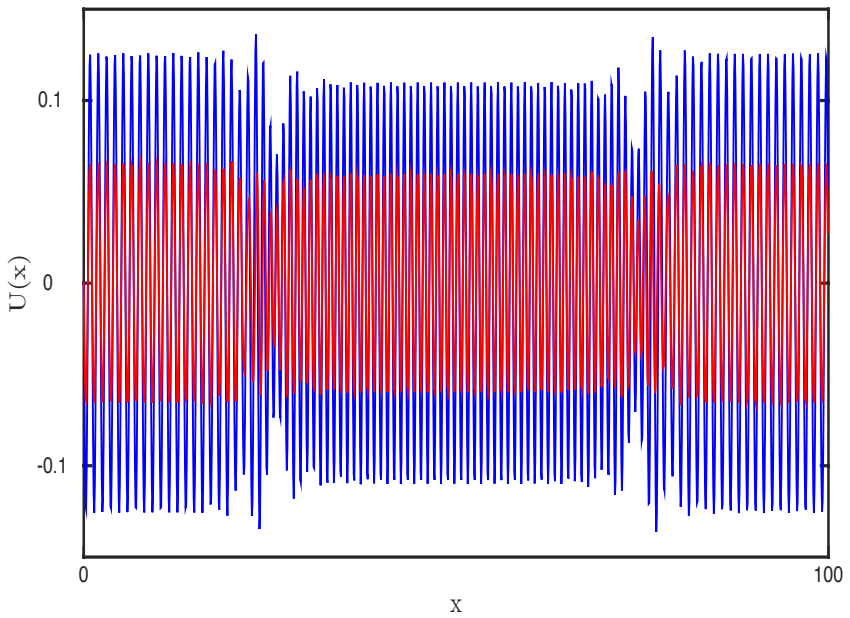

Figure 3.23: Localized solution in the PDE model (3.1) with two wavenumbers with $\mu = -0.255$, $\nu = -1$, $\alpha = -0.5$, $\beta = 1$, $\gamma = -0.25$, $\delta = 0.4825$, $F = 0.15$, $\epsilon = 0.1$, $\omega = 1 + \beta - \delta + (\epsilon^2\nu)$, and $v_g = -0.7$. $N_x = 1280$, $L_x = 200\pi$.

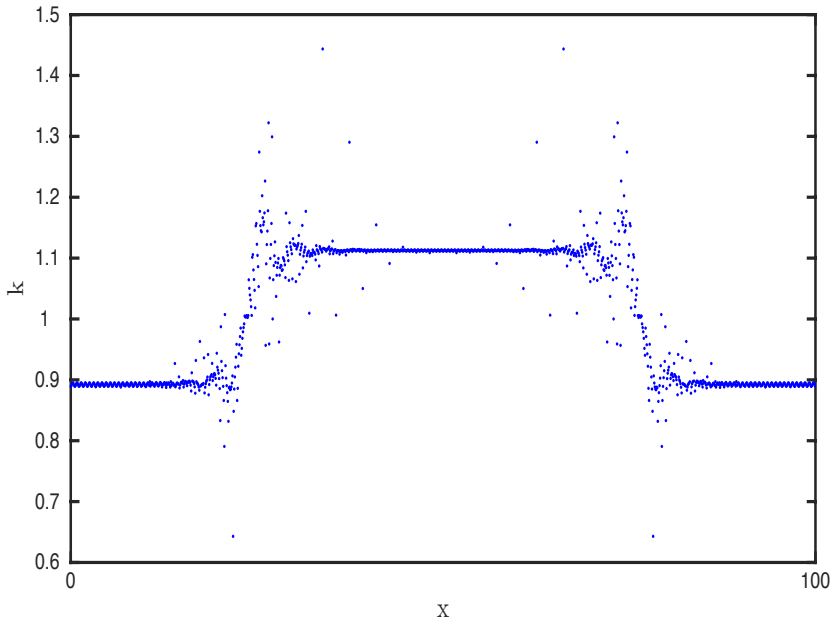

Figure 3.24: Approximation to the wavenumbers of the solution in Figure 3.23 with the same parameters.

existence of these solutions is subject to the scaling we applied in this chapter being valid; in particular we assumed that the group velocity is small. However, with such an assumption we have to be careful because waves with a wide range of wavenumbers can be excited. Figure 3.21 shows the dispersion curve for a fairly small group velocity ($v_g = 0.4$); it is clear that many wavenumbers are close to resonant (Ω is close to 1). It is also possible to get two wavenumbers being resonant; see Figure 3.22 for an example.

Localized solutions with two wavelengths have been observed in the PDE model (3.1). An example is given in Figure 3.23. We found more examples, but this problem is beyond this thesis. We will do more study in localized states with two wavenumbers in the future.

In order to avoid this problem, we might think of making the group velocity to be $O(1)$ and then reducing (3.1) to the averaged FCGL equation, rather than reducing it to the actual FCGL model, as was done in [57]. The averaged FCGL equation then might be reduced to the real Ginzburg–Landau equation, which could have sech solution. Therefore, spatially

localized oscillons can be found in the PDE model (3.1) even for $O(1)$ group velocity.

As we change the group velocity v_g we found that the biggest magnitude of the group velocity we can reach and still find localized oscillons is at $v_g = -0.75$. If we want to extend the group velocity more we need to reduce the forcing amplitude Γ and change β (see for example Figure 3.8).

In this chapter, we found oscillons in the model PDE (3.1), which give an idea of how oscillons might be studied in a model like the Zhang–Viñals model [93], and how the weakly nonlinear calculations of [77] might be extended to the oscillons observed in the Faraday wave experiment.

Chapter 4

Localized oscillons in the parametrically forced PDE model with a cubic–quintic nonlinearity

4.1 Introduction

In Chapter 3, spatially localized oscillons were found in the form of many oscillations of the periodic pattern underlying the envelope equation (see Figure 3.10). Our results did not give a single-peak oscillon as seen in Figure 1.2, observed in the Faraday wave experiment. We tried to find a single-peak oscillon in the PDE model (3.1), but we could not find any examples as Figure 2.9, where the preferred wavenumber is zero.

In the large amplitude regime, we need to control the subcriticality of the PDE model to make the oscillon sufficiently nonlinear that it will form a single-peak. The subcriticality in Chapter 3 comes from the forcing term balancing the $-|U|^2U$ term. An alternative way to control the subcriticality is to modify the PDE model (3.1) to include a quintic nonlinear term. With a $-|U|^4U$ term, it is possible to make the cubic coefficients as big (positive) as we want without losing the stable branch. An alternative way to control the subciticality would be to reinstate the quadratic nonlinearity. However, it is easier to

investigate the PDE model with cubic-quintic nonlinearity.

Localized solutions to the Swift–Hohenberg equation with cubic–quintic nonlinearity were studied first by Sakaguchi and Brand in [71–73]. Sakaguchi and Brand studied stationary stable localized solutions with a circular symmetry [72], in one and two dimensions [73]. These solutions depended on the initial conditions as expected, but not on the size of the domain. Burke and Knobloch in [13] investigated the Swift–Hohenberg equation with a cubic–quintic nonlinearity in order to give more detailed description of the resulting spatially localized solutions that were found in [71].

All previous work on cubic–quintic were done with autonomous PDEs. Here we are interested in explicit time-dependent forcing. Therefore, our analysis is carried out by altering the PDE model to include a quintic nonlinear term:

$$U_t = (\mu + i\omega)\, U + (\alpha + i\beta)\nabla^2 U + C_r|U|^2 U - |U|^4 U + i\Re(U) f(t), \qquad (4.1)$$

where $C_r \in \mathbb{R}$ and $C_r > 0$, and $f(t)$ is a 2π periodic function. We will study localized oscillons in this cubic–quintic PDE with strong damping, so we do not need the $\nabla^4 U$ term, and with values of parameters μ, ω, α, and β chosen so that the preferred wavenumber at onset is non-zero. This equation has a $U \to -U$ symmetry.

In the strong damping, strong forcing case, the linear part of the cubic–quintic PDE is reduced to the damped Mathieu equation, which has to be solved numerically to get the eigenfunction as we discussed in Chapter 2. We present the linear theory in the next section, and we present examples of spatially localized oscillons numerically in both one and two dimensions in Section 4.3 and 4.4.

4.2 Linear Theory

This chapter is based on studying the linearized PDE (4.1) in the strong damping and strong forcing case. The linear part of the PDE reduces to the damped Mathieu equation.

As in Chapter 2, we write the solution as $U = u + iv$, where $u(x,t)$ and $v(x,t)$ are real functions. Thus the PDE becomes

$$\begin{aligned}\frac{\partial u}{\partial t} &= \left(\mu + \alpha\frac{\partial^2}{\partial x^2}\right)u - \left(\omega + \beta\frac{\partial^2}{\partial x^2}\right)v + C_r(u^2+v^2)u - (u^2+v^2)^2u,\\ \frac{\partial v}{\partial t} &= \left(\omega + \beta\frac{\partial^2}{\partial x^2}\right)u + \left(\mu + \alpha\frac{\partial^2}{\partial x^2}\right)v + f(t)u + C_r(u^2+v^2)v - (u^2+v^2)^2v.\end{aligned} \tag{4.2}$$

We linearize the PDE problem about zero in order to reduce it to the damped Mathieu equation for a periodic forcing function $f(t) = F\cos(2t)$. The critical forcing amplitude F_c is the forcing at which the zero solution loses stability. Since in this case the critical wavenumber is not zero, we seek solution of the form

$$U = e^{ikx}(p_1(t) + iq_1(t)), \tag{4.3}$$

where $p_1(t)$ and $q_1(t)$ are 2π periodic functions. Note that this is different from the analysis in Chapter 2, and it is the same as the analysis in [70, Appendix A]. Substituting (4.3) into (4.2) leads to

$$\begin{aligned}\left[\frac{\partial}{\partial t} - (\mu - \alpha k^2)\right]p_1 &= -(\omega - \beta k^2)q_1,\\ \left[\frac{\partial}{\partial t} - (\mu - \alpha k^2)\right]q_1 &= (\omega - \beta k^2)p_1 + f(t)p_1,\end{aligned}$$

which can be combined to give a damped Mathieu equation

$$\ddot{p} + \hat{\gamma}\dot{p} + (\Omega^2 + f(t)\hat{\Omega})p = 0, \tag{4.4}$$

where $\hat{\gamma} = 2(-\mu + \alpha k^2)$, $\hat{\Omega} = \omega - \beta k^2$, and $\Omega = \sqrt{(\frac{\hat{\gamma}}{2})^2 + \hat{\Omega}^2}$. Thus a linear operator is defined as

$$L = \frac{\partial^2}{\partial t^2} + \hat{\gamma}\frac{\partial}{\partial t} + (\Omega^2 + f(t)\hat{\Omega}), \quad \text{with} \quad Lp = 0.$$

As in Chapter 2 we solve the damped Mathieu equation (4.4) numerically to determine the critical wavenumber k_c, and the critical forcing amplitude F_c. The critical forcing

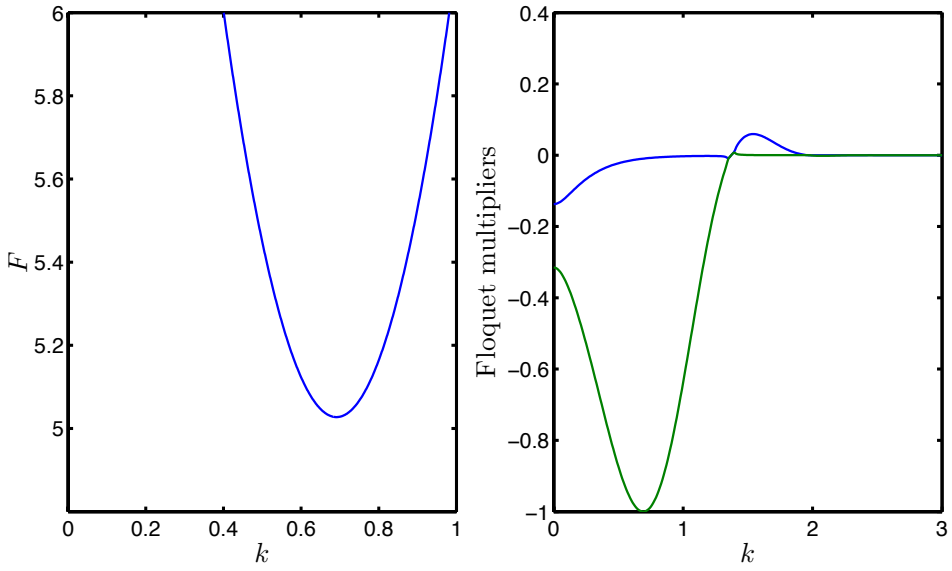

Figure 4.1: Linear theory for one-frequency forcing, with damping coefficients $\mu = -0.5$, $\alpha = 0.5$, and dispersion relation coefficients $\omega = \frac{1}{3}$, and $\beta = \frac{-2}{3}$. The left panel shows the critical forcing amplitude $F_c = 5.02736$, at $k_c = 0.69113$. The right panel presents the Floquet multipliers at $F = F_c$, with a critical Floquet multiplier $Fm = -1$ at $k = k_c$.

amplitude, where the transition between stable to unstable trivial state ocurrs, is given in the left panel of Figure 4.1. It shows that minimizing this forcing amplitude over k with $\mu = -0.5$, $\alpha = 0.5$, $\beta = \frac{-2}{3}$, and $\omega = \frac{1}{3}$ yields the critical wavenumber $k_c = 0.69113$ at $F_c = 5.02736$. The right panel of Figure 4.1 represents the Floquet multipliers at the critical forcing amplitude as a function of wavenumbers k (see Appendix B and C.1). We could apply weakly nonlinear theory to the PDE model (4.1) as in [70], but we are not going to do that in this thesis.

4.3 Numerical results: one dimension

In this section we solve the cubic–quintic PDE (4.1) by time-stepping. We use a pseudospectral method, and the exponential time differencing method ETD2 as in Chapter 2. We did continuation by using time-stepping to plot the stable periodic pattern curve

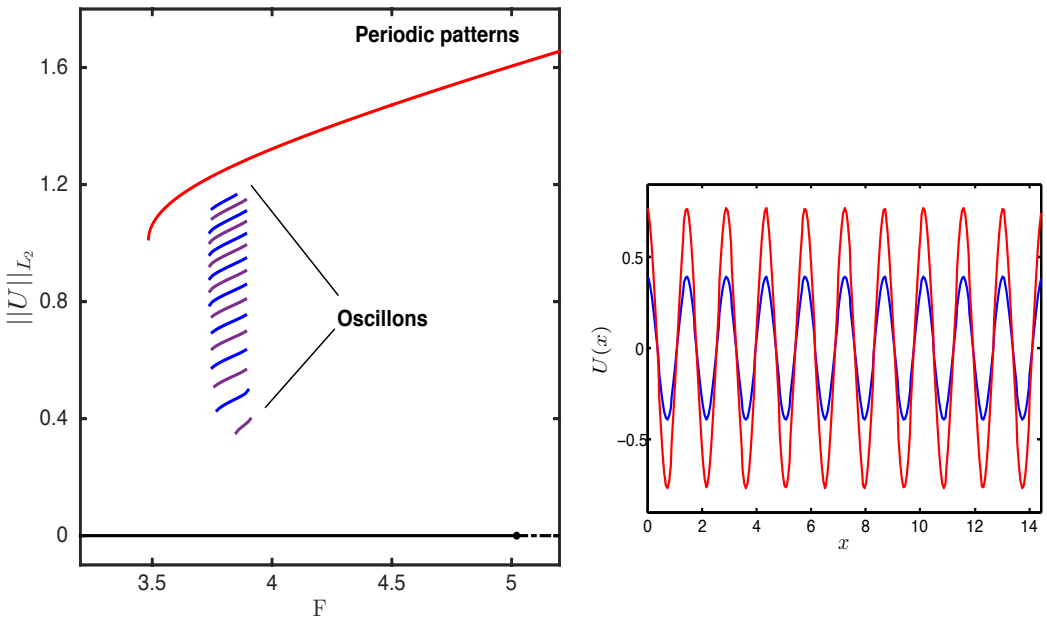

Figure 4.2: Bifurcation diagram of the cubic–quintic PDE (4.1), with $\mu = -0.5$, $\alpha = 0.5$, $\beta = \frac{-2}{3}$, $\omega = \frac{1}{3}$, and $C_r = 1$. Blue and purple branches present even and odd localized oscillons respectively. The right panel shows periodic patterns at $F = 3.8$.

and stable localization curves.

In one spatial dimension, we use a domain with size $L_x = \frac{20\pi}{k_c} = 91.0607$, and FFTs with up to 256 Fourier modes. Figure 4.2 shows the bifurcation diagram of (4.1) as computed by time-stepping. The right panel of Figure 4.2 presents the periodic pattern, which we use to do continuation to find the periodic patterns curve in the bifurcation diagram in the left panel.

Generally speaking, localized states arise as a result of bistability between a zero flat state and periodic patterns. The bistability region, as shown in the left panel of Figure 4.2, is between the bifurcation point $F_c = 5.021$ and the saddle-node point $F_d = 3.48$.

In order to find oscillons of different widths, we choose initial conditions that are different

combinations between the zero flat state at the edges and the periodic pattern in the center. Which spatially localized oscillons is found depends on the initial conditions. It is possible to detect them by setting a random initial condition, but this makes it difficult to generate oscillons in a systematic fashion. As we change the initial condition, we get different examples of spatially localized oscillons, which are shown in Figure 4.3 and 4.4. We continue each of these solutions, so we end up with a range of stable localized branches. Therefore, the bifurcation diagram in Figure 4.2 shows the region of localization in the bistability region. Since we use time-stepping to find spatially localized oscillons, the localized branches that we found are only the stable branches. Thus, they are not connected with unstable branches, which normally can be seen if we did continuation by AUTO.

Following the solutions in Figure 4.3 (a)-(h) shows that they are even about $x = \frac{L_x}{2}$, and so are maximum or minimum at midpoint . Figure 4.4 (a)-(h) shows that the localized state is always zero at $x = \frac{L_x}{2}$. Therefore, we expect that there are two curves of stable localized oscillons, which are similar to results found in the Swift–Hohenberg equation (see Figure 4.5, that is taken from [14]). In the Swift–Hohenberg equation, there have been many studies where similar results were discussed, for instance in [12–14, 39, 40, 71, 73]. We expect that branches in each of these curves be connected by unstable localized oscillons to give two snaking curves (see Figure 4.6). In Figure 4.3, we use the $U \to -U$ symmetry to present localized oscillons in such a way that their outer edges are all the same. As a consequence of this choice, (a), (c), (e), and (g) have a local maximum at the centre, while (b), (d), (f), and (h) have a local minimum. Similarly, we could use also the $U \to -U$ symmetry in Figure 4.4 to make the outer edges the same but instead we have chosen to have positive slope at the midpoint in all cases. All solutions were plotted at $x = \frac{L_x}{2\pi}$.

These results confirm the universal picture arising from the Swift–Hohenberg equation, even with parametric forcing. We expect that localized oscillons in Figure 4.3 to be connected by a snaking branch of even solutions, and localized oscillons in Figure 4.4 to be connected by another snaking branch of odd solutions. Figure 4.6 shows sketches

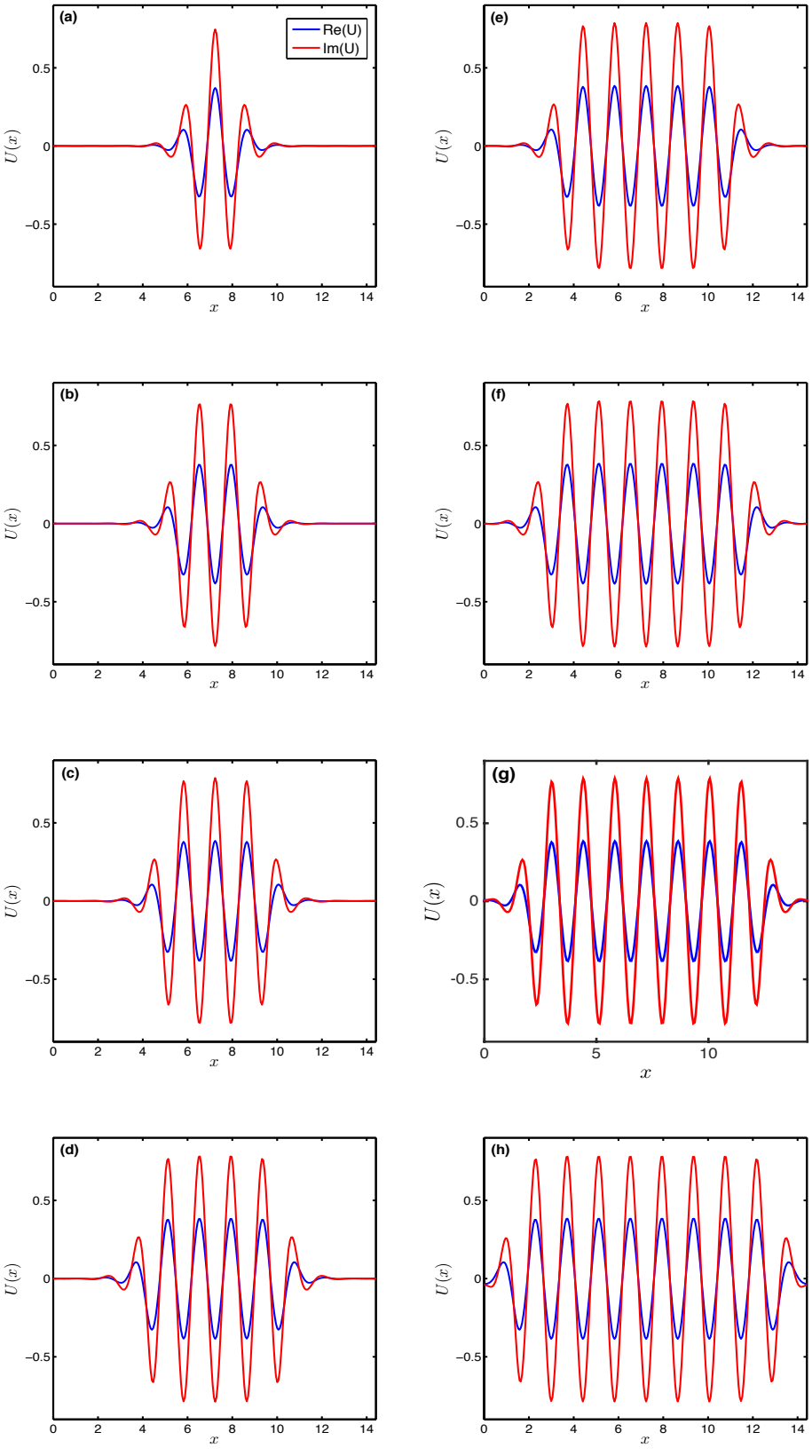

Figure 4.3: Examples of spatially periodic oscillons in the cubic–quintic PDE (4.1) along the blue branches in Figure 4.2 with parameters as in Figure 4.2. All these spatially localized oscillons arise at $F = 3.8$.

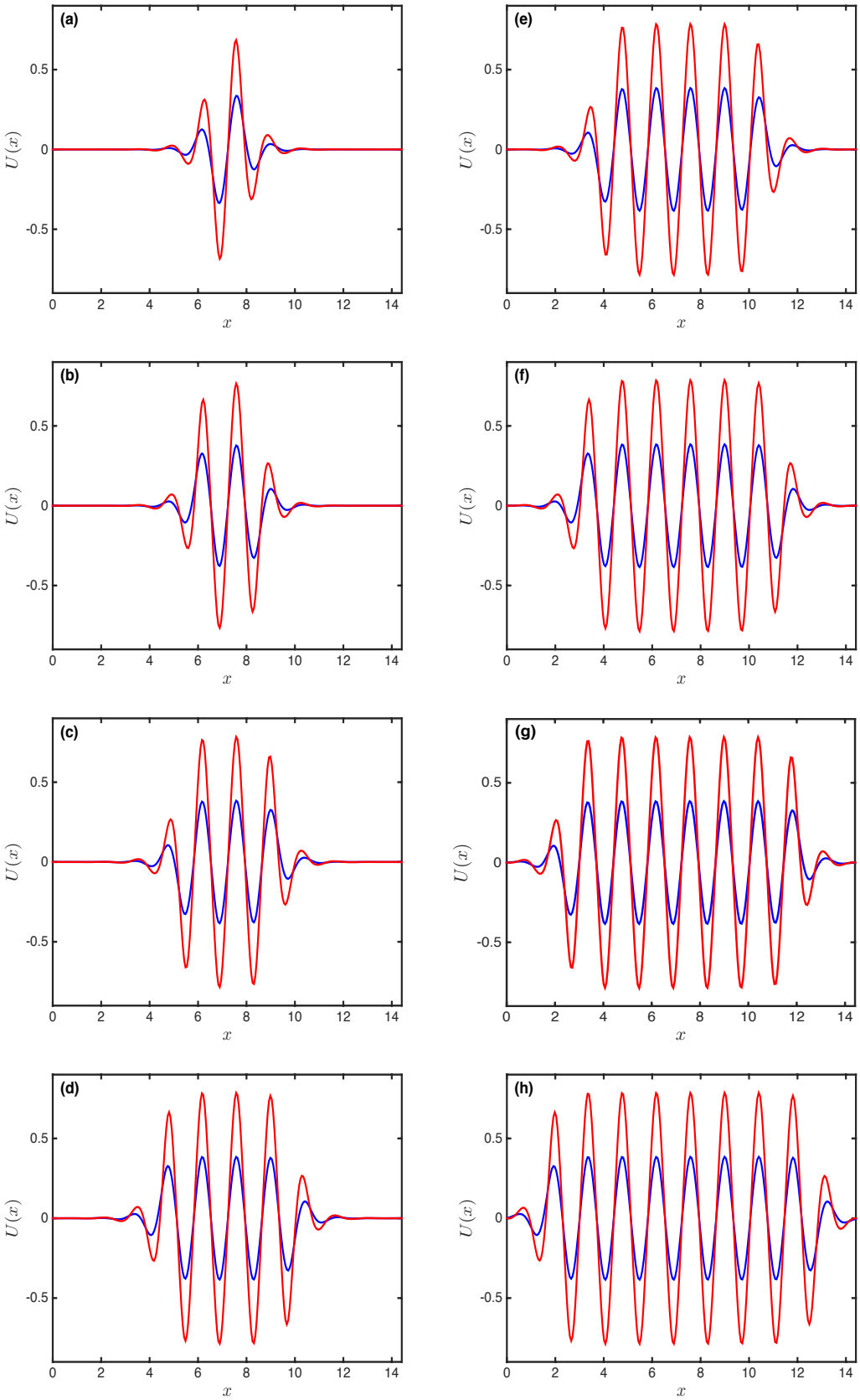

Figure 4.4: Examples of spatially periodic oscillons in the cubic–quintic PDE (4.1) along the purple branches in Figure 4.2 with parameters as in Figure 4.2. All these spatially localized oscillons are at $F = 3.8$ except (a) at $F = 3.85$.

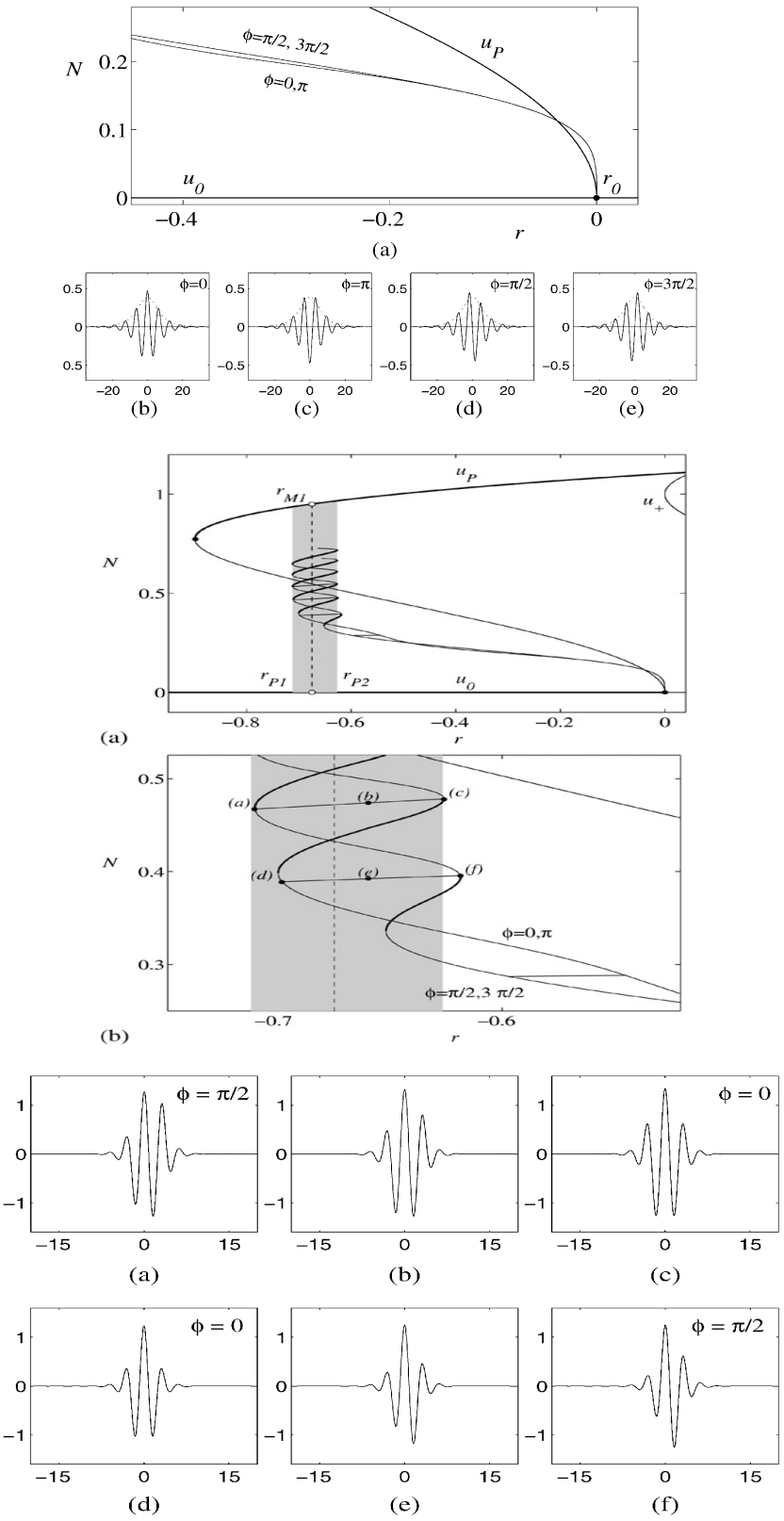

Figure 4.5: Bifurcation diagram and localized examples of the cubic–quintic Swift–Hohenberg equation, reproduced from [14]. Bifurcation diagram showing the two homoclinic branches. Thick lines indicate stable solutions.

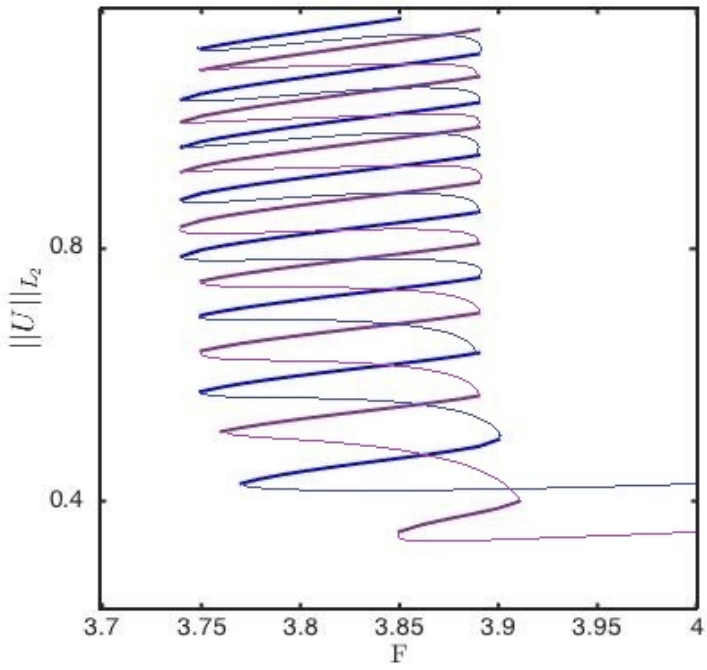

Figure 4.6: Localized branches from Figure 4.2 with the same parameter values. The thin lines are sketches of the expected unstable branches.

of the expected unstable branches. It had been found numerically in [13, 14] that the two snaking branches in the Swift–Hohenberg equation are connected by ladder branches. Therefore, we expect to have ladder branches that connect the two localization curves in the cubic–quintic PDE (4.1) model.

4.4 Numerical results: two dimensions

In two dimensions, we use a domain with size of $L_x = L_y = 91.0607$ and $N_x = N_y = 256$ Fourier modes to find spatially localized spots in the cubic-quintic PDE model (4.1), also by time-stepping. To find axisymmetric spots, we use axisymmetric initial conditions, centred in the middle of the box. Axisymmetric solutions $U(r)$ depend on the radial

variable $r = \sqrt{(x - \frac{L_x}{2})^2 + (y - \frac{L_y}{2})^2}$. In the Swift–Hohenberg equation, localized radial structures were studied by Lloyd and Sandstede [52], and also by McCalla and Sandstede [55]. In this section we investigate the existence of localized spots, which do not require bistability between the trivial state and a patterned state as in [52], and localized rings.

We set the initial condition to be one spot in the centre, which is surrounded by more rings, and then we set the rest of the domain to be zero. Specifically, we used in the time-stepping a function in radial coordinate $\cos(k_c r)$, multiplied by an amplitude. The initial condition is given in Appendix C.2 as

$$U(r) = \frac{0.65\cos(k_c r)}{1 + e^{0.5k_c(r-n)}}.$$

As we change n, we get different axisymmetric rings. The initial condition that is given in the Appendix is related to solution (e) in Figure 4.7. In our study we give only a sample of axisymmetric spots that can be found in the cubic–quintic PDE; more examples can be found by changing the initial condition.

Figure 4.7 shows 6 examples of axisymmetric spots. We follow these solutions to find the stable localization branches of the snaking curve. Figure 4.8 shows the bifurcation diagram of axisymmetric spots (blue branches) and stripes (red branch). Figure 4.9 represents stripes at $F = 3.8$. The longest stable blue branch at the bottom of Figure 4.8 refers to the one spot oscillon in Figure 4.7 (a). As we mentioned above, more examples of these type of spots can be found by changing the n in the initial condition. Our investigation shows that an initial condition with more rings than Figure 4.7 (f) breaks into stripes.

Next, we examine the existence of non-axisymmetric oscillons in the cubic–quintic PDE. In this case the domain size is the same as in the axisymmetric case, but with fewer Fourier modes $N_x = N_y = 128$. We used different initial condition in the time-stepping

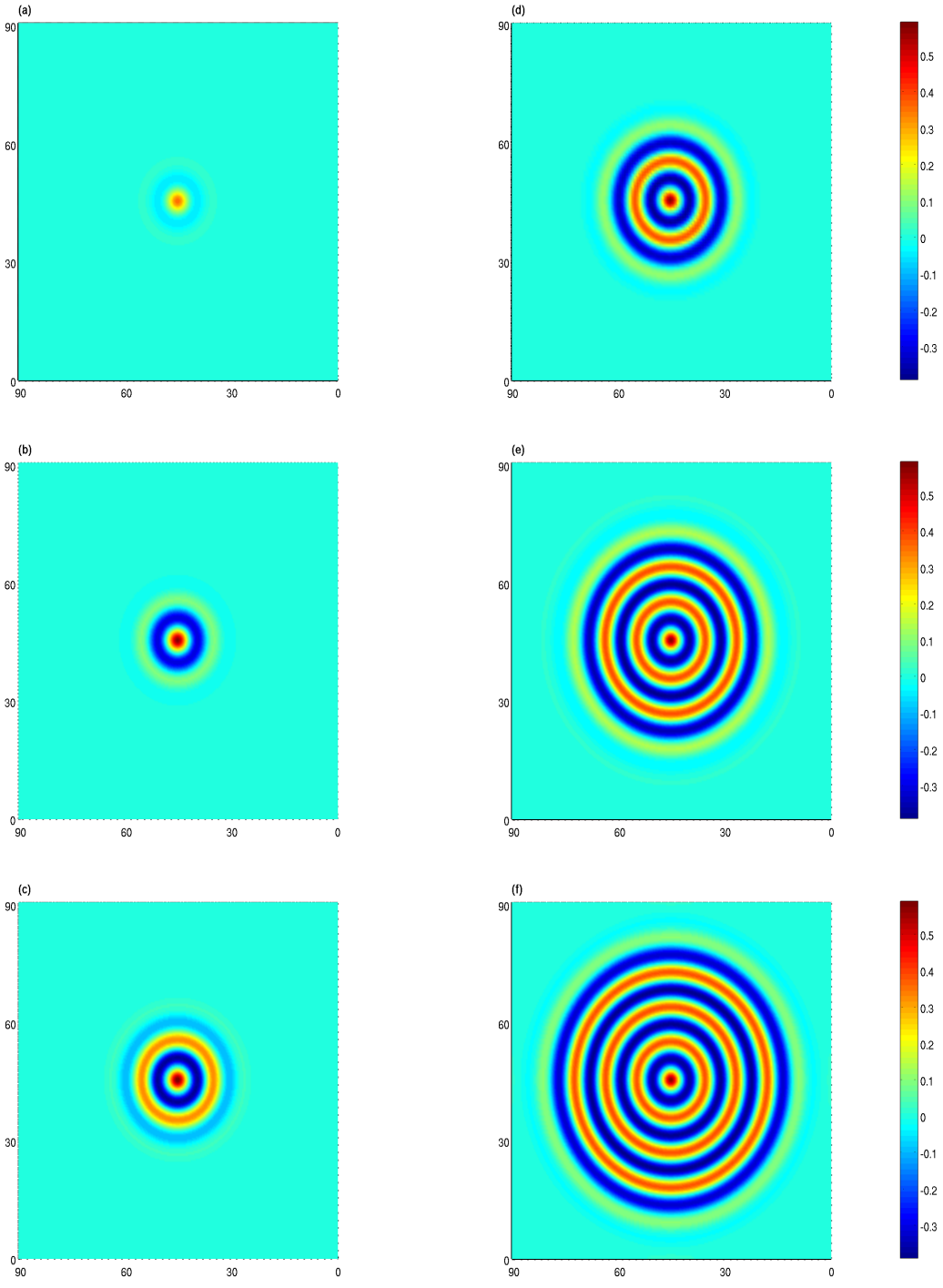

Figure 4.7: Solutions of the cubic–quintic PDE following the bifurcation diagram with $\mu = -0.5$, $\alpha = 0.5$, $\beta = -2/3$, $\omega = 1/3$, and $C_r = 1$.

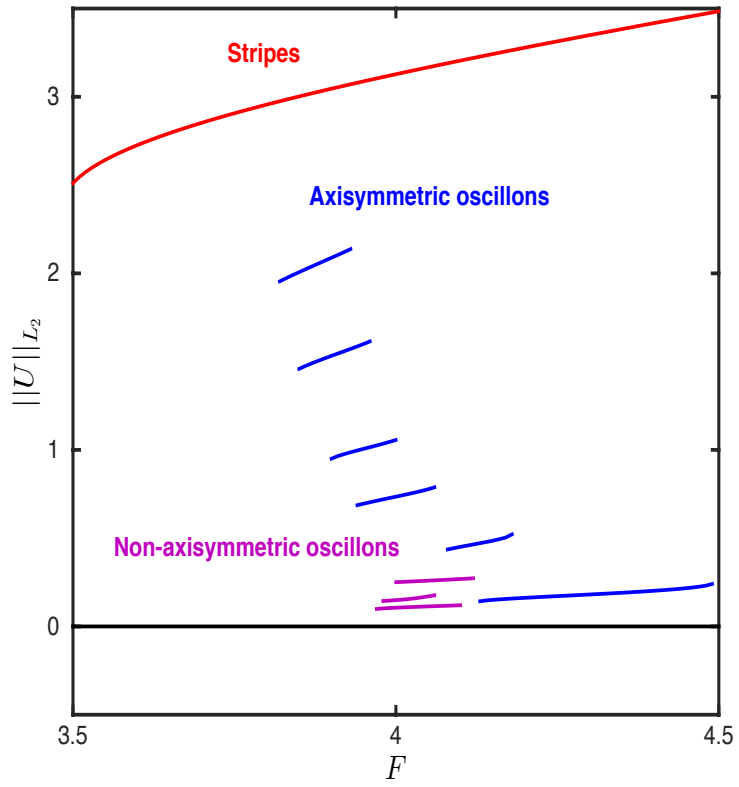

Figure 4.8: Bifurcation diagram of the cubic–quintic PDE in 2D spatial dimensions with branches of axisymmetric and non-axisymmetric oscillons with parameters as in Figure 4.7.

to find these non-axisymmetric oscillons, (see Appendix C.2). Figure 4.10 shows three examples of non-axisymmetric localized states. These solutions represents interaction between oscillons as expected in experiments (see Figure 1.2 in Chapter 1). These solutions include dipoles, triple, and chains of square polarity. Similar numerical results of non-axisymmetric oscillons were observed in the cubic–quintic Swift–Hohenberg equation [24]. As we continue these examples of oscillons, we find branches of stable localization, shown in Figure 4.8. In two spatial dimensions, we made movies to show the dynamic of axisymmetric and non-axisymmetric spots. Snapshots of axisymmetric and non-axisymmetric oscillons at different times are given in Figure 4.11 and 4.12 respectively.

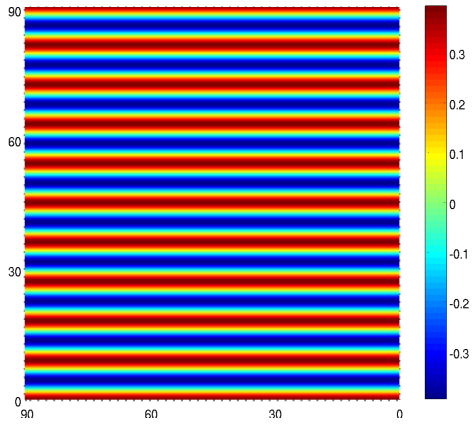

Figure 4.9: Example of stripes at $F = 3.8$ with other parameters the same as in Figure 4.7.

4.5 Conclusion

In this Chapter, we studied the cubic–quintic PDE with parametric forcing (4.1) numerically in one and two dimensions. In one spatial dimension, we found evidence for two snaking localization curves. Our expectation is that these two curves are connected by ladders as in the Swift–Hohenberg equation. The results we presented in this chapter were found by time-stepping, so the localization branches that we found are only the stable branches. It is complicated to do continuation by AUTO in the cubic–quintic PDE (4.1), because of the quintic nonlinearity. However, it would be interesting to find the stable and unstable branches in the bifurcation diagram. Also, by doing continuation using AUTO, it would be possible to find ladder branches. This is work for the future.

In two dimensions, examples of localized solutions can be found by varying the initial condition. We also expect to have more than one snaking curve for the axisymmetric oscillons. Non-axisymmetric examples can also be found in this problem. The cubic–quintic PDE is still an open problem for the future.

Analytically, we would expect weakly nonlinear calculations to lead to a cubic–quintic Complex Ginzburg–Landau equation close to the transition from a supercritical to a

subcritical bifurcation with non-zero wavenumber, if we scaled the cubic term to be small. This was studied in the Swift–Hohenberg equation by Kozyreff and Chapman [17,45] and by Dean, Matthews, Cox, and King [29] using exponential asymptotic. Weakly nonlinear analysis will be included in our future work.

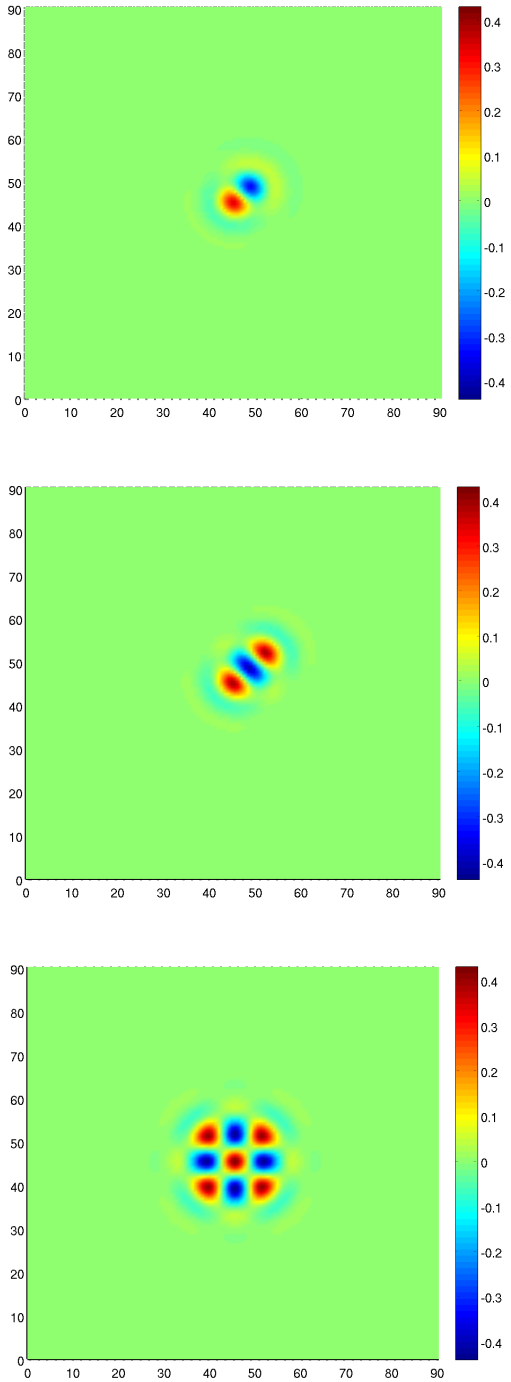

Figure 4.10: Non-axisymmetric oscillons with parameters as in Figure 4.7.

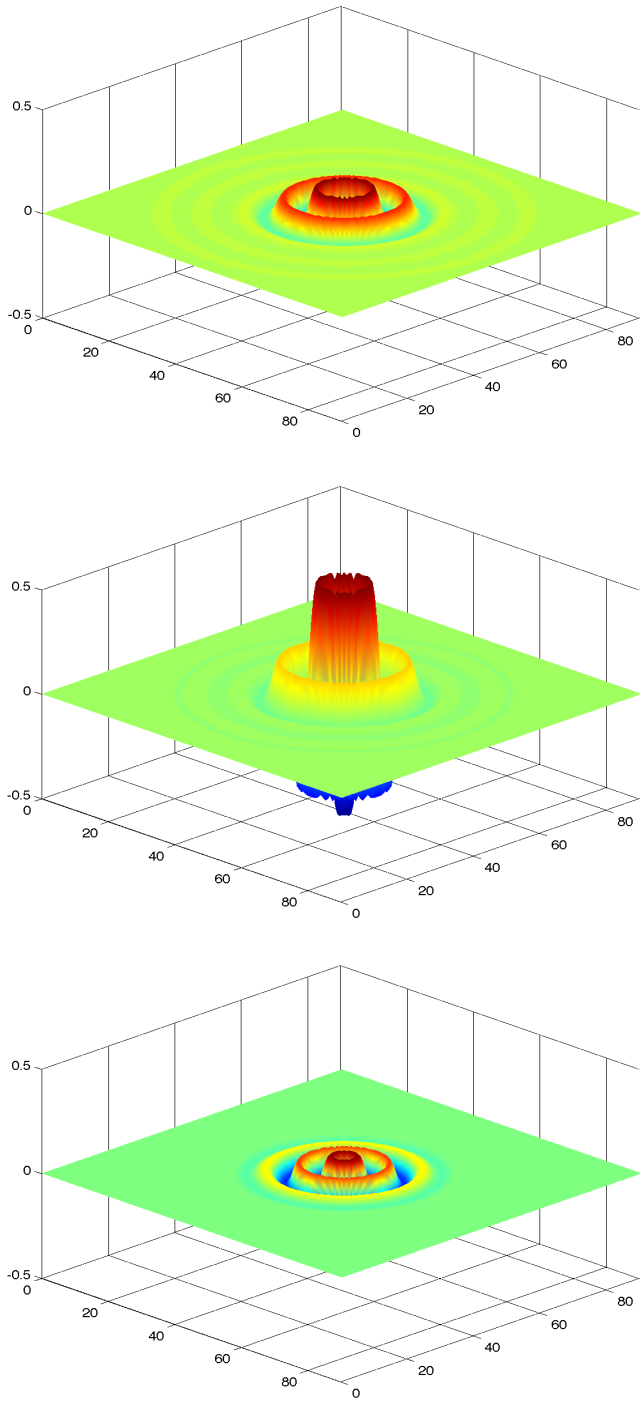

Figure 4.11: Sequence of snapshots of axisymmetric oscillons with parameters as in Figure 4.7 at times $t = \frac{1}{6}, \frac{13}{30}, \frac{18}{30}$.

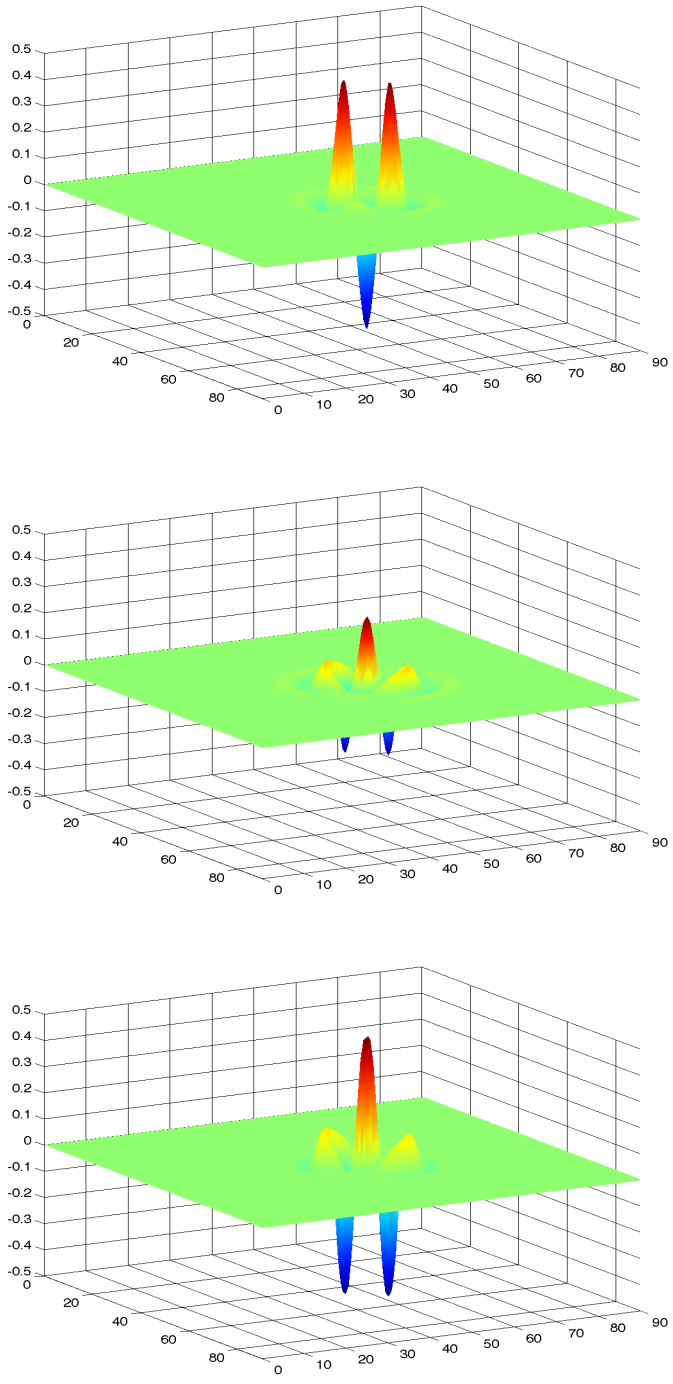

Figure 4.12: Sequence of snapshots of non-axisymmetric oscillons with parameters as in Figure 4.7 at times $t = 0, \frac{13}{60}, \frac{1}{3}$.

Chapter 5

Conclusion: summary and discussion

This thesis describes the existence of spatially localized states in a periodically forced system. The appearance of localized states is associated with the presence of bistability between the trivial state and the non-trivial state in the system. The subcriticality of the bifurcation diagram from the zero state is an essential element to find localized solutions. The localized solutions that we find are time dependent, unlike most previous work on this class of problems; they oscillate with half the frequency of the driving force. We have used the technique of weakly nonlinear theory to reduce the PDE model (1.12) with time dependent parametric forcing to its amplitude equations in order to find localized states that are presented in Chapters 2 and 3. In Chapter 4, examples of localized oscillons exhibited the typical snaking behavior that is familiar from the Swift–Hohenberg equation.

In Chapter 2, in the weak damping and weak forcing limit, the solutions and bifurcations of the PDE model (1.12) are accurately described by its amplitude equation, the FCGL equation (1.1). Analytically, we reduce the FCGL equation near onset to the Allen–Cahn equation (2.12) to find exact sech localized solution of the PDE. Numerically, we used continuation in the PDE model (1.12) to detect the branch of localized states. The saddle-node bifurcations on the snaking curve arise from pinning associated with the decaying spatial oscillations on either edge of the flat state. Numerical results show excellent

agreement between the PDE model and the FCGL equation. The agreement remains qualitatively good even with strong damping and strong forcing.

In this chapter our results are directly relevant to localized patterns found in Turing systems, such as those found in [80, 86]. These results are not directly relevant to the oscillons observed in the Faraday wave experiment, where the preferred wavenumber is non-zero. Therefore, in Chapter 3 we investigate spatially localized oscillons with non-zero wavenumber in the PDE model (1.12). Our study might indicate how localized solutions could be studied in (for example) the Zhang–Viñals model [93], and how the weakly nonlinear calculations of [77] might be extended to study the oscillons observed in the Faraday wave experiment. By using multiple scale analysis, and in the limit of weak damping, weak detuning, weak forcing, small group velocity, and small amplitude, we reduce the PDE model (1.12) to the coupled FCGL equations (1.2). We successfully found (for the first time) numerical examples of spatially localized oscillons in the coupled amplitude equations and in the PDE model at related parameter values.

The existence of localized solutions in the bistability region in the PDE model is subject to the scaling that we applied in this chapter being valid. We assumed that the group velocity is small, and with such an assumption we have to be careful not to get a wide range of wavenumbers excited. In the case where this happens, we found localized solutions with two wavelengths in the PDE model. These states resemble those found by Bentley [8] in an extended Swift–Hohenberg model, and by Riecke [67] in the coupled FCGL equations with small group velocity, in the supercritical case. We will study localized states with two wavenumbers in the future.

The coupled FCGL equations are derived with the assumption that the group velocity is small, of the same order as the amplitude of the solution, which is not true in reality. In fact, the group velocity is $O(1)$, but we consider the assumption that it is small in order to make progress in our problem. We have discussed the averaging approach taken by [57] in the $O(1)$ group velocity case in Chapter 3.

We also make further reduction of the coupled FCGL equations to the real Ginzburg–Landau equation, which has exact sech localized solutions. Numerically, we compare spatially localized oscillons in the model PDE with sech solutions of the real Ginzburg–Landau equation. In the strong damping, strong forcing limit, we could directly reduce the PDE model to the real Ginzburg–Landau equation (3.44) after solving the Mathieu equation numerically to get the eigenfunction from the linear terms of the PDE, and doing the weakly nonlinear theory numerically.

Numerically we studied in Chapter 4 the cubic–quintic PDE with parametric forcing (4.1) in the strong damping and strong forcing case. In one spatial dimension, we found evidence for two snaking localization curves, that are possibly connected by ladders as in the Swift–Hohenberg equation. It would be interesting in future to find the stable and unstable branches and ladders by doing continuation using AUTO. In two dimensions, we found examples of localized solutions by varying the initial condition. Our expectation is also to have more than one snaking curve for the axisymmetric oscillons. Examples of non-axisymmetric solutions were found in this problem. Analytically, we would expect weakly nonlinear calculations to lead to a cubic–quintic CGL equation close to the transition from a supercritical to a subcritical bifurcation with non-zero wavenumber, if we scaled the cubic term to be small. This was studied in the Swift–Hohenberg equation by Kozyreff and Chapman [17, 45] and by Dean, Matthews, Cox, and King [29] using exponential asymptotics. We will study weakly nonlinear analysis in our future work in the cubic–quintic PDE model.

Bibliography

[1] S. M. ALLEN AND J.W. CAHN, *A microscopic theory for antiphase boundary motion and its application to antiphase domain coarsening*, Acta. Metall, 27 (1978), pp. 1084-1095.

[2] A. S. ALNAHDI, J. NIESEN, A. M. RUCKLIDGE, AND T. WAGENKNECHT, *Localized patterns in periodically forced systems*, SIAM J. Appl. Dyn. Syst.,13 (2014), pp. 1311-1327.

[3] I. S. ARANSON AND L. S. TISIMRING, *Formation of periodic and localized patterns in an oscillating granular layer*, Phys. A, 249 (1998), pp. 103-110.

[4] H. ARBELL AND J. FINEBERG, *Temporally harmonic oscillons in Newtonian fluids*, Phys. Rev. Lett., 85 (2000), pp. 756-759.

[5] D. ARMBRUSTER AND T.-C. JO, *Pattern formation and parametric resonance. In: Dynamics and bifurcation of patterns in dissipative systems*, World Sci. Ser. Nonlinear Sci. Ser. B Spec. Theme Issues Proc. World Sci. Publ., Hackensack, NJ, (2004), pp. 158-173.

[6] AUTO, *1995-2010 Corporation on National Research Initiatives and 2001 Python Software Foundation*.

[7] T. B. BENJAMIN AND F. URSELL, *The stability of the plane free surface of a liquid in vertical periodic motion,* Proc. R. Soc. Lond. A, 225 (1954), pp. 505-515.

[8] D. C. BENTLEY, *Localised solutions in the magnetorotational Taylor-Couette flow with a quartic marginal stability curve*, thesis, University of Leeds (2012).

[9] C. BIZON, M. SHATTUCK, J. SWIFT, W. MCCORMICK AND H. SWINNEY, *Patterns in 3d vertically oscillated granular layers: simulation and experiment*, Phys. Rev. Lett., 80 (1998), pp. 57-60.

[10] M. BORDBAR AND P. ZAMANKHAN, *Dynamical states of bubbling in vertical vibrated granular materials. Part II: Theoretical analysis and simulations*, Commun. Nonlinear Sci. Numer. Simul., 12 (2007), pp. 273-99.

[11] J. BURKE AND J. H. P. DAWES, *Localized states in an extended Swift-Hohenberg equation*, SIAM J. Appl. Dyn. Syst., 11 (2012), pp. 261-284.

[12] J. BURKE AND E. KNOBLOCH, *Localized states in the generalized Swift-Hohenberg equation*, Phys. Rev. E, 73 (2006), 056211.

[13] J. BURKE AND E. KNOBLOCH, *Homoclinic snaking: structure and stability*, Chaos, 17 (2007), 037102.

[14] J. BURKE AND E. KNOBLOCH, *Snakes and ladders: Localized states in the Swift-Hohenberg equation*, Phys. Lett. A, 360 (2007), pp. 681-688.

[15] J. BURKE, A. YOCHELIS, AND E. KNOBLOCH, *Classification of spatially localized oscillations in periodically forced dissipative systems*, SIAM J. Appl. Math., 7 (2008), pp. 651-711.

[16] E. CERDA, F. MELO AND S. RICA, *Model for subharmonic waves in granular materials*, Phys. Rev. Lett., 79 (1997), pp. 4570-4573.

[17] S. J. CHAPMAN AND G. KOZYREFF, *Exponential asymptotics of localized patterns and snaking bifurcation diagrams*, Phys. D, 238 (2009), pp. 319-354.

[18] A. R CHAMPNEYS AND G. J LORD , *Computation of homoclinic solutions to periodic orbits in a reduced water-wave problem*, Phys. D, 102 (1997), pp. 101-124.

[19] C. CHONG, R. CARRETERO-GONZÁLEZ, B.A. MALOMED, AND P.G. KEVREKIDIS, *Multistable solitons in higher-dimensional cubic-quintic nonlinear Schrödinger lattices*, Phys. D, 238 (2009), pp.126-136.

[20] P. COULLET, *Commensurate-Incommensurate transition in nonequilibrium systems*, Phys. Rev. Lett., 56 (1986), pp. 724-727.

[21] P. COULLET AND K. EMILSSON, *Strong resonances of spatially distributed oscillators: a laboratory to study patterns and defects*, Phys. Lett. D, 61 (1992), pp. 119-131.

[22] P. COULLET, C. RIERA, AND C. TRESSER, *Stable static localized structures in one dimension*, Phys. Rev. Lett., 84 (2000), 3069.

[23] S. M. COX AND P.C. MATTHEWS, *Exponential Time Differencing for Stiff Systems*, J. Comput. Phys., 176 (2002), pp. 430-455.

[24] C. CRAWFORD AND H. RIECKE, *Oscillon-type structures and their interaction in a Swift-Hohenberg model*, Phys. D, 129 (1999), pp. 83-92.

[25] M. C. CROSS AND P. C. HOHENBERG, *Pattern formation outside of equilibrium*, Rev. Mod. Phys., 65 (1993), pp. 851-1112.

[26] J. H. P. DAWES, *Localized pattern formation with a large-scale mode: Slanted snaking*, SIAM J. Appl. Dyn. Syst., 7 (2008), pp. 186-206.

[27] J. H. P. DAWES, *The emergence of a coherent structure for coherent structures: localized states in nonlinear systems*, Philos. Trans. R. Soc. Lond. Ser. A Math. Phys. Eng. Sci., 368 (2010), pp. 3519-3534.

[28] J. DAWES AND S. LILLEY, *Localized states in a model of pattern formation in a vertically vibrated layer*, SIAM J. Appl. Dyn. Sys., 9 (2010), pp. 238-260.

[29] A. D. DEAN, P. C. MATTHEWS, S. M. COX AND J. R. KING, *Exponential asymptotics of homoclinic snaking*, Nonlinearity, 24 (2011), pp. 24-3323.

[30] J. EGGERS AND H. RIECKE, *Continuum description of vibrated sand*, Phys. Rev. E, 59 (1999), pp. 4476-4483.

[31] C. ELPHICK, G. IOOSS, AND E. TIRAPEGUI, *Normal form reduction for time-periodically driven differential equations*, Phys. Lett. A, 120 (1987), pp. 459-463.

[32] M. FARADAY, *On a peculiar class of acoustical figures; and on certain forms assumed by groups of particles*, Philos. Trans. R. Soc. Lond., 121 (1831), pp. 299-340.

[33] W. J. FIRTH, L. COLUMBO, AND T. MAGGIPINTO, *On homoclinic snaking in optical systems*, Chaos, 17 (2007), 037115.

[34] Y. FUKAO, Y. MORITA AND H. NINOMIYA, *Some entire solutions of the Allen–Cahn equation*, Taiwanese J. Math., 8 (2004), pp. 15-32.

[35] V. L. GINZBURG AND L. D. LANDAU, *On the theory of superconductivity*, Springer Berlin Heidelberg, (2009), pp. 113-137.

[36] A. GOLOVIN, B. MATKOWSKY AND A. NEPOMNYASHCHY, *A complex Swift–Hohenberg equation coupled to the Goldstone mode in the nonlinear dynamics of flames*, Phys. D, 179 (2003), pp. 183-210.

[37] M. GOLUBITSKY AND D. G. SCHAEFFER,, *Singularities and Groups in Bifurcation Theory*, Springer-Verlag, New York Berlin, 1 (1985).

[38] J. K. HALE AND H. KOCAK, *Dynamics and Bifurcations*, Springer-Verlag, New York, (1991).

[39] M' F. HILALI, S. MÉTENS, P. BORCKMANS, AND G. DEWEL, *Pattern selection in the generalized Swift–Hohenberg model*, Phys. Rev. E, 51 (1995), 2046.

[40] S. M. HOUGHTON AND E. KNOBLOCH, *Swift-Hohenberg equation with broken cubic–quintic nonlinearity*, Phys. Rev. E, 84 (2011), 016204.

[41] R. HOYLE, *Pattern Formation An introduction to methods*, Cambridge University Press (2006).

[42] D. W. JORDAN AND P. SMITH, *Nonlinear ordinary differential equations*, Oxford University Press Inc., New York, third edition (1999).

[43] C. A. KLAUSMEIER, *Floquet theory: a useful tool for understanding nonequilibrium dynamics*, Theor Ecol, 1 (2008), pp. 153-161.

[44] J. KNOBLOCH AND T. WAGENKNECHT, *Homoclinic snaking near a heteroclinic cycle in reversible systems*, Phys. D, 206 (2005), pp. 82-93.

[45] G. KOZYREFF AND S.J. CHAPMAN, *Asymptotics of large bound states of localized structures*, Phys. Rev. Lett., 97 (2006), 044502.

[46] E. KREYSZIG, *Introductory functional analysis with applications*, John Wiley and Sons. Inc (1978).

[47] K. V. KUMAR, J. S. BOIS, F. JÜLICHER, AND S. W. GRILL, *Pulsatory patterns in active fluids*, Phys. Rev. Lett. 112 (2014), 208101.

[48] C. R. LAING, W. C. TROY, B. GUTKIN, AND G. B. ERMENTROUT, *Multiple bumps in a neuronal model of working memory*, SIAM J. Appl. Math., 63 (2002), pp. 62-97.

[49] K. J. LEE, W. D. MCCORMICK, J. E. PEARSON, AND H. L. SWINNEY, *Experimental observation of self-replicating spots in a reaction-diffusion system*, Nature, 369 (1994), pp. 215-218.

[50] O. LIOUBASHEVSKI, H. ARBELL, AND J. FINEBERG, *Dissipative solitary states in driven surface waves*, Phys. Rev. Lett., 76 (1996), pp. 3959-3962.

[51] O. LIOUBASHEVSKI, Y. HAMIEL, A. AGNON, Z. RECHES, AND J. FINEBERG, *Oscillons and Propagating Solitary Waves in a Vertically Vibrated Colloidal Suspension*, Phys. Rev. Lett., 83 (1999), pp. 3190-3193.

[52] D. J. B. LLOYD AND B. SANDSTEDE, *Localized radial solutions of the Swift-Hohenberg equation*, Nonlinearity, 22 (2009), pp. 485-524.

[53] D. J. B. LLOYD, B. SANDSTEDE, D. AVITABILE, AND A. R. CHAMPNEYS, *Localized hexagon patterns of the planar Swift–Hohenberg equation*, SIAM J. Appl. Dyn. Syst., 7 (2008), 1049.

[54] S. LONGHI, *Spatial solitary waves in nondegenerate optical parametric oscillators near an inverted bifurcation*, Opt. Commun.,149 (1998), pp. 335-340.

[55] S. MCCALLA, B. SANDSTEDE, *Snaking of radial solutions of the multi-dimensional Swift-Hohenberg equation: a numerical study*, Physica D, 239 (2010), pp. 1581-1592.

[56] W. V. R. MALKUS AND G. VERONIS, *Finite amplitude cellular convection*, J. Fluid Mech., 4(1958), pp. 225-260.

[57] C. MARTEL, E. KNOBLOCH, J. M. VEGA, *Dynamics of counterpropagating waves in parametrically forced systems*, Phys. D, 137 (2000), pp. 94-123.

[58] Y.-P. MA, J. BURKE AND E. KNOBLOCH, *Defect-mediated snaking: A new growth mechanism for localized structures*, Phys. D, 239 (2010), pp. 1867-1883.

[59] J. MILES, *Parametrically excited solitary waves*, J. Fluid Mech., 148 (1984) , pp. 451-460.

[60] J. MILES AND D. HENDERSON, *Parametrically forced surface-waves*, Annual Reviews Inc, (1990), pp. 94303-0139.

[61] K. MCQUIGHAN AND B. SANDSTEDE, *Oscillons in the planar Ginzburg-Landau equation with 2:1 forcing*, Nonlinearity, 27 (2014), 3073.

[62] A. C. NEWELL, *Envelope equations*, Lect. Appl. Math., 15:157-163 (1974).

[63] A. C. NEWELL AND J.A. WHITEHEAD, *Finite bandwidth, finite amplitude convection*, J. Fluid Mech., 38 (1969), pp. 279-303.

[64] N. PERINET, D JURIC, L. S. TUCKERMAN, *Numerical simulation of Faraday waves*, J. Fluid Mech., 635 (2009), pp. 1-26.

[65] V. PETROV, Q. OUYANG AND H. SWINNEY, *Resonant pattern formation in a chemical system*, Nature, 388 (1997), pp. 655-657.

[66] Y. POMEAU, *Front motion, metastability and subcritical bifurcations in hydrodynamics*, Phys. D, 23 (1986), pp. 3-11.

[67] H. RIECKE, *Stable wave-number kinks in parametrically excited standing waves*, Europhys. Lett., 11 (1990), pp. 213-218.

[68] R. RICHTER AND I. V. BARASHENKOV, *Two-dimensional solitons on the surface of magnetic fluids*, Phys. Rev. Lett., 94 (2005), pp. 1-4.

[69] A. M. RUCKLIDGE AND W. J. RUCKLIDGE, *Convergence properties of the 8, 10 and 12 mode representations of quasipatterns*, Phys. D, 178 (2003), pp. 62-82.

[70] A. M. RUCKLIDGE AND M. SILBER, *Design of parametrically forced patterns and quasipatterns*, SIAM J. Appl. Math., 8 (2009), pp. 298-347.

[71] H. SAKAGUCHIA AND H. R. BRAND, *Stable localized solutions of arbitrary length for the quintic Swift-Hohenberg equation*, Phys. D, 97 (1996), pp. 274-285.

[72] H. SAKAGUCHIA AND H. R. BRAND, *Stable localized squares in pattern-forming nonequilibrium systems*, Europhys. Lett., 38 (1997), pp. 341-346.

[73] H. SAKAGUCHIA AND H. R. BRAND, *Localized patterns for the quintic complex Swift-Hohenberg equation*, Phys. D, 117 (1998), pp. 95-105.

[74] H. SCHMIDT AND S. COOMBES, *Snaking behavior of homoclinic solutions in a neural field model,* BMC Neuroscience, 10 (2009), (Suppl 1):P 297.

[75] L. A. SEGEL, *Distant side-walls cause slow amplitude modulation of cellular convection*, J. Fluid Mech., 38 (1969), pp. 203-224.

[76] M. SHATS, H. XIA AND H. PUNZMANN, *Parametrically excited water surface ripples as ensembles of oscillons*, Phys. Rev. Lett., 108 (2012), 034502.

[77] A. C. SKELDON AND G. GUIDOBONI, *Pattern selection for Faraday waves in an incompressible viscous fluid*, SIAM J. Appl. Math., 67 (2007), pp. 1064-1100.

[78] J. SWIFT AND P. C. HOHENBERG, *Hydrodynamic fluctuations at the convective instability*, Phys. Rev. A, 15 (1977), pp. 319-328.

[79] M. TLIDI, P. MANDEL, AND R. LEFEVER, *Localized structures and localized patterns in optical bistability*, Phys. Rev. Lett., 73 (1994), pp. 640-643.

[80] C. M. TOPAZ AND A.J. CATLLÁ, *Forced patterns near a Turing-Hopf bifurcation*, Phys. Rev. E, 81 (2010), 026213.

[81] A. M. TURING, *The chemical basis of morphogenesis*, Philos. Trans. R. Soc. Lond. Ser. B Math. Phys. Eng. Sci., 237 (1952), pp. 37-72.

[82] L. TSIMRING AND I. ARANSON, *Localized and cellular patterns in a vibrated granular layer*, Phys. Rev. Lett., 79 (1997), pp. 213-216.

[83] P. B. UMBANHOWAR, F. MELO, AND H. L. SWINNEY, *Localized excitations in a vertically vibrated granular layer*, Nature, 382 (1996), 793.

[84] V. VANAG AND I. EPSTEIN, *Stationary and oscillatory localized patterns, and subcritical bifurcations*, Phys. Rev. Lett., 92 (2004), 128301.

[85] V. VANAG AND I. EPSTEIN, *Subcritical wave instability in reaction-diffusion systems*, J. Chem. Phys. 121 (2004), 890.

[86] V. K. VANAG AND I.R. EPSTEIN, *Resonance-induced oscillons in a reaction-diffusion system*, Phys. Rev. E, 73 (2006), 016201.

[87] V. VANAG, A. ZHABOTINSKY AND I. EPSTEIN,*Oscillatory clusters in the periodically illuminated, spatially extended Belousov-Zhabotinsky reaction*, Phys. Rev. Lett. 86 (2001), 552-555.

[88] D. M. WINTERBOTTOM, *Pattern formation with a conservation law*, Thesis, University of Nottingham (2005).

[89] J. WU, R. KEOLIAN AND I. RUDNICK, *Observation of a non-propagating hydrodynamic soliton*, Phys. Rev. Lett., 52 (1984), pp. 1421-1424.

[90] A. YOCHELIS, J. BURKE, AND E. KNOBLOCH, *Reciprocal oscillons and nonmonotonic fronts in forced nonequilibrium systems*, Phys. Rev. Lett. 97 (2006), 254501.

[91] V. I. ZARNITSINA, F. I. ATAULLAKHANOV, A. I. LOBANOV, AND O. L. MOROZOVA, *Dynamics of spatially nonuniform patterning in the model of blood coagulation,* Chaos, 11 (2001), 57.

[92] P. ZAMANKHAN AND J. HUANG, *Localized structures in vertically vibrated granular materials*, J. Fluids Eng., 129 (2007), pp. 236-244.

[93] W. ZHANG AND J. VIÑALS, *Pattern formation in weakly damped parametric surface waves*, J. Fluid Mech., 336 (1996), pp. 301-330.

Appendix A

Generating ordinary differential equations from the PDE model and the FCGL equation in Fourier space

In this appendix we will derive the set of equations in Fourier space that we used to find the bifurcation diagram (Figure 2.8) of the PDE model (2.2) for the zero wavenumber case, and also for the non-zero wavenumber case. First, we will present the approximate equations that represent the FCGL equation (2.1) as a set of ordinary differential equations (ODEs).

A.1 Set of equations for the FCGL equation

AUTO treats localized solution as a periodic orbit, with $\mathbf{Y}(X) = \mathbf{Y}(X + L_X)$, so effectively we have periodic boundary condition with fixed period L_X. Often in pattern formation problems, using AUTO is problematic because of (multiple) neutral modes with zero eigenvalue. In this problem there is only one neutral mode correspond to spatial translation, and this neutral mode can be treated by AUTO in the same way that it treats the neutral time translation mode for periodic orbits in ordinary dynamical systems, and so it poses no difficulties.

Here we write A as $A = Y_1 + iY_3$, where Y_1 and Y_3 are functions of x, and $\frac{\partial A}{\partial X} = Y_2 + iY_4$.

The model is given as $\frac{\partial \mathbf{Y}}{\partial X} = F(\mathbf{Y})$, where $\mathbf{Y} = (Y_1, Y_2, Y_3, Y_4)$, and $F(\mathbf{Y})$ is given by

$$
\begin{aligned}
F(1) &= Y_2 \\
F(2) &= (1/(1+\alpha^2))(-\alpha(\mu Y_3 + \nu Y_1 - (Y_1^2 + Y_3^2)Y_3 - \beta(Y_1^2 + Y_3^2)Y_1 - \Gamma Y_3) - (\mu Y_1 - \nu Y_3 \\
&\quad - (Y_1^2 + Y_3^2)Y_1 + \beta(Y_1^2 + Y_3^2)Y_3 + \Gamma Y_1)) \\
F(3) &= Y_4 \\
F(4) &= (1/(1+\alpha^2))(\alpha(\mu Y_1 - \nu Y_3 - (Y_1^2 + Y_3^2)Y_1 + \beta(Y_1^2 + Y_3^2)Y_3 + \Gamma Y_1) - (\mu Y_3 + \nu Y_1 \\
&\quad - (Y_1^2 + Y_3^2)Y_3 - \beta(Y_1^2 + Y_3^2)Y_1 - \Gamma Y_3)) + \lambda Y_4.
\end{aligned}
$$

Homoclinic orbits are codimension-zero in this system because of the transversal in the intersection of the stable and unstable manifolds of origin. The solution is approximated by a periodic orbit of length L_X, and $L_X \gg 1$. To make this periodic orbit an isolated solution of the spatial dynamical system, the system needs to be modified slightly, which we do by adding a small term (λY_4) to the last equation. This breaks the Hamiltonian structure of the equation, thus allowing AUTO to continue the periodic orbit [18]. The value of λ is set to zero initially, but AUTO is allowed to vary it in order to continue the periodic orbit as a function of (e.g.) Γ. We monitored the value of λ and find that it satisfies $|\lambda| < 10^{-8}$, and is typically $O(10^{-10})$.

A.2 Equations for the PDE model in Fourier space: zero wavenumber case

We write solutions of the PDE model (2.2) with a truncated Fourier series in time with the frequencies -3, -1, 1 and 3 as

$$U = (Y_1 + iY_3)e^{-3it} + (Y_5 + iY_7)e^{-it} + (Y_9 + iY_{11})e^{it} + (Y_{13} + iY_{15})e^{3it}, \qquad \text{(A.2.1)}$$

where Y_1, Y_3, Y_5, Y_7, Y_9, Y_{11}, Y_{13}, and Y_{15} are functions of x. The choice of these modes is based on the choice of the forcing $\Re(U)\cos(2t)$. The dependent variables Y_2, Y_4, Y_6,

Y_8, Y_{10}, Y_{12}, Y_{14} and Y_{16} are the first derivatives in x of Y_1, Y_3, Y_5, Y_7, Y_9, Y_{11}, Y_{13}, and Y_{15} respectively. Here the problem is 16-dimensional since we have 8 complex variables in (A.2.1) and the problem is second order in space (see (2.2)). As discussed in A.1, AUTO treats the localized solution as a periodic orbit in space (with fixed period L_x), and the representation in (A.2.1) forces U to be periodic in time. For a domain size (for example) $L_x = 200\pi$, we use the order of 1000 grid points in AUTO ($NTST = 1000$, $NCOL = 4$). We add a term (λY_{16}) to the last equation to break the Hamiltonian structure.

We used Maple to generate the following equations for AUTO to do continuation and to find the bifurcation diagram:

$$
\begin{aligned}
F(1) &= Y_2 \\
F(2) &= (-0.4D1\beta Y_1 + 0.4D1\alpha Y_3 - \nu\epsilon^2\beta Y_1 + \nu\epsilon^2\alpha Y_3 - \mu\beta Y_3 - \mu\alpha Y_1 + E(\alpha Y_7 \\
&\quad /0.2D1 - \alpha Y_{11}/0.2D1 - \beta Y_5/0.2D1 - \beta Y_9/0.2D1)/0.2D1)/(\alpha^2+\beta^2) \\
&\quad - (2C_i\beta Y_1 {Y_9}^2 - 2C_i\alpha Y_3 {Y_9}^2 - C_i\beta {Y_7}^2 Y_9 + C_i\beta {Y_5}^2 Y_9 + 2C_i\beta Y_1 Y_{15}^2 \\
&\quad - 2C_i\alpha Y_3 {Y_{15}}^2 + C_i\beta {Y_3}^2 Y_1 - C_i\alpha {Y_1}^2 Y_3 + 2C_i\beta Y_1 {Y_{11}}^2 - 2C_i\alpha Y_3 \\
&\quad {Y_{11}}^2 - C_i\alpha {Y_7}^2 Y_{11} + C_i\alpha {Y_5}^2 Y_{11} + 2C_i\beta Y_1 {Y_7}^2 - 2C_i\alpha Y_3 {Y_7}^2 + 2C_i\beta Y_1 \\
&\quad {Y_5}^2 - 2C_i\alpha Y_3 {Y_5}^2 + 2C_i\beta Y_1 {Y_{13}}^2 - 2C_i\alpha Y_3 {Y_{13}}^2 - C_i\alpha {Y_3}^3 + 2C_r\alpha Y_1 \\
&\quad {Y_9}^2 + 2C_r\beta Y_3 {Y_9}^2 - C_r\alpha {Y_7}^2 Y_9 + C_r\alpha {Y_5}^2 Y_9 + 2C_r\alpha Y_1 {Y_{15}}^2 + 2C_r\beta \\
&\quad Y_3 {Y_{15}}^2 + C_r\beta {Y_1}^2 Y_3 + C_r\alpha {Y_3}^2 Y_1 + 2C_r\alpha Y_1 {Y_{11}}^2 - 2C_r\alpha Y_7 Y_{11} Y_{13} + 2C_i\beta \\
&\quad Y_5 Y_7 Y_{11} + C_i\beta {Y_1}^3 + 2C_r\beta Y_5 Y_7 Y_9 + 2C_r\alpha Y_5 Y_9 Y_{13} + 2C_r\beta Y_7 Y_9 Y_{13} + 2C_r \\
&\quad \beta Y_7 Y_{11} Y_{15} + C_r\alpha Y_1 3 - 2C_i\beta Y_7 Y_{11} Y_{13} - 2C_i\alpha Y_5 Y_{11} Y_{13} - 2C_i\alpha Y_7 Y_9 Y_{13} + 2 \\
&\quad C_i\beta Y_5 Y_9 Y_{13} + 2C_i\alpha Y_5 Y_9 Y_{15} + 2C_i\beta Y_5 Y_{11} Y_{15} - 2C_i\alpha Y_7 Y_{11} Y_{15} + 2C_i\beta Y_7 \\
&\quad Y_9 Y_{15} + C_r\beta {Y_3}^3 - 2C_i\alpha Y_5 Y_7 Y_9 + 2C_r\beta Y_5 Y_{11} Y_{13} + 2C_r\alpha Y_7 Y_9 Y_{15} + 2C_r\alpha Y_5 \\
&\quad Y_{11} Y_{15} - 2C_r\beta Y_5 Y_9 Y_{15} + 2C_r\alpha Y_5 Y_7 Y_{11} + 2C_r\beta Y_3 {Y_{11}}^2 - C_r\beta {Y_5}^2 Y_{11} + 2 \\
&\quad C_r\alpha Y_1 {Y_7}^2 + 2C_r\beta Y_3 {Y_7}^2 + 2C_r\alpha Y_1 {Y_5}^2 + 2C_r\beta Y_3 {Y_5}^2 + 2C_r\alpha Y_1 {Y_{13}}^2 \\
&\quad + 2C_r\beta Y_3 {Y_{13}}^2 + C_r\beta {Y_7}^2 Y_{11})/(\alpha^2+\beta^2)
\end{aligned}
$$

$$F(3) = Y_4$$

$$\begin{aligned}F(4) = (&-0.4D1\alpha Y_1 - 0.4D1\beta Y_3 - \nu\epsilon^2\alpha Y_1 - \mu\alpha Y_3 - \nu\epsilon^2\beta Y_3 \\ &+ \mu\beta Y_1 - E(\alpha Y_5/0.2D1 + \alpha Y_9/0.2D1 + \beta Y_7/0.2D1 - \beta Y_{11}/0.2D1)/0.2D1) \\ &/(\alpha^2+\beta^2) - (C_r\alpha {Y_3}^3 - C_r\beta {Y_1}^3 + 2C_i\alpha Y_7 Y_9 \\ &Y_{15} - 2C_r\beta Y_5 Y_7 Y_{11} + 2C_i\alpha Y_1 {Y_{11}}^2 + C_i\beta {Y_3}^3 + C_i\alpha {Y_3}^2 Y_1 + 2C_r\alpha Y_7 Y_{11} \\ &Y_{15} - 2C_r\beta Y_5 Y_9 Y_{13} + 2C_r\alpha Y_7 Y_9 Y_{13} + 2C_r\alpha Y_5 Y_{11} Y_{13} + 2C_r\beta Y_7 Y_{11} Y_{13} - 2C_r \\ &\beta Y_7 Y_9 Y_{15} - 2C_r\alpha Y_5 Y_9 Y_{15} - C_i\beta {Y_5}^2 Y_{11} + C_i\alpha {Y_1}^3 + 2C_i\beta Y_3 {Y_9}^2 + 2C_i\alpha \\ &Y_1 {Y_9}^2 + C_i\alpha {Y_5}^2 Y_9 - C_i\alpha {Y_7}^2 Y_9 + 2C_i\beta Y_3 {Y_{15}}^2 + 2C_i\alpha Y_1 {Y_{15}}^2 + C_i\beta \\ &{Y_1}^2 Y_3 + C_i\beta {Y_7}^2 Y_{11} + 2C_i\beta Y_3 {Y_{11}}^2 + 2C_i\beta Y_5 Y_7 Y_9 - 2C_i\beta Y_5 Y_9 Y_{15} + 2C_i \\ &\alpha Y_5 Y_{11} Y_{15} + 2C_i\alpha Y_5 Y_7 Y_{11} + 2C_i\beta Y_7 Y_9 Y_{13} + 2C_i\alpha Y_5 Y_9 Y_{13} + 2C_i\beta Y_5 \\ &Y_{11} Y_{13} - 2C_i\alpha Y_7 Y_{11} Y_{13} + 2C_i\beta Y_3 {Y_7}^2 + 2C_i\alpha Y_1 {Y_7}^2 + 2C_i\beta Y_3 {Y_5}^2 + 2C_i \\ &\alpha Y_1 {Y_5}^2 + 2C_i\beta Y_3 {Y_{13}}^2 + 2C_i\alpha Y_1 {Y_{13}}^2 - 2C_r\beta Y_5 Y_{11} Y_{15} - 2C_r\beta Y_1 {Y_9}^2 \\ &+ 2C_r\alpha Y_3 {Y_9}^2 + C_r\beta {Y_7}^2 Y_9 - C_r\beta {Y_5}^2 Y_9 + 2C_r\alpha Y_3 {Y_{15}}^2 - 2C_r\beta Y_1 {Y_{15}}^2 \\ &- C_r\beta Y_1 {Y_3}^2 - 2C_r\beta Y_1 {Y_{11}}^2 - C_r\alpha {Y_5}^2 Y_{11} + C_r\alpha {Y_7}^2 Y_{11} + 2C_r\alpha Y_3 {Y_{11}}^2 \\ &- 2C_r\beta Y_1 {Y_7}^2 + 2C_r\alpha Y_3 {Y_7}^2 - 2C_r\beta Y_1 {Y_5}^2 + 2C_r\alpha Y_3 {Y_5}^2 + C_r\alpha {Y_1}^2 Y_3 \\ &- 2C_r\beta Y_1 {Y_{13}}^2 + 2C_r\alpha Y_3 {Y_{13}}^2 + 2C_i\beta Y_7 Y_{11} Y_{15} + 2C_r\alpha Y_5 Y_7 Y_9)/(\alpha^2+\beta^2)\end{aligned}$$

$$F(5) = Y_6$$

$$F(6) = (-0.2D1\beta Y_5 + 0.2D1\alpha Y_7 - \nu\epsilon^2\beta Y_5 - \mu\beta Y_7 + \nu\epsilon^2\alpha Y_7 - \mu\alpha Y_5 + E(-\alpha Y_7/0.2D1 + \alpha Y_{11}/0.2D1 - \beta Y_5/0.2D1 - \beta Y_9/0.2D1)/0.2D1 + E(-\alpha Y_{15}/0.2D1 + \alpha Y_3/0.2D1 - \beta Y_1/0.2D1 - \beta Y_{13}/0.2D1)/0.2D1)/(\alpha^2 + \beta^2) - (-2C_i\alpha Y_3Y_9Y_{13} - 2C_r\beta Y_1Y_7Y_9 - 2C_i\beta Y_3Y_5Y_{11} + 2C_i\beta Y_1Y_7Y_{11} - 2C_i\alpha Y_3Y_7Y_{11} - 2C_i\alpha Y_3Y_5Y_9 - 2C_i\alpha Y_3Y_{11}Y_{15} - 2C_i\alpha Y_1Y_9Y_{15} + 2C_i\beta Y_1Y_{11}Y_{15} + 2C_i\beta Y_1Y_9Y_{13} + 2C_i\alpha Y_1Y_{11}Y_{13} - 2C_i\alpha Y_9Y_{11}Y_{13} + 2C_i\alpha Y_1Y_7Y_9 + 2C_i\beta Y_3Y_7Y_9 + 2C_r\alpha Y_9Y_{11}Y_{15} + 2C_r\beta Y_1Y_9Y_{15} + 2C_r\alpha Y_1Y_5Y_9 - 2C_r\beta Y_1Y_{11}Y_{13} + 2C_r\beta Y_3Y_9Y_{13} - 2C_i\beta Y_3Y_9Y_{15} + C_i\beta {Y_5}^3 - C_i\alpha {Y_7}^3 - 2C_r\alpha Y_3Y_9Y_{15} + 2C_r\alpha Y_1Y_7Y_{11} + 2C_r\alpha Y_3Y_7Y_9 + 2C_r\beta Y_3Y_5Y_9 + 2C_r\beta Y_3Y_{11}Y_{15} + 2C_r\alpha Y_1Y_{11}Y_{15} - 2C_r\alpha Y_3Y_5Y_{11} + 2C_r\beta Y_9Y_{11}Y_{13} + 2C_r\alpha Y_3Y_{11}Y_{13} + 2C_r\alpha Y_1Y_9Y_{13} + 2C_r\beta Y_3Y_7Y_{11} + 2C_r\beta Y_1Y_5Y_{11} + 2C_i\beta Y_9Y_{11}Y_{15} + 2C_i\beta Y_3Y_{11}Y_{13} - 2C_i\alpha Y_1Y_5Y_{11} + C_r\alpha {Y_5}^3 + C_r\beta {Y_7}^3 + 2C_i\beta Y_5{Y_9}^2 - 2C_i\alpha Y_7{Y_9}^2 - C_i\beta {Y_{11}}^2Y_{13} + 2C_i\beta Y_5{Y_{13}}^2 - 2C_i\alpha Y_7{Y_{13}}^2 + C_i\alpha Y_9{}^2Y_{15} - C_i\alpha {Y_{11}}^2Y_{15} + 2C_i\beta Y_5{Y_{15}}^2 - 2C_i\alpha Y_7{Y_{15}}^2 + 2C_i\beta Y_5{Y_{11}}^2 - 2C_i\alpha Y_7{Y_{11}}^2 + 2C_i\beta {Y_1}^2Y_5 + 2C_i\beta {Y_3}^2Y_5 - C_i\alpha {Y_5}^2Y_7 - 2C_i\alpha {Y_1}^2Y_7 - 2C_i\alpha {Y_3}^2Y_7 + C_i\beta {Y_7}^2Y_5 + C_i\beta {Y_9}^2Y_{13} + 2C_i\beta Y_1Y_5Y_9 + 2C_r\alpha Y_5{Y_9}^2 + 2C_r\beta Y_7{Y_9}^2 + 2C_r\alpha Y_5{Y_{13}}^2 - C_r\alpha {Y_{11}}^2Y_{13} + 2C_r\beta Y_7{Y_{13}}^2 - C_r\beta {Y_9}^2Y_{15} + 2C_r\alpha Y_5{Y_{15}}^2 + C_r\beta {Y_{11}}^2Y_{15} + 2C_r\beta Y_7{Y_{15}}^2 + 2C_r\alpha Y_5{Y_{11}}^2 + 2C_r\beta Y_7{Y_{11}}^2 + 2C_r\alpha {Y_1}^2Y_5 + C_r\alpha {Y_7}^2Y_5 + C_r\beta {Y_5}^2Y_7 + 2C_r\beta {Y_1}^2Y_7 + 2C_r\beta {Y_3}^2Y_7 + C_r\alpha {Y_9}^2Y_{13} + 2C_r\alpha {Y_3}^2Y_5)/(\alpha^2 + \beta^2)$$

$$F(7) = Y_8$$

$$\begin{aligned}F(8) = (&-0.2D1\alpha Y_5 - 0.2D1\beta Y_7 - \nu\epsilon^2\alpha Y_5 + \mu\beta Y_5 - \nu\epsilon^2\beta Y_7 - \mu\alpha Y_7 \\ &- E(\alpha Y_5/0.2D1 + \alpha Y_9/0.2D1 - \beta Y_7/0.2D1 + \beta Y_{11}/0.2D1)/0.2D1 \\ &- E(\alpha Y_1/0.2D1 + \alpha Y_{13}/0.2D1 - \beta Y_{15}/0.2D1 + \beta Y_3/0.2D1)/0.2D1)/(\alpha^2+\beta^2) \\ &- (-2C_r\beta Y_1Y_7Y_{11} + 2C_i\alpha {Y_1}^2Y_5 - 2C_r\beta Y_1Y_5Y_9 + 2C_r\alpha Y_3Y_9Y_{13} + 2C_r\alpha \\ &Y_9Y_{11}Y_{13} - 2C_r\beta Y_3Y_{11}Y_{13} - 2C_r\alpha Y_1Y_{11}Y_{13} + 2C_r\alpha Y_1Y_9Y_{15} + 2C_r\beta Y_3Y_9 \\ &Y_{15} - 2C_r\beta Y_1Y_{11}Y_{15} - 2C_r\beta Y_9Y_{11}Y_{15} + 2C_r\alpha Y_3Y_{11}Y_{15} + 2C_r\alpha Y_3Y_7Y_{11} + 2C_r \\ &\beta Y_3Y_5Y_{11} + 2C_r\alpha Y_1Y_5Y_{11} - 2C_r\beta Y_1Y_9Y_{13} + C_i\alpha {Y_5}^3 + 2C_i\beta Y_1Y_9Y_{15} + C_r\alpha \\ &{Y_7}^3 - 2C_i\beta Y_1Y_7Y_9 + 2C_i\alpha Y_1Y_5Y_9 + 2C_i\alpha Y_3Y_7Y_9 + 2C_i\beta Y_3Y_5Y_9 + 2C_i \\ &\alpha Y_1Y_9Y_{13} + 2C_i\beta Y_3Y_9Y_{13} + 2C_i\beta Y_9Y_{11}Y_{13} + 2C_i\alpha Y_3Y_{11}Y_{13} - 2C_i\beta Y_1 \\ &Y_{11}Y_{13} - 2C_i\alpha Y_3Y_9Y_{15} + 2C_i\alpha Y_1Y_{11}Y_{15} + 2C_i\alpha Y_9Y_{11}Y_{15} + 2C_i\beta Y_3Y_7Y_{11} + 2 \\ &C_i\beta Y_1Y_5Y_{11} - 2C_i\alpha Y_3Y_5Y_{11} - 2C_r\alpha Y_1Y_7Y_9 - C_r\beta {Y_5}^3 + C_i\beta {Y_7}^3 + 2C_i\beta \\ &Y_3Y_{11}Y_{15} - 2C_r\beta Y_3Y_7Y_9 + 2C_i\beta Y_7{Y_{11}}^2 + 2C_i\alpha Y_5{Y_{11}}^2 + C_i\beta {Y_5}^2Y_7 + C_i \\ &\alpha {Y_7}^2Y_5 + 2C_i\beta {Y_3}^2Y_7 + 2C_i\beta Y_7{Y_9}^2 + 2C_i\alpha Y_5{Y_9}^2 - C_i\alpha {Y_{11}}^2Y_{13} \\ &+ C_i\alpha {Y_9}^2Y_{13} + 2C_i\alpha Y_5{Y_{13}}^2 + 2C_i\beta Y_7{Y_{13}}^2 + C_i\beta {Y_{11}}^2Y_{15} - C_i\beta {Y_9}^2Y_{15} \\ &+ 2C_i\alpha Y_5{Y_{15}}^2 + 2C_i\beta Y_7{Y_{15}}^2 + 2C_i\alpha {Y_3}^2Y_5 + 2C_i\beta {Y_1}^2Y_7 + 2C_r\alpha Y_3 \\ &Y_5Y_9 + 2C_r\alpha Y_7{Y_{11}}^2 - 2C_r\beta Y_5{Y_{11}}^2 + C_r\alpha {Y_5}^2Y_7 + 2C_r\alpha {Y_3}^2Y_7 + 2C_r\alpha \\ &Y_7{Y_9}^2 - 2C_r\beta Y_5{Y_9}^2 - C_r\beta Y_5{Y_7}^2 + C_r\beta {Y_{11}}^2Y_{13} + 2C_r\alpha Y_7{Y_{13}}^2 - C_r\beta \\ &{Y_9}^2Y_{13} - 2C_r\beta Y_5{Y_{13}}^2 + C_r\alpha {Y_{11}}^2Y_{15} + 2C_r\alpha Y_7{Y_{15}}^2 - C_r\alpha {Y_9}^2Y_{15} - 2C_r \\ &\beta Y_5{Y_{15}}^2 - 2C_r\beta {Y_1}^2Y_5 - 2C_r\beta {Y_3}^2Y_5 + 2C_r\alpha {Y_1}^2Y_7 + 2C_i\alpha Y_1Y_7Y_{11})/(\alpha^2+\beta^2)\end{aligned}$$

$$F(9) = Y_{10}$$

$$\begin{aligned}F(10) = {} & (-\mu\alpha Y_9 - \mu\beta Y_{11} + \nu\epsilon^2\alpha Y_{11} - \nu\epsilon^2\beta Y_9 + E(-\alpha Y_3/0.2D1 \\ & + \alpha Y_{15}/0.2D1 - \beta Y_1/0.2D1 - \beta Y_{13}/0.2D1)/0.2D1 + E(\alpha Y_7/0.2D1 \\ & - \alpha Y_{11}/0.2D1 - \beta Y_5/0.2D1 - \beta Y_9/0.2D1)/0.2D1)/(\alpha^2 + \beta^2) \\ & - (2C_r\beta Y_{11}{Y_{13}}^2 + 2C_r\alpha Y_9{Y_{13}}^2 + 2C_r\beta Y_{11}{Y_{15}}^2 + 2C_r\alpha Y_9{Y_{15}}^2 + 2C_r\alpha {Y_1}^2 Y_9 \\ & + 2C_r\alpha {Y_3}^2 Y_9 + 2C_i\beta {Y_7}^2 Y_9 + 2C_i\beta {Y_5}^2 Y_9 - 2C_i\alpha {Y_7}^2 Y_{11} - 2C_i\alpha {Y_5}^2 Y_{11} \\ & - C_i\beta Y_1 {Y_7}^2 - C_i\alpha Y_3 {Y_7}^2 + C_i\beta Y_1 {Y_5}^2 + C_i\alpha Y_3 {Y_5}^2 + C_i\beta {Y_9}^3 - C_i\alpha {Y_{11}}^3 \\ & + 2C_r\alpha {Y_7}^2 Y_9 + 2C_r\alpha {Y_5}^2 Y_9 + 2C_r\alpha Y_7 Y_{11} Y_{13} + 2C_r\beta Y_5 Y_7 Y_1 + 2C_r\alpha Y_5 Y_7 Y_3 \\ & - 2C_r\beta Y_1 Y_7 Y_{13} + 2C_r\alpha Y_1 Y_5 Y_{13} + 2C_r\beta Y_3 Y_7 Y_{15} + 2C_r\beta Y_1 Y_5 Y_{15} - 2C_r\alpha Y_3 Y_5 Y_{15} \\ & + 2C_r\alpha Y_1 Y_7 Y_{15} - 2C_i\alpha Y_3 Y_7 Y_{15} - 2C_i\alpha Y_5 Y_7 Y_1 + 2C_i\beta Y_5 Y_7 Y_3 + 2C_i\beta {Y_3}^2 Y_9 \\ & + 2C_i\beta Y_3 Y_7 Y_{13} + 2C_i\alpha Y_1 Y_7 Y_{13} + 2C_i\beta Y_1 Y_5 Y_{13} - 2C_i\alpha Y_3 Y_5 Y_{13} + 2C_i\beta Y_1 \\ & Y_7 Y_{15} - 2C_i\alpha Y_1 Y_5 Y_{15} - 2C_i\beta Y_3 Y_5 Y_{15} + 2C_r\beta Y_3 Y_5 Y_{13} + 2C_r\alpha Y_5 Y_9 Y_{13} + 2 \\ & C_r\beta Y_7 Y_9 Y_{13} + 2C_r\beta Y_7 Y_{11} Y_{15} + 2C_r\alpha Y_3 Y_7 Y_{13} + C_r\alpha {Y_9}^3 + 2C_i\beta Y_7 Y_{11} Y_{13} \\ & + 2C_i\alpha Y_5 Y_{11} Y_{13} - 2C_i\alpha Y_7 Y_9 Y_{13} + 2C_i\beta Y_5 Y_9 Y_{13} - 2C_i\alpha Y_5 Y_9 Y_{15} + 2C_i\beta \\ & Y_5 Y_{11} Y_{15} - 2C_i\alpha Y_7 Y_{11} Y_{15} - 2C_i\beta Y_7 Y_9 Y_{15} - 2C_i\alpha {Y_1}^2 Y_{11} + C_i\beta {Y_{11}}^2 Y_9 - C_i \\ & \alpha {Y_9}^2 Y_{11} - 2C_i\alpha {Y_3}^2 Y_{11} - 2C_i\alpha Y_{11}{Y_{13}}^2 + 2C_i\beta Y_9 {Y_{13}}^2 - 2C_i\alpha Y_{11}{Y_{15}}^2 \\ & + 2C_i\beta Y_9 {Y_{15}}^2 + 2C_i\beta {Y_1}^2 Y_9 - 2C_r\beta Y_5 Y_{11} Y_{13} - 2C_r\alpha Y_7 Y_9 Y_{15} + 2C_r \\ & \alpha Y_5 Y_{11} Y_{15} + 2C_r\beta Y_5 Y_9 Y_{15} + 2C_r\beta {Y_5}^2 Y_{11} - C_r\alpha Y_1 {Y_7}^2 + C_r\beta Y_3 {Y_7}^2 + C_r \\ & \alpha Y_1 {Y_5}^2 - C_r\beta Y_3 {Y_5}^2 + 2C_r\beta {Y_1}^2 Y_{11} + C_r\beta {Y_9}^2 Y_{11} + C_r\alpha {Y_{11}}^2 Y_9 + 2C_r \\ & \beta {Y_3}^2 Y_{11} + 2C_r\beta {Y_7}^2 Y_{11} + C_r\beta {Y_{11}}^3)/(\alpha^2 + \beta^2)\end{aligned}$$

$$F(11) = Y_{12}$$

$$\begin{aligned}F(12) = {} & (-\nu\epsilon^2\beta Y_{11} + \mu\beta Y_9 - \mu\alpha Y_{11} - \nu\epsilon^2\alpha Y_9 - E(\alpha Y_1/0.2D1 + \alpha Y_{13}/0.2D1 \\ & - \beta Y_3/0.2D1 + \beta Y_{15}/0.2D1)/0.2D1 - E(\alpha Y_5/0.2D1 + \alpha Y_9/0.2D1 \\ & + \beta Y_7/0.2D1 - \beta Y_{11}/0.2D1)/0.2D1)/(\alpha^2 + \beta^2) - (2C_r\alpha {Y_1}^2 Y_{11} - C_r\beta Y_9 {Y_{11}}^2 \\ & + C_r\alpha Y_9{}^2 Y_{11} + 2C_r\alpha Y_3{}^2 Y_{11} + 2C_r\alpha Y_{11} {Y_{13}}^2 - 2C_r\beta Y_9 {Y_{13}}^2 - 2C_r\beta Y_9 {Y_{15}}^2 \\ & + 2C_r\alpha Y_{11} {Y_{15}}^2 - 2C_r\beta {Y_1}^2 Y_9 - 2C_r\beta Y_3{}^2 Y_9 + C_i\alpha Y_9{}^3 + 2C_i\beta Y_5 Y_7 \\ & Y_1 - 2C_i\alpha Y_7 Y_9 Y_{15} - 2C_r\beta Y_3 Y_7 Y_{13} - 2C_r\beta Y_1 Y_5 Y_{13} + 2C_r\alpha Y_3 Y_5 Y_{13} - 2C_r\alpha \\ & Y_1 Y_7 Y_{13} + 2C_r\alpha Y_1 Y_5 Y_{15} + 2C_r\beta Y_3 Y_5 Y_{15} + 2C_r\alpha Y_5 Y_7 Y_1 - 2C_r\beta Y_5 Y_7 Y_3 \\ & - 2C_r\beta Y_1 Y_7 Y_{15} + 2C_r\alpha Y_3 Y_7 Y_{15} + C_r\alpha {Y_{11}}^3 + 2C_i\beta {Y_1}^2 Y_{11} + C_i\beta Y_9{}^2 Y_{11} \\ & + C_i\alpha Y_9 {Y_{11}}^2 + 2C_i\beta Y_3{}^2 Y_{11} + 2C_i\beta Y_{11} {Y_{13}}^2 + 2C_i\beta Y_{11} {Y_{15}}^2 + 2C_i\alpha Y_9 \\ & {Y_{15}}^2 + 2C_i\alpha {Y_1}^2 Y_9 + 2C_i\alpha Y_3{}^2 Y_9 + 2C_i\alpha Y_9 {Y_{13}}^2 + 2C_i\alpha Y_3 Y_7 Y_{13} + 2C_i \\ & \alpha Y_1 Y_5 Y_{13} + 2C_i\beta Y_3 Y_5 Y_{13} - 2C_i\beta Y_1 Y_7 Y_{13} + 2C_i\alpha Y_1 Y_7 Y_{15} + 2C_i\beta Y_3 Y_7 \\ & Y_{15} + 2C_i\beta Y_1 Y_5 Y_{15} - 2C_i\alpha Y_3 Y_5 Y_{15} + 2C_i\alpha Y_5 Y_7 Y_3 + 2C_r\alpha Y_7 Y_{11} Y_{15} \\ & - 2C_r\beta Y_5 Y_9 Y_{13} + 2C_r\alpha Y_7 Y_9 Y_{13} - 2C_r\alpha Y_5 Y_{11} Y_{13} - 2C_r\beta Y_7 Y_{11} Y_{13} \\ & + 2C_r\beta Y_7 Y_9 Y_{15} + 2C_r\alpha Y_5 Y_9 Y_{15} + C_i\beta {Y_{11}}^3 + 2C_i\beta Y_5{}^2 Y_{11} + 2C_i\alpha Y_5{}^2 Y_9 \\ & + 2C_i\alpha Y_7{}^2 Y_9 + 2C_i\beta Y_7{}^2 Y_{11} + 2C_i\beta Y_5 Y_9 Y_{15} + 2C_i\alpha Y_5 Y_{11} Y_{15} + 2C_i\beta Y_7 Y_9 Y_{13} \\ & + 2C_i\alpha Y_5 Y_9 Y_{13} - 2C_i\beta Y_5 Y_{11} Y_{13} + 2C_i\alpha Y_7 Y_{11} Y_{13} + C_i\beta Y_3 {Y_7}^2 - C_i\alpha Y_1 {Y_7}^2 \\ & - C_i\beta Y_3 {Y_5}^2 + C_i\alpha Y_1 {Y_5}^2 - 2C_r\beta Y_5 Y_{11} Y_{15} - C_r\beta Y_9{}^3 - 2C_r\beta Y_7{}^2 Y_9 \\ & - 2C_r\beta Y_5{}^2 Y_9 + 2C_r\alpha Y_5{}^2 Y_{11} + 2C_r\alpha Y_7{}^2 Y_{11} + C_r\beta Y_1 Y_7{}^2 + C_r\alpha Y_3 Y_7{}^2 \\ & - C_r\beta Y_1 {Y_5}^2 - C_r\alpha Y_3 {Y_5}^2 + 2C_i\beta Y_7 Y_{11} Y_{15})/(\alpha^2 + \beta^2)\end{aligned}$$

$$F(13) \quad = Y_{14}$$

$$F(14) \quad = (0.2D1\beta Y_{13} - 0.2D1\alpha Y_{15} + \nu\epsilon^2\alpha Y_{15} - \mu\alpha Y_{13} - \nu\epsilon^2\beta Y_{13} - \mu\beta$$
$$Y_{15} + E(-\alpha Y_7/0.2D1 + \alpha Y_{11}/0.2D1 - \beta Y_5/0.2D1 - \beta Y_9/0.2D1)/0.2D1)$$
$$/(\alpha^2 + \beta^2) - (2C_r\beta {Y_7}^2 Y_{15} + C_r\beta {Y_{13}}^2 Y_{15} + C_r$$
$$\alpha {Y_{15}}^2 Y_{13} + 2C_r\beta {Y_1}^2 Y_{15} + 2C_r\beta {Y_5}^2 Y_{15} + 2C_r\beta {Y_3}^2 Y_{15} + 2C_r\alpha {Y_7}^2 Y_{13}$$
$$+ 2C_r\alpha {Y_1}^2 Y_{13} + 2C_r\alpha {Y_5}^2 Y_{13} + 2C_r\alpha {Y_3}^2 Y_{13} + 2C_r\beta Y_1 Y_7 Y_9 + 2C_i\beta$$
$$Y_3 Y_5 Y_{11} - 2C_i\beta Y_1 Y_7 Y_{11} - 2C_i\alpha Y_3 Y_7 Y_{11} + 2C_i\alpha Y_3 Y_5 Y_9 - 2C_i\alpha Y_1 Y_7 Y_9 + 2$$
$$C_i\beta Y_3 Y_7 Y_9 + 2C_r\alpha Y_1 Y_5 Y_9 - C_i\alpha {Y_{15}}^3 + C_i\beta {Y_{13}}^3 + 2C_r\beta Y_9 Y_{11} Y_5 - 2C_i$$
$$\alpha {Y_7}^2 Y_{15} - C_i\alpha {Y_{13}}^2 Y_{15} - 2C_i\alpha {Y_1}^2 Y_{15} - 2C_i\alpha {Y_5}^2 Y_{15} - 2C_i\alpha {Y_3}^2 Y_{15}$$
$$+ C_i\beta {Y_{15}}^2 Y_{13} + 2C_i\beta {Y_1}^2 Y_{13} + 2C_i\beta {Y_5}^2 Y_{13} + 2C_i\beta {Y_3}^2 Y_{13} + 2C_i\beta {Y_7}^2 Y_{13}$$
$$+ 2C_i\beta Y_9 Y_{11} Y_7 - 2C_i\alpha Y_9 Y_{11} Y_5 + C_r\beta {Y_{15}}^3 - 2C_r\alpha Y_1 Y_7 Y_{11} + 2C_r\alpha$$
$$Y_3 Y_7 Y_9 - 2C_r\beta Y_3 Y_5 Y_9 + 2C_r\alpha Y_3 Y_5 Y_{11} + 2C_r\beta Y_3 Y_7 Y_{11} + 2C_r\beta Y_1 Y_5 Y_{11}$$
$$- 2C_i\alpha Y_1 Y_5 Y_{11} + C_i\beta Y_5 {Y_9}^2 + C_i\alpha Y_7 {Y_9}^2 + 2C_i\beta {Y_{11}}^2 Y_{13} - 2C_i\alpha {Y_9}^2 Y_{15}$$
$$- 2C_i\alpha {Y_{11}}^2 Y_{15} - C_i\beta Y_5 {Y_{11}}^2 - C_i\alpha Y_7 {Y_{11}}^2 + 2C_i\beta {Y_9}^2 Y_{13} + 2C_i\beta Y_1 Y_5$$
$$Y_9 + C_r\alpha Y_5 {Y_9}^2 - C_r\beta Y_7 {Y_9}^2 + 2C_r\alpha {Y_{11}}^2 Y_{13} + 2C_r\beta {Y_9}^2 Y_{15} + 2C_r\beta {Y_{11}}$$
$${}^2 Y_{15} - C_r\alpha Y_5 {Y_{11}}^2 + C_r\beta Y_7 {Y_{11}}^2 + 2C_r\alpha {Y_9}^2 Y_{13} + C_r\alpha {Y_{13}}^3 + 2C_r\alpha Y_9$$
$$Y_{11} Y_7)/(\alpha^2 + \beta^2)$$

$$F(15) = Y_{16}$$

$$\begin{aligned}F(16) = {} & (0.2D1\alpha Y_{13} + 0.2D1\beta Y_{15} - \nu\epsilon^2\alpha Y_{13} - \mu\alpha Y_{15} - \nu\epsilon^2\beta Y_{15} \\ & + \mu\beta Y_{13} - E(\alpha Y_5/0.2D1 + \alpha Y_9/0.2D1 - \beta Y_7/0.2D1 \\ & + \beta Y_{11}/0.2D1)/0.2D1)/(\alpha^2+\beta^2) - (C_i\beta {Y_{15}}^3 - 2C_r\beta {Y_7}^2 Y_{13} - 2C_r \\ & \beta {Y_1}^2 Y_{13} - 2C_r\beta {Y_5}^2 Y_{13} - 2C_r\beta {Y_3}^2 Y_{13} + 2C_r\alpha {Y_7}^2 Y_{15} - C_r\beta Y_{13} {Y_{15}}^2 \\ & + C_r\alpha {Y_{13}}^2 Y_{15} + 2C_r\alpha {Y_1}^2 Y_{15} + 2C_r\alpha {Y_5}^2 Y_{15} + 2C_r\alpha {Y_3}^2 Y_{15} + 2C_r\beta Y_1 \\ & Y_7 Y_{11} - 2C_r\beta Y_1 Y_5 Y_9 + 2C_r\alpha Y_3 Y_7 Y_{11} - 2C_r\beta Y_3 Y_5 Y_{11} + 2C_r\alpha Y_1 Y_5 Y_{11} + 2C_i \\ & \beta {Y_5}^2 Y_{15} + 2C_i\beta {Y_3}^2 Y_{15} + C_i\alpha {Y_{13}}^3 + 2C_i\beta Y_9 Y_{11} Y_5 - C_r\beta {Y_{13}}^3 + 2C_r\alpha \\ & Y_9 Y_{11} Y_5 - 2C_r\beta Y_9 Y_{11} Y_7 + 2C_i\alpha Y_9 Y_{11} Y_7 + 2C_i\beta {Y_1}^2 Y_{15} + 2C_i\beta Y_1 Y_7 Y_9 \\ & + 2C_i\alpha Y_1 Y_5 Y_9 + 2C_i\alpha Y_3 Y_7 Y_9 - 2C_i\beta Y_3 Y_5 Y_9 + 2C_i\beta Y_3 Y_7 Y_{11} + 2C_i\beta Y_1 \\ & Y_5 Y_{11} + 2C_i\alpha Y_3 Y_5 Y_{11} + 2C_i\alpha {Y_7}^2 Y_{13} + 2C_i\alpha {Y_1}^2 Y_{13} + 2C_i\alpha {Y_5}^2 Y_{13} + 2 \\ & C_i\alpha {Y_3}^2 Y_{13} + 2C_i\beta {Y_7}^2 Y_{15} + C_i\beta {Y_{13}}^2 Y_{15} + C_i\alpha Y_{13} {Y_{15}}^2 + 2C_r\alpha Y_1 Y_7 Y_9 \\ & - 2C_r\beta Y_3 Y_7 Y_9 + C_i\beta Y_7 {Y_{11}}^2 - C_i\alpha Y_5 {Y_{11}}^2 - C_i\beta Y_7 {Y_9}^2 + C_i\alpha Y_5 {Y_9}^2 + 2 \\ & C_i\alpha {Y_{11}}^2 Y_{13} + 2C_i\alpha {Y_9}^2 Y_{13} + 2C_i\beta {Y_{11}}^2 Y_{15} + 2C_i\beta {Y_9}^2 Y_{15} \\ & + C_r\alpha {Y_{15}}^3 - 2C_r\alpha Y_3 Y_5 Y_9 + C_r\alpha Y_7 {Y_{11}}^2 + C_r\beta {Y_5} \\ & {Y_{11}}^2 - C_r\alpha Y_7 {Y_9}^2 - C_r\beta Y_5 {Y_9}^2 - 2C_r\beta {Y_{11}}^2 Y_{13} - 2C_r\beta {Y_9}^2 Y_{13} + 2C_r\alpha \\ & {Y_{11}}^2 Y_{15} + 2C_r\alpha {Y_9}^2 Y_{15} - 2C_i\alpha Y_1 Y_7 Y_{11})/(\alpha^2+\beta^2) + \lambda Y_{16}\end{aligned}$$

A.3 Equations of the PDE model generated by Maple in Fourier space: non-zero wavenumber case

We write solutions of the PDE model (1.12) with a truncated Fourier series in time with the frequencies -3, -1, 1 and 3. We expand U in Fourier space as

$$U = (Y_1 + iY_5)e^{-3it} + (Y_9 + iY_{13})e^{-it} + (Y_{17} + iY_{21})e^{it} + (Y_{25} + iY_{29})e^{3it}.$$

Here, with four derivatives in space, we need $Y_2 = \frac{\partial Y_1}{\partial x}$, $Y_3 = \frac{\partial^2 Y_1}{\partial x^2}$, $Y_4 = \frac{\partial^3 Y_1}{\partial x^3}$ and so on. We also add a term ($\lambda Y_3 2$) to the last equation to break the Hamiltonian structure as before. The equations are

$$
\begin{aligned}
F(1) &= Y_2 \\
F(2) &= Y_3 \\
F(3) &= Y_4 \\
F(4) &= (-0.3D1\delta Y_1 + 0.3D1\rho Y_5 - \mu\rho Y_1 + \omega\rho Y_5 - \omega\delta Y_1 - \mu\delta Y_5 - \alpha\rho Y_3 - \alpha\delta Y_7 \\
&\quad + \beta\rho Y_7 - \beta\delta Y_3 + E(\rho Y_{13}/0.2D1 - \rho Y_{21}/0.2D1 - \delta Y_9/0.2D1 - \delta Y_{17}/0.2D1) \\
&\quad /0.2D1)/(\rho^2 + \delta^2) - (2C_i\delta Y_1 Y_{17}^2 - 2C_i\rho Y_5 Y_{17}^2 - C_i\delta Y_{13}^2 Y_{17} + C_i\delta Y_9^2 Y_{17} \\
&\quad + 2C_i\delta Y_1 {Y_{29}}^2 - 2C_i\rho Y_5 Y_{29}^2 + C_i\delta Y_5^2 Y_1 - C_i\rho Y_1^2 Y_5 + 2C_i\delta Y_1 Y_{21}^2 - 2C_i\rho Y_5 \\
&\quad Y_{21}^2 - C_i\rho Y_{13}^2 Y_{21} + C_i\rho Y_9^2 Y_{21} + 2C_i\delta Y_1 Y_{13}^2 - 2C_i\rho Y_5 Y_{13}^2 + 2C_i\delta Y_1 \\
&\quad Y_9^2 - 2C_i\rho Y_5 Y_9^2 + 2C_i\delta Y_1 Y_{25}^2 - 2C_i\rho Y_5 Y_{25}^2 - C_i\rho Y_5^3 + 2C_r\rho Y_1 \\
&\quad Y_{17}^2 + 2C_r\delta Y_5 Y_{17}^2 - C_r\rho Y_{13}^2 Y_{17} + C_r\rho Y_9^2 Y_{17} + 2C_r\rho Y_1 Y_{29}^2 + 2C_r\delta \\
&\quad Y_5 Y_{29}^2 + C_r\delta Y_1^2 Y_5 + C_r\rho Y_5^2 Y_1 + 2C_r\rho Y_1 Y_{21}^2 - 2C_r\rho Y_{13} Y_{21} Y_{25} + 2C_i\delta \\
&\quad Y_9 Y_{13} Y_{21} + C_i\delta Y_1^3 + 2C_r\delta Y_9 Y_{13} Y_{17} + 2C_r\rho Y_9 Y_{17} Y_{25} + 2C_r\delta Y_{13} Y_{17} Y_{25} + 2C_r \\
&\quad \delta Y_{13} Y_{21} Y_{29} + C_r\rho Y_1^3 - 2C_i\delta Y_{13} Y_{21} Y_{25} - 2C_i\rho Y_9 Y_{21} Y_{25} - 2C_i\rho Y_{13} Y_{17} Y_{25} + 2 \\
&\quad C_i\delta Y_9 Y_{17} Y_{25} + 2C_i\rho Y_9 Y_{17} Y_{29} + 2C_i\delta Y_9 Y_{21} Y_{29} - 2C_i\rho Y_{13} Y_{21} Y_{29} + 2C_i\delta Y_{13} \\
&\quad Y_{17} Y_{29} + C_r\delta Y_5^3 - 2C_i\rho Y_9 Y_{13} Y_{17} + 2C_r\delta Y_9 Y_{21} Y_{25} + 2C_r\rho Y_{13} Y_{17} Y_{29} + 2C_r\rho Y_9 \\
&\quad Y_{21} Y_{29} - 2C_r\delta Y_9 Y_{17} Y_{29} + 2C_r\rho Y_9 Y_{13} Y_{21} + 2C_r\delta Y_5 Y_{21}^2 - C_r\delta Y_9^2 Y_{21} + 2 \\
&\quad C_r\rho Y_1 Y_{13}^2 + 2C_r\delta Y_5 Y_{13}^2 + 2C_r\rho Y_1 Y_9^2 + 2C_r\delta Y_5 Y_9^2 + 2C_r\rho Y_1 {Y_{25}}^2 \\
&\quad + 2C_r\delta Y_5 Y_{25}^2 + C_r\delta Y_{13}^2 Y_{21})/(\rho^2 + \delta^2)
\end{aligned}
$$

$$F(5) = Y_6$$

$$F(6) = Y_7$$

$$F(7) = Y_8$$

$$\begin{aligned}F(8) = (&-0.3D1\rho Y_1 - 0.3D1\delta Y_5 + \mu\delta Y_1 - \mu\rho Y_5 - \omega\rho Y_1 - \omega\delta Y_5 - \alpha\rho \\ &Y_7 + \alpha\delta Y_3 - \beta\rho Y_3 - \beta\delta Y_7 - E(\rho Y_9/0.2D1 + \rho Y_{17}/0.2D1 + \delta \\ &Y_{13}/0.2D1 - \delta Y_{21}/0.2D1)/0.2D1)/(\rho^2 + \delta^2) - (C_r\rho Y_5^3 - C_r\delta Y_1^3 + 2C_i\rho Y_{13}Y_{17} \\ &Y_{29} - 2C_r\delta Y_9 Y_{13}Y_{21} + 2C_i\rho Y_1 Y_{21}^2 + C_i\delta Y_5^3 + C_i\rho Y_5^2 Y_1 + 2C_r\rho Y_{13}Y_{21} \\ &Y_{29} - 2C_r\delta Y_9 Y_{17}Y_{25} + 2C_r\rho Y_{13}Y_{17}Y_{25} + 2C_r\rho Y_9 Y_{21}Y_{25} + 2C_r\delta Y_{13}Y_{21}Y_{25} - 2C_r \\ &\delta Y_{13}Y_{17}Y_{29} - 2C_r\rho Y_9 Y_{17}Y_{29} - C_i\delta Y_9^2 Y_{21} + C_i\rho Y_1^3 + 2C_i\delta Y_5 Y_{17}^2 + 2C_i\rho \\ &Y_1 Y_{17}^2 + C_i\rho Y_9^2 Y_{17} - C_i\rho Y_{13}^2 Y_{17} + 2C_i\delta Y_5 Y_{29}^2 + 2C_i\rho Y_1 Y_{29}^2 + C_i\delta \\ &Y_1^2 Y_5 + C_i\delta Y_{13}^2 Y_{21} + 2C_i\delta Y_5 Y_{21}^2 + 2C_i\delta Y_9 Y_{13}Y_{17} - 2C_i\delta Y_9 Y_{17}Y_{29} + 2C_i \\ &Y_{13}Y_{17}Y_{25} + 2C_i\rho Y_9 Y_{17}Y_{25} + 2C_i\delta Y_9 Y_{21}Y_{25} - 2C_i\rho Y_{13}Y_{21}Y_{25} + 2C_i\delta Y_5 Y_{13}^2 \\ &+ 2C_i\rho Y_1 Y_{13}^2 + 2C_i\delta Y_5 Y_9^2 + 2C_i\rho Y_1 Y_9^2 + 2C_i\delta Y_5 Y_{25}^2 + 2C_i\rho Y_1 \\ &Y_{25}^2 - 2C_r\delta Y_9 Y_{21}Y_{29} - 2C_r\delta Y_1 Y_{17}^2 + 2C_r\rho Y_5 Y_{17}^2 + C_r\delta Y_{13}^2 Y_{17} - C_r\delta Y_9^2 \\ &Y_{17} + 2C_r\rho Y_5 Y_{29}^2 - 2C_r\delta Y_1 {Y_{29}}^2 - C_r\delta Y_1 Y_5^2 - 2C_r\delta Y_1 Y_{21}^2 - C_r\rho \\ &Y_9^2 Y_{21} + C_r\rho Y_{13}^2 Y_{21} + 2C_r\rho Y_5 {Y_{21}}^2 - 2C_r\delta Y_1 Y_{13}^2 + 2C_r\rho Y_5 Y_{13}^2 - 2C_r \\ &\delta Y_1 Y_9^2 + 2C_r\rho Y_5 Y_9^2 + C_r\rho Y_1^2 Y_5 - 2C_r\delta Y_1 Y_{25}^2 + 2C_r\rho Y_5 Y_{25}^2 \\ &+ 2C_i\delta Y_{13}Y_{21}Y_{29} + 2C_r\rho Y_9 Y_{13}Y_{17})/(\rho^2 + \delta^2)\end{aligned}$$

$$F(9) = Y_{10}$$

$$F(10) = Y_{11}$$

$$F(11) = Y_{12}$$

$$\begin{aligned}F(12) = {} & (-\delta Y_9 + \rho Y_{13} - \omega\delta Y_9 - \mu\delta Y_{13} - \mu\rho Y_9 + \omega\rho Y_{13} - \alpha\rho Y_{11} \\ & - \alpha\delta Y_{15} + \beta\rho Y_{15} - \beta\delta Y_{11} + E(-\rho Y_{13}/0.2D1 + \rho Y_{21}/0.2D1 - \delta Y_9 \\ & /0.2D1 - \delta Y_{17}/0.2D1)/0.2D1 + E(-\rho Y_{29}/0.2D1 + \rho Y_5/0.2D1 - \delta Y_1/0.2D1 \\ & - \delta Y_{25}/0.2D1)/0.2D1)/(\rho^2 + \delta^2) - (-2C_i\rho Y_5 Y_{17} Y_{25} - 2C_r\delta Y_1 Y_{13} Y_{17} - 2 \\ & C_i\delta Y_5 Y_9 Y_{21} + 2C_i\delta Y_1 Y_{13} Y_{21} - 2C_i\rho Y_5 Y_{13} Y_{21} - 2C_i\rho Y_5 Y_9 Y_{17} - 2C_i\rho Y_5 Y_{21} \\ & Y_{29} - 2C_i\rho Y_1 Y_{17} Y_{29} + 2C_i\delta Y_1 Y_{21} Y_{29} + 2C_i\delta Y_1 Y_{17} Y_{25} + 2C_i\rho Y_1 Y_{21} Y_{25} - 2 \\ & C_i\rho Y_{17} Y_{21} Y_{25} + 2C_i\rho Y_1 Y_{13} Y_{17} + 2C_i\delta Y_5 Y_{13} Y_{17} + 2C_r\rho Y_{17} Y_{21} Y_{29} + 2C_r\delta Y_1 Y_{17} \\ & Y_{29} + 2C_r\rho Y_1 Y_9 Y_{17} - 2C_r\delta Y_1 Y_{21} Y_{25} + 2C_r\delta Y_5 Y_{17} Y_{25} - 2C_i\delta Y_5 Y_{17} Y_{29} + C_i\delta \\ & Y_9^3 - C_i\rho Y_{13}^3 - 2C_r\rho Y_5 Y_{17} Y_{29} + 2C_r\rho Y_1 Y_{13} Y_{21} + 2C_r\rho Y_5 Y_{13} Y_{17} + 2C_r\delta \\ & Y_5 Y_9 Y_{17} + 2C_r\delta Y_5 Y_{21} Y_{29} + 2C_r\rho Y_1 Y_{21} Y_{29} - 2C_r\rho Y_5 Y_9 Y_{21} + 2C_r\delta Y_{17} Y_{21} Y_{25} \\ & + 2C_r\rho Y_5 Y_{21} Y_{25} + 2C_r\rho Y_1 Y_{17} Y_{25} + 2C_r\delta Y_5 Y_{13} Y_{21} + 2C_r\delta Y_1 Y_9 Y_{21} + 2C_i\delta \\ & Y_{17} Y_{21} Y_{29} + 2C_i\delta Y_5 Y_{21} Y_{25} - 2C_i\rho Y_1 Y_9 Y_{21} + C_r\rho Y_9^3 + C_r\delta Y_{13}^3 + 2C_i\delta Y_9 \\ & Y_{17}^2 - 2C_i\rho Y_{13} Y_{17}^2 - C_i\delta Y_{21}^2 Y_{25} + 2C_i\delta Y_9 Y_{25}^2 - 2C_i\rho Y_{13} Y_{25}^2 + C_i\rho \\ & Y_{17}^2 Y_{29} - C_i\rho Y_{21}^2 Y_{29} + 2C_i\delta Y_9 Y_{29}^2 - 2C_i\rho Y_{13} Y_{29}^2 + 2C_i\delta Y_9 Y_{21}^2 - 2 \\ & C_i\rho Y_{13} Y_{21}^2 + 2C_i\delta Y_1^2 Y_9 + 2C_i\delta Y_5^2 Y_9 - C_i\rho Y_9^2 Y_{13} - 2C_i\rho Y_1^2 Y_{13} \\ & - 2C_i\rho Y_5^2 Y_{13} + C_i\delta Y_{13}^2 Y_9 + C_i\delta Y_{17}^2 Y_{25} + 2C_i\delta Y_1 Y_9 Y_{17} + 2C_r\rho Y_9 Y_{17}^2 \\ & + 2C_r\delta Y_{13} Y_{17}^2 + 2C_r\rho Y_9 Y_{25}^2 - C_r\rho Y_{21}^2 Y_{25} + 2C_r\delta Y_{13} Y_{25}^2 - C_r\delta Y_{17}^2 \\ & Y_{29} + 2C_r\rho Y_9 Y_{29}^2 + C_r\delta Y_{21}^2 Y_{29} + 2C_r\delta Y_{13} Y_{29}^2 + 2C_r\rho Y_9 Y_{21}^2 + 2C_r\delta \\ & Y_{13} Y_{21}^2 + 2C_r\rho Y_1^2 Y_9 + C_r\rho Y_{13}^2 Y_9 + C_r\delta Y_9^2 Y_{13} + 2C_r\delta Y_1^2 Y_{13} + 2C_r\delta \\ & Y_5^2 Y_{13} + C_r\rho Y_{17}^2 Y_{25} + 2C_r\rho Y_5^2 Y_9)/(\rho^2 + \delta^2)\end{aligned}$$

$$F(13) = Y_{14}$$

$$F(14) = Y_{15}$$

$$F(15) = Y_{16}$$

$$\begin{aligned}F(16) = {} & (-\rho Y_9 - \delta Y_{13} - \omega\rho Y_9 - \mu\rho Y_{13} + \mu\delta Y_9 - \omega\delta Y_{13} - \alpha\rho Y_{15} \\ & + \alpha\delta Y_{11} - \beta\rho Y_{11} - \beta\delta Y_{15} - E(\rho Y_9/0.2D1 + \rho Y_{17}/0.2D1 - \delta Y_{13} \\ & /0.2D1 + \delta Y_{21}/0.2D1)/0.2D1 - E(\rho Y_1/0.2D1 + \rho Y_{25}/0.2D1 - \delta Y_{29}/0.2D1 \\ & + \delta Y_5/0.2D1)/0.2D1)/(\rho^2 + \delta^2) - (-2C_r\delta Y_1 Y_{13} Y_{21} + 2C_i\rho Y_1^2 Y_9 - 2 \\ & C_r\delta Y_1 Y_9 Y_{17} + 2C_r\rho Y_5 Y_{17} Y_{25} + 2C_r\rho Y_{17} Y_{21} Y_{25} - 2C_r\delta Y_5 Y_{21} Y_{25} - 2C_r\rho Y_1 \\ & Y_{21} Y_{25} + 2C_r\rho Y_1 Y_{17} Y_{29} + 2C_r\delta Y_5 Y_{17} Y_{29} - 2C_r\delta Y_1 Y_{21} Y_{29} - 2C_r\delta Y_{17} Y_{21} Y_{29} \\ & + 2C_r\rho Y_5 Y_{21} Y_{29} + 2C_r\rho Y_5 Y_{13} Y_{21} + 2C_r\delta Y_5 Y_9 Y_{21} + 2C_r\rho Y_1 Y_9 Y_{21} - 2C_r\delta Y_1 \\ & Y_{17} Y_{25} + C_i\rho Y_9^3 + 2C_i\delta Y_1 Y_{17} Y_{29} + C_r\rho Y_{13}^3 - 2C_i\delta Y_1 Y_{13} Y_{17} + 2C_i\rho Y_1 Y_9 Y_{17} \\ & + 2C_i\rho Y_5 Y_{13} Y_{17} + 2C_i\delta Y_5 Y_9 Y_{17} + 2C_i\rho Y_1 Y_{17} Y_{25} + 2C_i\delta Y_5 Y_{17} Y_{25} + 2C_i\delta \\ & Y_{17} Y_{21} Y_{25} + 2C_i\rho Y_5 Y_{21} Y_{25} - 2C_i\delta Y_1 Y_{21} Y_{25} - 2C_i\rho Y_5 Y_{17} Y_{29} + 2C_i\rho Y_1 Y_{21} Y_{29} \\ & + 2C_i\rho Y_{17} Y_{21} Y_{29} + 2C_i\delta Y_5 Y_{13} Y_{21} + 2C_i\delta Y_1 Y_9 Y_{21} - 2C_i\rho Y_5 Y_9 Y_{21} - 2C_r\rho \\ & Y_1 Y_{13} Y_{17} - C_r\delta Y_9^3 + C_i\delta Y_{13}^3 + 2C_i\delta Y_5 Y_{21} Y_{29} - 2C_r\delta Y_5 Y_{13} Y_{17} + 2C_i\delta Y_{13} \\ & Y_{21}^2 + 2C_i\rho Y_9 Y_{21}^2 + C_i\delta Y_9^2 Y_{13} + C_i\rho Y_{13}^2 Y_9 + 2C_i\delta Y_5^2 Y_{13} + 2C_i\delta Y_{13} \\ & Y_{17}^2 + 2C_i\rho Y_9 Y_{17}^2 - C_i\rho Y_{21}^2 Y_{25} + C_i\rho Y_{17}^2 Y_{25} + 2C_i\rho Y_9 Y_{25}^2 + 2C_i\delta \\ & Y_{13} Y_{25}^2 + C_i\delta Y_{21}^2 Y_{29} - C_i\delta Y_{17}^2 Y_{29} + 2C_i\rho Y_9 Y_{29}^2 + 2C_i\delta Y_{13} Y_{29}^2 + 2C_i \\ & \rho Y_5^2 Y_9 + 2C_i\delta Y_1^2 Y_{13} + 2C_r\rho Y_5 Y_9 Y_{17} + 2C_r\rho Y_{13} Y_{21}^2 - 2C_r\delta Y_9 Y_{21}^2 \\ & + C_r\rho Y_9^2 Y_{13} + 2C_r\rho Y_5^2 Y_{13} + 2C_r\rho Y_{13} Y_{17}^2 - 2C_r\delta Y_9 Y_{17}^2 - C_r\delta Y_9 Y_{13}^2 \\ & + C_r\delta Y_{21}^2 Y_{25} + 2C_r\rho Y_{13} Y_{25}^2 - C_r\delta Y_{17}^2 Y_{25} - 2C_r\delta Y_9 Y_{25}^2 + C_r\rho Y_{21}^2 \\ & Y_{29} + 2C_r\rho Y_{13} Y_{29}^2 - C_r\rho Y_{17}^2 Y_{29} - 2C_r\delta Y_9 Y_{29}^2 - 2C_r\delta Y_1^2 Y_9 - 2C_r\delta {Y_5}^2 Y_9 \\ & + 2C_r\rho Y_1^2 Y_{13} + 2C_i\rho Y_1 Y_{13} Y_{21})/(\rho^2 + \delta^2)\end{aligned}$$

$$F(17) = Y_{18}$$

$$F(18) = Y_{19}$$

$$F(19) = Y_{20}$$

$$\begin{aligned}F(20) = {} & (\delta Y_{17} - \gamma Y_{21} - \mu\delta Y_{21} - \omega\delta Y_{17} + \omega\gamma Y_{21} - \mu\gamma Y_{17} - \alpha\gamma Y_{19} \\ & - \alpha\delta Y_{23} + \beta\gamma Y_{23} - \beta\delta Y_{19} + E(-\gamma Y_5/0.2D1 + \gamma Y_{29}/0.2D1 - \delta Y_1 \\ & /0.2D1 - \delta Y_{25}/0.2D1)/0.2D1 + E(\gamma Y_{13}/0.2D1 - \gamma Y_{21}/0.2D1 - \delta Y_9/0.2D1 \\ & - \delta Y_{17}/0.2D1)/0.2D1)/(\gamma^2 + \delta^2) - (2C_r\delta Y_{21}Y_{25}^2 + 2C_r\gamma Y_{17}Y_{25}^2 \\ & + 2C_r\delta Y_{21}Y_{29}^2 + 2C_r\gamma Y_{17}Y_{29}^2 + 2C_r\gamma Y_1^2Y_{17} + 2C_r\gamma Y_5^2Y_{17} + 2C_i\delta {Y_{13}}^2Y_{17} \\ & + 2C_i\delta Y_9^2Y_{17} - 2C_i\gamma Y_{13}^2Y_{21} - 2C_i\gamma Y_9^2Y_{21} - C_i\delta Y_1Y_{13}^2 - C_i\gamma Y_5 \\ & Y_{13}^2 + C_i\delta Y_1Y_9^2 + C_i\gamma Y_5Y_9^2 + C_i\delta Y_{17}^3 - C_i\gamma Y_{21}^3 + 2C_r\gamma Y_{13}^2Y_{17} + 2C_r \\ & \gamma Y_9^2Y_{17} + 2C_r\gamma Y_{13}Y_{21}Y_{25} + 2C_r\delta Y_9Y_{13}Y_1 + 2C_r\gamma Y_9Y_{13}Y_5 - 2C_r\delta Y_1Y_{13} \\ & Y_{25} + 2C_r\gamma Y_1Y_9Y_{25} + 2C_r\delta Y_5Y_{13}Y_{29} + 2C_r\delta Y_1Y_9Y_{29} - 2C_r\gamma Y_5Y_9Y_{29} + 2C_r \\ & \gamma Y_1Y_{13}Y_{29} - 2C_i\gamma Y_5Y_{13}Y_{29} - 2C_i\gamma Y_9Y_{13}Y_1 + 2C_i\delta Y_9Y_{13}Y_5 + 2C_i\delta Y_5^2Y_{17} \\ & + 2C_i\delta Y_5Y_{13}Y_{25} + 2C_i\gamma Y_1Y_{13}Y_{25} + 2C_i\delta Y_1Y_9Y_{25} - 2C_i\gamma Y_5Y_9Y_{25} + 2C_i\delta Y_1 \\ & Y_{13}Y_{29} - 2C_i\gamma Y_1Y_9Y_{29} - 2C_i\delta Y_5Y_9Y_{29} + 2C_r\delta Y_5Y_9Y_{25} + 2C_r\gamma Y_9Y_{17}Y_{25} + 2 \\ & C_r\delta Y_{13}Y_{17}Y_{25} + 2C_r\delta Y_{13}Y_{21}Y_{29} + 2C_r\gamma Y_5Y_{13}Y_{25} + C_r\gamma Y_{17}^3 + 2C_i\delta Y_{13}Y_{21}Y_{25} \\ & + 2C_i\gamma Y_9Y_{21}Y_{25} - 2C_i\gamma Y_{13}Y_{17}Y_{25} + 2C_i\delta Y_9Y_{17}Y_{25} - 2C_i\gamma Y_9Y_{17}Y_{29} + 2C_i\delta \\ & Y_9Y_{21}Y_{29} - 2C_i\gamma Y_{13}Y_{21}Y_{29} - 2C_i\delta Y_{13}Y_{17}Y_{29} - 2C_i\gamma Y_1^2Y_{21} + C_i\delta Y_{21}^2Y_{17} - C_i \\ & \gamma Y_{17}^2Y_{21} - 2C_i\gamma Y_5^2Y_{21} - 2C_i\gamma Y_{21}Y_{25}^2 + 2C_i\delta Y_{17}Y_{25}^2 - 2C_i\gamma Y_{21}Y_{29}^2 \\ & + 2C_i\delta Y_{17}Y_{29}^2 + 2C_i\delta Y_1^2Y_{17} - 2C_r\delta Y_9Y_{21}Y_{25} - 2C_r\gamma Y_{13}Y_{17}Y_{29} + 2C_r \\ & \gamma Y_9Y_{21}Y_{29} + 2C_r\delta Y_9Y_{17}Y_{29} + 2C_r\delta Y_9^2Y_{21} - C_r\gamma Y_1Y_{13}^2 + C_r\delta Y_5Y_{13}^2 + C_r \\ & \gamma Y_1Y_9^2 - C_r\delta Y_5Y_9^2 + 2C_r\delta Y_1^2Y_{21} + C_r\delta Y_{17}^2Y_{21} + C_r\gamma Y_{21}^2Y_{17} + 2C_r \\ & \delta Y_5^2Y_{21} + 2C_r\delta Y_{13}^2Y_{21} + C_r\delta Y_{21}^3)/(\gamma^2 + \delta^2)\end{aligned}$$

$$F(21) = Y_{22}$$

$$F(22) = Y_{23}$$

$$F(23) = Y_{24}$$

$$\begin{aligned}F(24) = {} & (\gamma Y_{17} + \delta Y_{21} - \omega\delta Y_{21} - \mu\gamma Y_{21} + \mu\delta Y_{17} - \omega\gamma Y_{17} - \alpha\gamma Y_{23} \\ & + \alpha\delta Y_{19} - \beta\gamma Y_{19} - \beta\delta Y_{23} - E(\gamma Y_1/0.2D1 + \gamma Y_{25}/0.2D1 - \delta Y_5 \\ & /0.2D1 + \delta Y_{29}/0.2D1)/0.2D1 - E(\gamma Y_9/0.2D1 + \gamma Y_{17}/0.2D1 + \delta Y_{13}/0.2D1 \\ & - \delta Y_{21}/0.2D1)/0.2D1)/(\gamma 2 + \delta 2) - (2C_r\gamma Y_1 2Y_{21} - C_r\delta Y_{17}Y_{21}2 + C_r\gamma \\ & Y_{17}2Y_{21} + 2C_r\gamma Y_5 2Y_{21} + 2C_r\gamma Y_{21}Y_{25}2 - 2C_r\delta Y_{17}Y_{25}2 - 2C_r\delta Y_{17}Y_{29}2 \\ & + 2C_r\gamma Y_{21}Y_{29}2 - 2C_r\delta Y_1 2Y_{17} - 2C_r\delta Y_5 2Y_{17} + C_i\gamma Y_{17}3 + 2C_i\delta Y_9 Y_{13} \\ & Y_1 - 2C_i\gamma Y_{13}Y_{17}Y_{29} - 2C_r\delta Y_5 Y_{13}Y_{25} - 2C_r\delta Y_1 Y_9 Y_{25} + 2C_r\gamma Y_5 Y_9 Y_{25} - 2C_r\gamma \\ & Y_1 Y_{13}Y_{25} + 2C_r\gamma Y_1 Y_9 Y_{29} + 2C_r\delta Y_5 Y_9 Y_{29} + 2C_r\gamma Y_9 Y_{13}Y_1 - 2C_r\delta Y_9 Y_{13}Y_5 \\ & - 2C_r\delta Y_1 Y_{13}Y_{29} + 2C_r\gamma Y_5 Y_{13}Y_{29} + C_r\gamma Y_{21}3 + 2C_i\delta Y_1 2Y_{21} + C_i\delta Y_{17}2Y_{21} \\ & + C_i\gamma Y_{17}Y_{21}2 + 2C_i\delta Y_5 2Y_{21} + 2C_i\delta Y_{21}Y_{25}2 + 2C_i\delta Y_{21}Y_{29}2 + 2C_i\gamma Y_{17} \\ & Y_{29}2 + 2C_i\gamma Y_1 2Y_{17} + 2C_i\gamma Y_5 2Y_{17} + 2C_i\gamma Y_{17}Y_{25}2 + 2C_i\gamma Y_5 Y_{13}Y_{25} + 2C_i \\ & \gamma Y_1 Y_9 Y_{25} + 2C_i\delta Y_5 Y_9 Y_{25} - 2C_i\delta Y_1 Y_{13}Y_{25} + 2C_i\gamma Y_1 Y_{13}Y_{29} + 2C_i\delta Y_5 Y_{13} \\ & Y_{29} + 2C_i\delta Y_1 Y_9 Y_{29} - 2C_i\gamma Y_5 Y_9 Y_{29} + 2C_i\gamma Y_9 Y_{13}Y_5 + 2C_r\gamma Y_{13}Y_{21}Y_{29} - 2C_r\delta \\ & Y_9 Y_{17}Y_{25} + 2C_r\gamma Y_{13}Y_{17}Y_{25} - 2C_r\gamma Y_9 Y_{21}Y_{25} - 2C_r\delta Y_{13}Y_{21}Y_{25} + 2C_r\delta Y_{13}Y_{17}Y_{29} \\ & + 2C_r\gamma Y_9 Y_{17}Y_{29} + C_i\delta Y_{21}^3 + 2C_i\delta Y_9^2 Y_{21} + 2C_i\gamma Y_9^2 Y_{17} + 2C_i\gamma Y_{13}^2 \\ & Y_{17} + 2C_i\delta Y_{13}^2 Y_{21} + 2C_i\delta Y_9 Y_{17}Y_{29} + 2C_i\gamma Y_9 Y_{21}Y_{29} + 2C_i\delta Y_{13}Y_{17}Y_{25} + 2C_i \\ & \gamma Y_9 Y_{17}Y_{25} - 2C_i\delta Y_9 Y_{21}Y_{25} + 2C_i\gamma Y_{13}Y_{21}Y_{25} + C_i\delta Y_5 Y_{13}^2 - C_i\gamma Y_1 Y_{13}^2 - C_i \\ & \delta Y_5 Y_9^2 + C_i\gamma Y_1 Y_9^2 - 2C_r\delta Y_9 Y_{21}Y_{29} - C_r\delta Y_{17}^3 - 2C_r\delta Y_{13}^2 Y_{17} - 2C_r\delta \\ & Y_9^2 Y_{17} + 2C_r\gamma Y_9^2 Y_{21} + 2C_r\gamma Y_{13}^2 Y_{21} + C_r\delta Y_1 Y_{13}^2 + C_r\gamma Y_5 Y_{13}^2 - C_r\delta \\ & Y_1 Y_9^2 - C_r\gamma Y_5 Y_9^2 + 2C_i\delta Y_{13}Y_{21}Y_{29})/(\gamma^2 + \delta^2)\end{aligned}$$

$$F(25) = Y_{26}$$

$$F(26) = Y_{27}$$

$$F(27) = Y_{28}$$

$$\begin{aligned}F(28) = {} & (0.3D1\delta Y_{25} - 0.3D1\gamma Y_{29} - \mu\gamma Y_{25} - \omega\delta Y_{25} - \mu\delta Y_{29} + \omega\gamma Y_{29} \\ & - \alpha\gamma Y_{27} - \alpha\delta Y_{31} + \beta\gamma Y_{31} - \beta\delta Y_{27} + E(-\gamma Y_{13}/0.2D1 + \gamma Y_{21} \\ & /0.2D1 - \delta Y_9/0.2D1 - \delta Y_{17}/0.2D1)/0.2D1)/(\gamma^2 + \delta^2) \\ & - (2C_r\delta Y_{13}^2 Y_{29} + C_r\delta Y_{25}^2 Y_{29} + C_r\gamma Y_{29}^2 Y_{25} + 2C_r\delta Y_1^2 Y_{29} + 2C_r\delta Y_9^2 Y_{29} \\ & + 2C_r\delta Y_5^2 Y_{29} + 2C_r\gamma Y_{13}^2 Y_{25} + 2C_r\gamma Y_1^2 Y_{25} + 2C_r\gamma Y_9^2 Y_{25} + 2C_r\gamma Y_5^2 Y_{25} \\ & + 2C_r\delta Y_1 Y_{13} Y_{17} + 2C_i\delta Y_5 Y_9 Y_{21} - 2C_i\delta Y_1 Y_{13} Y_{21} - 2C_i\gamma Y_5 Y_{13} \\ & Y_{21} + 2C_i\gamma Y_5 Y_9 Y_{17} - 2C_i\gamma Y_1 Y_{13} Y_{17} + 2C_i\delta Y_5 Y_{13} Y_{17} + 2C_r\gamma Y_1 Y_9 Y_{17} \\ & - C_i\gamma {Y_{29}}^3 + C_i\delta Y_{25}^3 + 2C_r\delta Y_{17} Y_{21} Y_9 - 2C_i\gamma Y_{13}^2 Y_{29} - C_i\gamma Y_{25}^2 Y_{29} - 2C_i\gamma Y_1^2 \\ & Y_{29} - 2C_i\gamma Y_9^2 Y_{29} - 2C_i\gamma Y_5^2 Y_{29} + C_i\delta Y_{29}^2 Y_{25} + 2C_i\delta Y_1^2 Y_{25} + 2C_i \\ & \delta Y_9^2 Y_{25} + 2C_i\delta Y_5^2 Y_{25} + 2C_i\delta {Y_{13}}^2 Y_{25} + 2C_i\delta Y_{17} Y_{21} Y_{13} - 2C_i\gamma Y_{17} Y_{21} Y_9 \\ & + C_r\delta Y_{29}^3 - 2C_r\gamma Y_1 Y_{13} Y_{21} + 2C_r\gamma Y_5 Y_{13} Y_{17} - 2C_r\delta Y_5 Y_9 Y_{17} + 2C_r\gamma Y_5 Y_9 \\ & Y_{21} + 2C_r\delta Y_5 Y_{13} Y_{21} + 2C_r\delta Y_1 Y_9 Y_{21} - 2C_i\gamma Y_1 Y_9 Y_{21} + C_i\delta Y_9 Y_{17}^2 + C_i\gamma Y_{13} \\ & Y_{17}^2 + 2C_i\delta Y_{21}^2 Y_{25} - 2C_i\gamma Y_{17}^2 Y_{29} - 2C_i\gamma Y_{21}^2 Y_{29} - C_i\delta Y_9 Y_{21}^2 - C_i\gamma \\ & Y_{13} Y_{21}^2 + 2C_i\delta Y_{17}^2 Y_{25} + 2C_i\delta Y_1 Y_9 Y_{17} + C_r\gamma Y_9 Y_{17}^2 - C_r\delta Y_{13} Y_{17}^2 + 2C_r\gamma \\ & Y_{21}^2 Y_{25} + 2C_r\delta Y_{17}^2 Y_{29} + 2C_r\delta {Y_{21}}^2 Y_{29} - C_r\gamma Y_9 Y_{21}^2 + C_r\delta Y_{13} Y_{21}^2 + 2 \\ & C_r\gamma Y_{17}^2 Y_{25} + C_r\gamma Y_{25}^3 + 2C_r\gamma Y_{17} Y_{21} Y_{13})/(\gamma^2 + \delta^2)\end{aligned}$$

$$F(29) = Y_{30}$$

$$F(30) = Y_{31}$$

$$F(31) = Y_{32}$$

$$\begin{aligned}F(32) = {} & (0.3D1\gamma Y_{25} + 0.3D1\delta Y_{29} - \mu\gamma Y_{29} - \omega\gamma Y_{25} - \omega\delta Y_{29} + \mu\delta Y_{25} \\ & - \alpha\gamma Y_{31} + \alpha\delta Y_{27} - \beta\gamma Y_{27} - \beta\delta Y_{31} - E(\gamma Y_9/0.2D1 + \gamma Y_{17} \\ & /0.2D1 - \delta Y_{13}/0.2D1 + \delta Y_{21}/0.2D1)/0.2D1)/(\gamma^2 + \delta^2) \\ & - (C_i\delta Y_{29}^3 - 2C_r\delta Y_{13}^2 Y_{25} - 2C_r\delta Y_1^2 Y_{25} - 2C_r\delta Y_9^2 Y_{25} - 2C_r\delta Y_5^2 \\ & Y_{25} + 2C_r\gamma Y_{13}^2 Y_{29} - C_r\delta Y_{25} Y_{29}^2 + C_r\gamma Y_{25}^2 Y_{29} + 2C_r\gamma Y_1^2 Y_{29} + 2C_r\gamma \\ & Y_9^2 Y_{29} + 2C_r\gamma Y_5^2 Y_{29} + 2C_r\delta Y_1 Y_{13} Y_{21} - 2C_r\delta Y_1 Y_9 Y_{17} + 2C_r\gamma Y_5 Y_{13} Y_{21} \\ & - 2C_r\delta Y_5 Y_9 Y_{21} + 2C_r\gamma Y_1 Y_9 Y_{21} + 2C_i\delta Y_9^2 Y_{29} + 2C_i\delta Y_5^2 Y_{29} + C_i\gamma Y_{25}^3 \\ & + 2C_i\delta Y_{17} Y_{21} Y_9 - C_r\delta Y_{25}^3 + 2C_r\gamma Y_{17} Y_{21} Y_9 - 2C_r\delta Y_{17} Y_{21} Y_{13} + 2C_i\gamma Y_{17} Y_{21} \\ & Y_{13} + 2C_i\delta Y_1^2 Y_{29} + 2C_i\delta Y_1 Y_{13} Y_{17} + 2C_i\gamma Y_1 Y_9 Y_{17} + 2C_i\gamma Y_5 Y_{13} Y_{17} - 2C_i \\ & \delta Y_5 Y_9 Y_{17} + 2C_i\delta Y_5 Y_{13} Y_{21} + 2C_i\delta Y_1 Y_9 Y_{21} + 2C_i\gamma Y_5 Y_9 Y_{21} + 2C_i\gamma Y_{13}^2 Y_{25} \\ & + 2C_i\gamma Y_1^2 Y_{25} + 2C_i\gamma Y_9^2 Y_{25} + 2C_i\gamma Y_5^2 Y_{25} + 2C_i\delta Y_{13}^2 Y_{29} + C_i\delta Y_{25} \\ & {}^2 Y_{29} + C_i\gamma Y_{25} Y_{29}^2 + 2C_r\gamma Y_1 Y_{13} Y_{17} - 2C_r\delta Y_5 Y_{13} Y_{17} + C_i\delta Y_{13} Y_{21}^2 - C_i\gamma Y_9 \\ & Y_{21}^2 - C_i\delta Y_{13} Y_{17}^2 + C_i\gamma Y_9 Y_{17}^2 + 2C_i\gamma Y_{21}^2 Y_{25} + 2C_i\gamma Y_{17}^2 Y_{25} + 2C_i\delta \\ & Y_{21}^2 Y_{29} + 2C_i\delta Y_{17}^2 Y_{29} + C_r\gamma Y_{29}^3 - 2C_r\gamma Y_5 Y_9 Y_{17} + C_r\gamma Y_{13} Y_{21}^2 + C_r\delta Y_9 \\ & Y_{21}^2 - C_r\gamma Y_{13} Y_{17}^2 - C_r\delta Y_9 Y_{17}^2 - 2C_r\delta Y_{21}^2 Y_{25} - 2C_r\delta Y_{17}^2 Y_{25} + 2C_r\gamma \\ & Y_{21}^2 Y_{29} + 2C_r\gamma Y_{17}^2 Y_{29} - 2C_i\gamma Y_1 Y_{13} Y_{21})/(\gamma^2 + \delta^2) + \lambda Y_{32}\end{aligned}$$

Appendix B

Floquet multiplier theorem

Consider an n-dimensional first-order system as

$$\dot{\vec{x}} = A(t)\vec{x} \tag{B.2}$$

where A is an $n \times n$ matrix function with minimal period T, which satisfies

$$A(t+T) = A(t), \quad -\infty < t < \infty,$$

for the smallest positive T. The Floquet multiplier theorem [42] stats that the system has at least one non-trivial solution. Under some conditions, solutions of (B.2) take the form

$$\vec{x}(t) = \Sigma_{i=1}^{n} c_i e^{\mu_i t} \vec{p}_i(t) \tag{B.3}$$

where c_i are constants that depend on initial conditions, $\vec{p}_i(t)$ are vector-valued functions with period T, and μ_i are called characteristic numbers or Floquet multipliers of (B.2). The Floquet exponents are related to μ_i by the relationship

$$\rho_i = e^{\mu_i T}.$$

The zero equilibrium is stable if all Floquet multipliers have magnitude less than 1, or if all Floquet exponents have negative real parts. The zero equilibrium is unstable if any

Floquet exponent has a positive real part or, equivalently a Floquet multiplier has modulus greater than one [43]. More information can be found in [38, 42].

Appendix C

Matlab programs

C.0 Mathieu equation

```
function zdot = ode1(t,p,F,k,n);
 f =F*cos(n*t);
 % strong damping k=0 case
 %mu=-0.125; beta=-2; omega=1.5; alpha=1; gamma=0; delta=0;
%strong damping k=0.6911 case.
   mu=-.5; beta=-2/3; omega=1/3; alpha=.5; gamma=0; delta=0;
%weak damping case k=1
% mu=-.255; beta=1;  alpha=-1/2; gamma=-1/4; delta=0.495;
%    rho=-0.5;
%    epsilon=sqrt((mu-alpha+gamma)/rho);
%    nu=2;
%    w=beta+1+(epsilon^2 *nu);
Om_hat = omega-beta*k.^2+delta*k.^4;
Ga = 2*(-mu+alpha*k.^2-gamma*k.^4);
    Om = sqrt((Ga.^2/4)+ Om_hat.^2);
      zdot = [p(2);-Ga*p(2)-(Om^2 + Om_hat*f)*p(1)];
```

C.1 Floquet multipliers

Eigenvalue of Mathieu equation with $F = F_c$ and vary the wavenumber k.

```
F=5.02736;
n=2;
E1=[];E2=[];
for  k=0:0.01:3
     tspan= [0 2*pi/n]; p0 = [1; 0]; t= [0 2*pi/n];
   options = odeset('reltol',1e-10);
   [t,p] = ode45(@(t,p) me(t,p,F,k,n), tspan , p0,options);
   v = p(:,1); w = p(:,2);
   a=v(end);
   c=w(end);
   p0 = [0; 1];
   [t,p] = ode45(@(t,p) me(t,p,F,k,n), tspan , p0,options);
   v = p(:,1); w = p(:,2);
   b=v(end);
   d=w(end);
   A=[a b; c d];
   e=eig(A);
  E1=[E1;e(1)];
  E2=[E2;e(2)];
end
k=0:0.01:3;
figure(1);
plot(k,E1,k,E2,'LineWidth',1.5);
xlabel('k'),ylabel('e-values');
set(gca,'fontsize',14)
ylabel('Floquet multipliers','Interpreter','latex',
```

```
27 'FontSize',18)
28 xlabel('$\boldmath{k}$','Interpreter','latex','FontSize'
       ,18)
```

C.2 Cubic–quintic PDE model in 2D

The cubic-quintic PDE model in 2D

```
1 kc=0.6911;
2  F=3.98;
3 Nx =128 ; Lx=(2*pi/kc)*10;
4 Ny = 128; Ly=(2*pi/kc)*10;
5 x =(Lx/Nx)*(0:Nx-1)';
6 y =(Ly/Ny)*(0:Ny-1)';
7 [xx,yy]=meshgrid(x,y);
8  mu=-0.5; beta=-2/3;nu=0; alpha=0.5; gamma=0; delta=0;
9  omega=1/3;
10 C=1;
11  Nits_twic_per=120;% the number of points in two period
12  h = 4*pi/Nits_twic_per;
13  number_twic_per=20;
14 tmax=4*pi*number_twic_per;
15 nmax=number_twic_per* Nits_twic_per;
16 nplt = Nits_twic_per*floor(number_twic_per/10);
17
18 %Initial condition of axisymmetric oscillon
19  r = sqrt((xx-Lx/2).^2+(yy-Ly/2).^2);
20  u = 0.65*cos(kc*r)./(1+exp(0.5*kc*(r-27)));
21  u=u+1.0e-6*(2*rand(Nx,Ny)-1);
```

```
%Initial conditions should be even in r if U_xx is to be
    finite.
%This initial condition is not quite even but it gives
    rings
% Initial condition of nonaxisymmetric (example 1)
 r = sqrt(xx.^2+yy.^2);
  u = 1.9*r.*sech(r/4).*besselj(1,r);
u=u+1.0e-6*(2*rand(Nx,Ny)-1);
  u=circshift(u,[Nx/2,Ny/2]);
 u_hat = fft2(u);
 udata = u_hat; tdata = 0;udata1=u_hat(11);
 % set wavenumbers
kx = [0:Nx/2-1 Nx/2 -Nx/2+1:-1]'*2*pi/Lx;
ky = [0:Ny/2-1 Ny/2 -Ny/2+1:-1]'*2*pi/Ly;
[kkx,kky]=meshgrid(kx,ky);
k1=kx.*kx;
k2=ky.*ky;
 % linear part
c = (mu+1i*omega) - (alpha+(1i*beta))*(kkx.^2+kky.^2)
     + (gamma+(1i*delta))*(kkx.^4+kky.^4);
E = exp(h*c);
etd =(E-1)./c;
etd2a = (E.*(1 +1./c/h) - 1./c/h - 2 )./ c;
etd2b = (E.*(-1./c/h) + 1./c/h + 1 )./ c;

u = ifft2(u_hat);
 t = 0;
 f=F*cos(2*t);
 nlold=fft2(Q1*u.^2+Q2*abs(u).^2+C*u.*abs(u).^2
```

```
49            -u.*abs(u).^4+ f.*1i*real(u));
50 nldata=[];
51 % start the main loop n is step No.
52 for n = 1:round(nmax)
53   u =(ifft2(u_hat));
54   t = (n-1) * h;
55   f = F*cos(2*t);
56   nl=fft2(Q1*u.^2+Q2*abs(u).^2+C*u.*abs(u).^2
57       -u.*abs(u).^4+ f.*1i*real(u));
58   u_hat= E.*u_hat + nl.*etd2a + nlold.*etd2b;  % ETD2
59   nlold = nl;
60  %u_hat= E.*u_hat + nl.*etd ; % ETD1
61  if mod(n-1,nplt)==0
62       u = ifft2(u_hat);
63  udata = [udata,u_hat];
64  udata1=[udata1,u_hat(11)];
65  nldata=[nldata,nlold];
66  tdata = [tdata,t];
67   umax=max(max(u));
68  figure(1);
69  surf(xx,yy,real(u));view([-90 90]);
70          shading interp; axis equal; axis tight; drawnow;
71          colorbar
72  end
73 end
74  u_last2r=ifft2(u_hat);
75 u_hat;
```